ALGAL CULTIVATION AND BIOMASS UTILIZATION FOR SUSTAINABLE CARBON CAPTURE FROM THE POWER INDUSTRY

By

Ashley Cutshaw

A DISSERTATION

Submitted to
Michigan State University
in partial fulfillment of the requirements
for the degree of

Biosystems Engineering—Doctor of Philosophy
Environmental Science and Policy—Dual Major

2022

ABSTRACT

ALGAL CULTIVATION AND BIOMASS UTILIZATION FOR SUSTAINABLE CARBON CAPTURE FROM THE POWER INDUSTRY

By

Ashley Cutshaw

Anthropogenic climate change is a critical issue that must be addressed with a systems approach. Greenhouse gas (GHG) emissions, like carbon dioxide (CO_2), are key contributors to the climate crisis and originate from several different sources. Namely, the power industry is responsible for approximately 30% of U.S. CO_2 emissions and 45% of global CO_2 emissions. These emissions result from the combustion of carbon-based fuels, like coal and natural gas, and are emitted into the atmosphere in the form of flue gas. Being a large contributor of CO_2 emissions has made the power industry the focus of research efforts to develop post-combustion carbon capture technologies. This work represents a comprehensive examination of microalgal cultivation and biomass utilization as methods for post-combustion carbon capture and replacement of fossil-dependent technologies and products.

Optimized pilot-scale cultivation represents a sustainable post-combustion carbon capture technology with downstream economic value. An initial study of a 100 L photobioreactor (PBR) within a 100 MW power plant was conducted to optimize the long-term, continuous cultivation of the green microalgae *Chlorella sorokiniana*. The culture utilized flue gas as a source of CO_2 and successfully operated continuously over a year long period. Insights from this study include the growth kinetics of *C. sorokiniana*, optimal cultivation conditions of the PBR, and an in-depth analysis of the microbial-microalgal assemblage throughout the study. The biomass produced during the 12-month study was stored and subsequently utilized to develop methods for cell disruption and protein recovery. This work investigated a mechanochemical method, using ball

milling technology and chemically induced pH changes, to efficiently extract and recover microalgal proteins. The results of this study indicate that the mechanochemical method requires less energy than existing mechanical methods, while achieving similar levels of cell disruption.

In addition to protein extraction and recovery, an alternate pathway for biomass utilization was explored. Microalgal biomass and microalgal proteins contain the foundational building blocks required for synthesis of chemicals like polyols. Polyols, used for polyurethane (PU) foam production, represent another value-added product that could provide the economic incentive to invest in microalgal cultivation for post-combustion carbon capture. Using biomass and recovered proteins as feedstocks, polyols were synthesized using a one-pot, two step method. Two microalgal polyols were selected based on their characterization and were evaluated using life cycle and techno-economic frameworks. The results elucidated the environmental and economic advantages when using microalgal biomass as an alternative to petrochemicals as a feedstock for polyol synthesis. Finally, this work evaluated a combined biological and chemical post-combustion carbon capture system using microalgal cultivation and a novel microalgal amino acid salt solution (MAASS). Life cycle and techno-economic frameworks were used to compare the MAASS to a standard amine-based solvent. The results of these assessments show that the MAASS capture system performs significantly better than an amine capture system, both in terms of environmental impacts and the cost of capture. This comprehensive collection of data and analysis represents advances in the field, as well as innovative methods and technologies that further demonstrate the viability of microalgal cultivation and biomass utilization for carbon capture from the power industry.

ACKNOWLEDGEMENTS

The author greatly appreciates the financial support from the U.S. Department of Energy (DOE) National Energy Technology Laboratory (NETL) (Award No.: DE-FE0030977). The author would also like to thank the Research Technology Support Facility (RTSF) of Michigan State University for their support.

TABLE OF CONTENTS

LIST OF TABLES

LIST OF FIGURES

KEY TO ABBREVIATIONS

AASS Amino acid salt solution

PBR Algae Photobioreactor

CEMS Continuous Emissions Monitoring System

CO_2 Carbon dioxide

GHG Greenhouse gas

LCA Life cycle assessment

LED Light Emitting Diode

MAASS Microalgal amino acid salt solution

MEA Monoethanolamine

MPSP Minimum polyol selling price

PBR Photobioreactor

PC Propylene carbonate

PPFD Photosynthetic Photon Flux Density

PU Polyurethane

TAP Tris-Acetate-Phosphate

TEA Techno-economic assessment

TN Total Nitrogen

TP Total Phosphorous

INTRODUCTION

Problem background

High atmospheric carbon dioxide (CO_2) levels continue to pose a threat to our climate and planet. In 2018, carbon dioxide (CO_2) emissions totaled nearly 5,500 million metric tons, accounting for 81% of all greenhouse gas (GHG) emissions [1]. The energy sector is responsible for nearly one-third of all CO_2 emissions and is therefore the focus of post-combustion carbon capture research efforts. Current technologies for post-combustion carbon capture include adsorption, membrane absorption and separation, and chemical absorption [2]. While there is ongoing investigation into the advance of these currently implemented technologies, there are also alternatives that have garnered continued interest, such as microalgal cultivation.

Microalgal cultivation continues to be a desirable carbon capture method due to its CO_2 fixation capabilities and the downstream potential of high value metabolites [3, 4]. Decades of research on lab-scale microalgal cultivation have demonstrated both the possibilities and the limitations of microalgal cultivation as a carbon capture method [5, 6]. The challenges with microalgal cultivation as a method for post-combustion carbon capture are primarily economic in nature [7]. However, the economic potential of co-product biorefineries and efficient development value-added products has elucidated emerging pathways to sustainable and economically viable microalgal systems [8-10]. While there are several reports demonstrating the feasibility of large-scale cultivation systems, very few studies have demonstrated the practicality of a co-located biorefinery [11-14]. Cultivation on flue gas has many advantages, most notably the sequestration of carbon emissions and the delivery of a low-cost, concentrated stream of CO_2. However, operating conditions and emissions profiles vary considerably between power plants and co-located cultivation should be evaluated on a case-by-case basis. Establishing protocols for long term, continuous cultivation is critical for establishing co-located cultivation as a practical

post-combustion carbon capture method with downstream benefits.

Additional challenges to implementation include the lack of standard procedures for efficient cell disruption, and subsequent protein recovery, and the need to establish microalgal biotechnology as a viable alternative to existing products [15]. Decades of research have been dedicated to the development and optimization of lipid synthesis and extraction, and microalgal biofuels continue to be of interest [16]. However, this resulted in under-developed research on protein extraction, until recently, when microalgal proteins became a topic of interest. Protein extraction methods have been evaluated, however, yields are low relative to energy demand, energy data is scarce, and process scale analysis is limited [17]. Another under-developed area of research is the production of chemicals from microalgal biomass. Recent studies have presented microalgal proteins and oil as substitutes for petrochemicals like ethylene glycol, polyols for polyurethane (PU) foams, and thermoplastics [18-23]. However, there are no available studies on the use of whole microalgal biomass for chemical synthesis and additional research is necessary to establish the feasibility of existing methods at a process scale.

Current post-combustion carbon capture techniques primarily use alkanolamines, like monoethanolamine (MEA), for chemical capture [24, 25]. However, a recent study proved that microalgal biomass, once it's been hydrolyzed to release free amino acids, can achieve efficient carbon capture with high CO_2 loading (paper under review). This novel solvent has elicited interest due to its non-toxic nature, recyclability, and sustainability. Life cycle and techno-economic assessment are essential frameworks for appraising the sustainability of emerging technologies, and the microalgal solvent should be evaluated as such.

The purpose of this work was to address the identified knowledge and data gaps in microalgal biotechnology. The primary goal was to collect empirical data and perform analyses

that would validate the viability of co-located microalgal cultivation and biorefineries, and advance microalgal biorefinery research. A secondary goal of this work was to identify current limitations in this area of research and opportunities for future work.

Literature Review

Long-term and pilot-scale cultivation systems

Reactor type, culture stability, nutrients and operating conditions are the main factors that affect large cultivation systems in the long-term. When deciding between using an open pond system or a photobioreactor (PBR), there are several factors to consider. Open pond systems are much less costly, both in capital costs and operating costs, as they require little infrastructure and use only sunlight to drive photosynthesis [26]. However, because pond cultures are inherently open to their environment, they are much more susceptible to their local climate and contamination by heterotrophic bacteria and other algal species. Although PBRs have higher capital and operating costs, their infrastructure allows for better growth and higher productivity [27].

Culture stability is another challenge when it comes to maintaining long-term cultivation systems. Two factors have been identified that can greatly impact the stability and long-term success of an algal culture: pH and biological contamination. Although there are several microalgal species that are resilient under different culture conditions, most species have very specific pH ranges that are required for successful growth [28]. Culture systems often achieve a stable pH through the addition of a strong acid or base, using acid-base chemistry to cause a direct and immediate change in the pH. Unfortunately, this method requires the addition of a chemical that would not otherwise be added to a culture, adding further cost to the cultivation

system. An alternative to directly manipulating the pH is creating different formulations of nutrients that can indirectly create steady pH conditions [29]. These unique formulations take advantage of the nutrient assimilation processes of selected microalgal species and result in biochemical pH stabilization [30]. Although biological contamination often carries a negative connotation, there is evidence of positive bacterial-microalgal interactions in microalgal-dominant cultures [31]. More specifically, bacterial respiration can elicit changes to O_2 and CO_2 levels and substrate exchange between bacteria and microalgae can improve productivity and growth [32]. Considering these important factors that affect culture stability, the ideal microalgal species is one that demonstrates compatibility with evolving culture conditions, while maintaining high growth and productivity rates.

Culture media and the subsequent delivery of sufficient nutrients are critical components of any culture system, lab- or pilot-scale. Carbon, nitrogen, and phosphorous make up the major nutrients and sodium, potassium and calcium are among several other (Mg, S, Fe, Mo, Sr, Mn, Ba, Zn, and Al) minor nutrients [33]. In photoautotrophic cultures, carbon is introduced into the system as CO_2. An advantageous source of CO_2, both economically and environmentally, is flue gas that is expelled from natural gas and coal fired power plants. While co-locating PBRs with power plants is advantageous, flue gas can also contain other components, such as sulfur oxides (SO_x), that may negatively impact an algal culture [34]. This inadvertent addition of SO_x into the culture could impact the growth and composition of a microalgal culture and these conditions need to be investigated in a long-term culture.

Although photobioreactors are more efficient and customizable, the energy inputs regarding water and light are problematic when it comes to scale-up and commercial applications. To determine how reliant microalgal growth and productivity are on light exposure, a light/dark

cycle (X hours on, X hours off) can be applied in order to compare with continuous light (24 hours on). Harvesting amount, or harvesting rate, is another parameter that is critical to successful algal cultivation. Choosing an optimal harvesting rate is a balance between productivity (g/L/day) and biomass concentration (g/L). Ultimately, the growth rate of the selected algal species will determine the appropriate harvesting rate and residence time that optimizes both productivity and biomass concentration in the PBR [35].

There are decades of research on lab scale microalgal cultivation and its optimization, however, data demonstrating the stability and productivity of a large, pilot-scale PBR over extended periods of time are inadequate. A majority of the focus has been on standalone, open pond operations and theoretical scales as large as 5,000 acres [36]. While these studies are critical for establishing the feasibility of future large-scale operations, co-located pilot and process scale systems are more practical and achievable in the short term, and should be investigated further.

Microalgal protein extraction and isolation techniques

Despite its capacity for CO_2 fixation, microalgal cultivation has significant energy and cost demands, leading to economic disparities between the cost to grow and the financial benefits of harvested biomass [26]. Although microalgal lipids and biofuels have been thoroughly investigated for decades, microalgal biofuels remain uncompetitive with fossil fuels when it comes to price, and have yet to be accepted as a viable alternative fuel source [37, 38]. In addition to lipids, microalgae are a rich source of protein, often making up more than 50% of the dry matter [39, 40]. In 2019 the global market for microalgal protein exceeded $700 million and is expected to increase over 6% by 2026, reaching over $1 billion [41]. The *Chlorella* species in

particular has become a popular alternative nutrition source and interest in its use as a plant-based protein source for human consumption continues to grow [17].

Once microalgal biomass has been harvested and dewatered, the next step in converting biomass into value-added products is cell disruption. Downstream products receive their value from intracellular components, like lipids and proteins, that are transformed into goods like biofuels or nutraceuticals. Several different techniques have been tested to achieve different degrees of disruption, such that the integrity of the target component is not compromised during the process. These techniques include alkali/acid treatment, enzymatic treatment, microwave, sonication, high pressure homogenizers, thermochemical conversion, pulsed electric field treatment, and milling with beads or balls [37, 42, 43]. Several reports indicate that despite the high energy demands of mechanical methods, like homogenizers and mills, they are the most efficient techniques for cell disruption and offer the best opportunities for scalability [43].

High pressure or high speed homogenizers can be very effective methods for total cell disruption as the intense conditions works in combination with inertia, shear, and cavitation to quickly rupture cells [44]. Despite the effectiveness of these homogenizers, analysis of the required energy input and the resulting energy and economic outputs of the microalgal biomass show that there is a discrepancy between the two [45]. Bead milling, or ball milling, are similar mechanical disruption processes that require less energy. Both use the help of beads/balls to enhance an induced agitation for fractionation of a material. Bead and ball mills either have a stirring mechanism (i.e., discs on a rotor) that assist the beads in their disruption through transfer of kinetic energy, or centrifugal and inertial energy is created through movement of the vessel itself [46]. Bead mills and ball mills come in varying sizes (i.e., 0.5-26 L) and are widely used in industrial applications, thus making them an attractive scalable method for microalgal cell

disruption [47].

Once the biomass has been disrupted or homogenized, the component of interest can be extracted. There are several techniques for extraction of microalgal metabolites, including the use of alkali or organic solvents, ionic liquids, and aqueous two-phase extraction [15, 48]. Most research on the extraction of components from microalgal biomass is concerned with lipid extraction and the subsequent development of biofuels. Only recently did protein become of widespread interest, and thus, the methods for protein recovery from processed biomass are scarce and under-developed. An established procedure for efficient cell disruption and subsequent protein recovery has yet to be determined [15].

Biobased polyol production

A polyol is a liquid substance that will react with isocyanate and are generally classified as hydroxyl-terminated or amino-terminated [49]. Polyols are a major component of PU foams, and can yield either a rigid or flexible foam that can have several different applications from mattresses to home insulation. The hydroxyl number, given in units of mg KOH equivalent for every 1 g of sample (mg KOH/g), is a key characteristic of polyols that indicate the type of PU foam it will form [50]. This number represents how many hydroxyl groups are present in the sample to react with isocyanate and can range from 28-160 for flexible PU foams and from 300-800 for rigid PU foams [49, 50]. The polyurethane market is expected to grow significantly in coming years due to its continued use in adhesives and foams. This growth is expected to be accompanied by a shift towards using renewable and sustainable sources of nitrogen and carbon to produce biobased polyols [22, 51].

There are several established biobased feedstocks currently being used and researched for polyol synthesis, ranging from natural sugars like sucrose and glucose to lignin [50]. One of the

most common starting materials is vegetable oil. Unsaturated vegetable oils, like soybean and castor oil, have characteristic double bonds that can be chemically transformed into hydroxyl groups, a key component of a reactive polyol. While these polyols are well documented and even commercially utilized, continued demand for vegetable oils in the food industry and the additional cost required for oil extraction pose some challenges [52]. Emerging research is showing the potential of protein as a starting material for polyols and as a filler in polyurethane production, namely from protein-rich sources such as microalgal biomass [22, 50]. Further research is needed to evaluate the performance of protein polyols and explore the use of whole biomass as a polyol feedstock. Life cycle and techno-economic assessment frameworks are excellent tools for evaluating emerging technologies like those that need to be developed for biobased polyols.

Post-combustion carbon capture solvents

Chemical post-combustion carbon capture technologies are based on the principal that CO_2 can readily react with amines or amino groups. The general reaction mechanisms have been studied extensively and summarized [25, 53]. Due to the diversity of molecules containing amine or amino groups, there are several different compounds that can react with CO_2. An alkanolamine ($OHRNH_2$) is a compound that contains a hydroxyl group and an amino group that are attached by an alkane chain. Both hydroxyl and amine functional groups make an alkanolamine a good reagent to bind and capture CO_2. Alkanolamine scrubbing systems have been implemented in power plants for post-combustion carbon capture for decades [54]. Despite the success of alkanolamine solutions for CO_2 capture, there are concerns with the cost of the energy input needed for the capture process [55]. In addition, some alkanolamines have very

high volatility and are sensitive to oxygen, which can lead to loss of the amine solvent and degradation to harmful chemicals with may have environmental impacts [56].

Due to the disadvantages of alkanolamine capture systems, research efforts have been focused on developing alternative solvents. Amino acids ($COOHRHCNH_2$) are a class of compounds that have a carboxyl group and an amino group attached by an alpha carbon atom that has an attached hydrogen atom and a unique side chain, R. Unlike amines, amino acid solutions have very low volatility and can absorb CO_2 at much higher temperatures [57]. This is an important characteristic for a post-combustion capture solvent being used in a power plant where operating temperatures are high. This low volatility is due to the addition of chemicals such as potassium or sodium, making the amino acid solutions salt solutions, which prevents evaporation from happening during the absorption process [58]. In addition to their low volatility, amino acid salt solutions (AASS) are less susceptible to oxidative degradation and are more environmentally friendly [59, 60]. Analysis of both capture systems show that the capital costs, operating costs, and energy consumption for an AASS system are less than those for an amine-based system [61].

Despite the success of these bench-scale and modelling studies, there has not been widespread adoption of AASS for post-combustion carbon capture. Issues such as the reactivity of single amino acid and mixed amino acid solutions, corrosivity, solubility, and general lack of data, must be addressed before extensive implementation [60]. Currently, amino acids used for carbon capture are purchased at technical or lab grade from chemical companies, or at food grade in the form of nutritional supplements. Finding biological sources of amino acids may further reduce the cost of capture while being more sustainable than using synthetic amino acids. One candidate for sourcing amino acids is microalgae, as it has high protein content and thus, high

amino acid content [62]. Developing efficient techniques for total hydrolysis and solvent preparation represent challenges to making microalgal biomass a feasible source of amino acids.

A recent study developed a method for hydrolysis of microalgal biomass and explored the use of hydrolyzed microalgal biomass as a CO_2 capture solvent (paper under review). Results from this study showed that the microalgal amino acid salt solution (MAASS) has an absorption capacity of 1.27 mol CO_2/mol amine, which is significantly higher than the absorption capacity of conventional amine solvents and synthetic AASS [25, 63]. This notable result suggests that the complex mixture within the MAASS may create synergistically enhanced capture conditions. Data from a mass and energy balance indicate that the recyclability of the MAASS is a critical indicator of the process scale feasibility of this technology. The results of this study warrant further investigation of the MAASS. Life cycle and techno-economic assessments could provide additional rationale and support for continued research on a MAASS capture system.

CHAPTER 1: A LONG-TERM PILOT-SCALE ALGAL CULTIVATION ON POWER PLANT FLUE GAS – CULTIVATION STABILITY AND BIOMASS ACCUMULATION

Introduction

Carbon dioxide (CO_2) accounts for 82% of greenhouse gas emissions in the U.S., with electricity and power generation totaling 33% of total U.S. CO_2 emissions [1]. Net CO_2 emissions from coal fired power plants are nearly 770 kg/MWh, while emissions from natural gas power plants are approximately 340 kg/MWh [64]. As a result, power generation has become a point of interest with regards to reducing greenhouse gas and CO_2 emissions. The search for a sustainable, post-combustion carbon capture method is ongoing, and microalgal cultivation continues to be a preferable solution due to its capacity for CO_2 fixation and the possibility for downstream revenue from value-added products [3, 4]. Decades of valuable lab-scale research has been done on microalgal cultivation, identifying growth limitations and optimal conditions, techniques for growing and harvesting, and the possibilities for downstream processes [5, 6]. However, data on long-term, pilot-scale cultivation are still inadequate to determine feasible solutions for commercial applications. Reactor configuration, cultivation stability, nutrient selection, and operational conditions are the main factors that long-term, pilot-scale cultivation studies need to focus on.

The debate between using photobioreactors (PBRs) or open pond systems for cultivation is ongoing, as they both have their respective advantages and disadvantages. Open ponds require low capital cost and less energy input as they rely solely on sunlight to drive photosynthesis [26]. However, open ponds are very susceptible to their climate (i.e. temperature, weather and sunlight), making location an important consideration. In addition, open ponds are inherently vulnerable to contamination by other algae and heterotrophic bacteria, and consequently only certain, robust algal species are suitable for outdoor open pond systems [26]. In contrast, PBRs are suitable for a range of algal species as contamination is much easier to control. Light

intensity can be enhanced by using high efficiency light emitting diodes (LEDs) as supplemental light source to the sunlight. Unlike open pond systems, where light penetration is a known limitation, PBR's have a considerably shorter and manipulatable length of light path, which results in better growth and higher efficiency and productivity [27]. In addition, PBRs require a relatively smaller footprint, creating several opportunities for placement.

Besides reactor types, another challenge regarding long-term cultivation of microalgae is maintaining culture stability. In order to ensure successful culture growth, the selected algal species should be robust. When comparing algal species, *Chlorella* were found to have higher rates of production and carbon fixation, making them an ideal species for PBR cultivation and carbon capture [4]. The long-term cultivation of a *Chlorella* species, *C. vulgaris*, was previously demonstrated over a 6-month period in an PBR, with productivity reaching 0.40 g/L/day [65]. Microalgae strains, like *Chlorella* species, have very specific pH ranges that lead to optimal growth [28]. Thus, pH stability and control are major challenges associated with microalgal cultivation. This is often realized by the addition of pH stabilizers (i.e. acid or base) and unfortunately leads to inescapable additional costs on both chemicals and equipment. One way to avoid this complication is to control the pH of a culture using different formulations of nutrients that inherently create steady pH conditions [29]. Biological contamination is another major factor influencing culture stability. Microalgae growth should be maintained at the desired level despite the existence of other biological agents, typically heterotrophic bacteria, by controlling their metabolic activities, via mutual symbiotic relationships, microalgae growth prevails during operational cycles [66]. Despite negative perceptions of biological contamination, microalgal-bacterial interactions can be beneficial for an algal-dominant cultivation system [31]. Algal growth and productivity can be enhanced via substrate exchange from bacteria to algae and by

modification of O_2/CO_2 levels as a result of bacterial respiration [32]. Although bacteria in the culture of algal assemblage is not always intentional, the inherent contamination could result in enhanced growth conditions for an algal culture.

Cultivation medium is also critical to large-scale algal cultivation systems. The mass production media should be cost effective while providing the major (C, N, P) and minor (Na, K, Ca, Mg, S, Fe, Mo, Sr, Mn, Ba, Zn, and Al) nutrients essential for the microalgae growth [33]. When implementing an PBR in an operating power plant using flue gas as a source of CO_2, other components present in the flue gas, such as sulfur oxides (SO_x), can be introduced into the PBR simultaneously [34]. Although concentrations of such impurities from flue gas are low, they may still impact an algal culture. Thus, the robustness of microalgae is critical to overcome the inhibitory effects of impurities [67].

In addition, the mass production of microalgae and its commercialization are directly related to the operation of PBRs. To maximize and stabilize algal biomass accumulation rate, light cycle (continuous light versus light/dark cycles) and harvesting rate (hydraulic retention time) are two major parameters which must be optimized for continuous, large-scale cultivations. Lighting condition can be controlled relatively easily in PBRs, wherein light limitation can be alleviated and microalgae growth can be enhanced [68]. Harvesting rate is inherently linked with microalgae residence time in PBRs and should be adjusted based on growth rate of the selected microalgae species [35]. Optimization of lighting condition and harvesting rate can be determined using traditional microalgae cultivation metrics, including biomass concentration and biomass productivity.

This study aimed to evaluate the long-term culture of the selected freshwater microalgal assemblage from Great Lakes region in a pilot-scale PBR located in the T.B. Simon Power Plant

(East Lansing, MI) using flue gas as the CO_2 source. Biomass composition (major and minor components of biomass) and biological diversity (relative abundance at different taxa) of the culture, biomass production and algal assemblage stability were investigated under different culture conditions: light cycle, harvesting amount, pH stabilization, and SO_x content in the culture medium. The results were analyzed to obtain an in-depth understanding of a long-term cultivation of an PBR in a power plant.

Materials and methods

Algal assemblage and culture medium

The microalgae *Chlorella sorokiniana MSU* was selected from the Great Lakes region and was stored on Tris-Acetate-Phosphate (TAP) agar medium at room temperature under constant fluorescent light until it was used to seed the algae photobioreactor (PBR) [69]. Modified liquid TAP media (without agar) was used for photoautotrophic cultures. The modified medium contained the following substances: 3.75 mmol/L of NH_4NO_3 or 7.5 mmol/L of NH_4Cl, 0.34 mmol/L of $CaCl_2 \cdot 2H_2O$, 0.4 mmol/L of $MgSO_4 \cdot 7H_2O$, 0.68 mmol/L of K_2HPO_4 (anhydrous), 0.45 mmol/L of KH_2PO_4 (anhydrous), and 0.09 mmol/L $FeCl_3 \cdot 6H_2O$. In the medium, NH_4NO_3 and NH_4Cl were both used as nitrogen sources but were not used simultaneously. When NH_4NO_3 was used in the medium, it acted as the nitrogen source and its ability to independently balance the pH was tested [29]. As a comparison, when NH_4Cl was used as the nitrogen source, NaOH solution (100 g/L) was used for pH stabilization. $FeCl_3 \cdot 6H_2O$ was added to increase cell density and growth rate [70]. The potential effect of sulfur oxides was tested with the addition of SO_2 in the form of Na_2SO_3 at a concentration of 0.23 mmol/L. The stock solutions of nutrients and trace

elements were prepared using deionized water. The water used for the culture was fresh water from the power plant tap. All media, water, and equipment were unsterilized.

Pilot photobioreactor system

The PHYCO$_2$ PBR unit previously installed in the T.B. Simon Power Plant was used in this study (Figure 1). The operating mechanism of the PBR has been previously described [65]. Briefly, the 118 L PBR (100 L working volume) includes a vertical up-tube, helical coil, and light source. A gas sparger at the bottom of the up-tube delivers natural gas fired flue gas to the unit, where medium is driven upward through the up-tube. The medium is then gravitationally circulated back down through the helical coil to the bottom of the PBR and is then pushed vertically upward once again by the gas sparger. The unit was updated with 12, 8-foot LED light bars (Independence LED Lighting LLC, USA) containing forty-four red and twelve blue diodes each. The red and blue diodes provided light at 660 nm and 450 nm, respectively. The LED bars were arranged such that there were 4 equally distributed bars in the center of the coil and 8 around the up-tube, providing a continuous photosynthetic photon flux density (PPFD) of approximately 407 μmol/m^2/s to support algae growth. PPFD was measured using a LI-190R Quantum Sensor paired with a LI-250A light meter (LI-COR, Lincoln, Nebraska). The natural gas fired flue gas, containing 7.2 ± 0.06% v/v of CO_2, and 76.9 ± 0.4 ppmv of NO_x, was directly pumped from the stack into the PBR at a flow rate of 120 L/min. The emissions of CO_2 and NO_x were determined using a continuous emissions monitoring system (CEMS) as regulated by the United States Environmental Protection Agency (EPA).

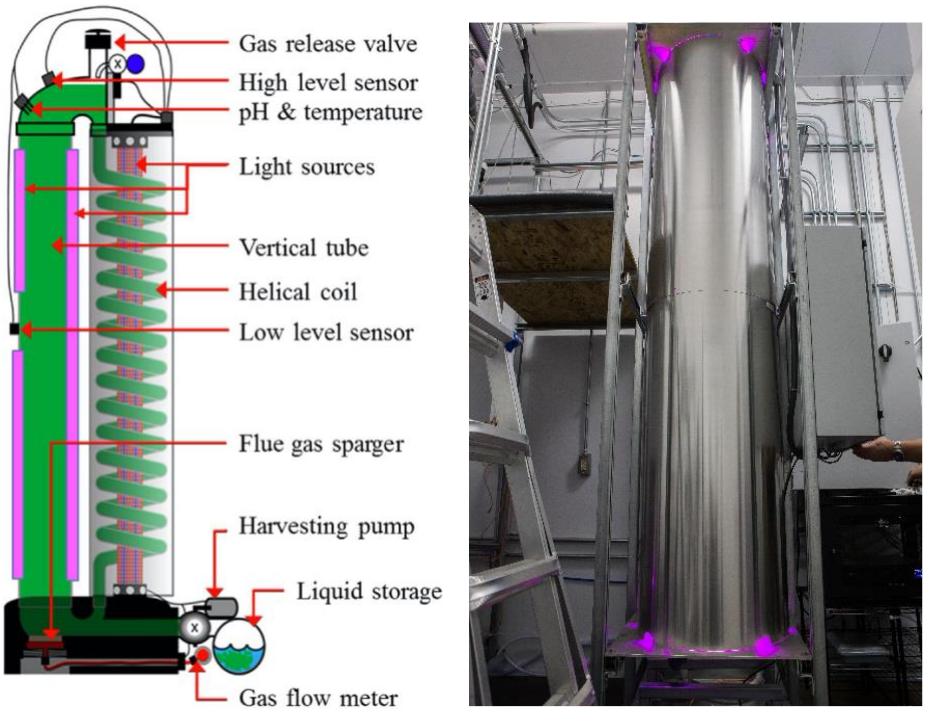

(a) (b)

Figure 1. PHYCO₂ PBR unit [65]. (a) Diagram of the photobioreactor; (b) The photobioreactor at the MSU. T.B. Simon power plant.

Kinetic study of the algal assemblage

Cultivation of the microalgae species for the growth kinetics study was carried out in the PBR unit with inoculum of 1% v/v. The kinetic study was run at 20 ± 2 °C under a continuous light of 407 μmol/m^2/s with flue gas rate of 120 L/min. A total of 18 samples were collected over a period of 5 days, resulting in a total cultivation time of approximately 108 h. Temperature (PHH-257 Micro pH Meter, Omega Engineering™, USA) and pH (Pocket Pro pH, HACH Company, Loveland, Colorado) were monitored daily to ensure stability and thus, proper growth conditions. Nutrient concentrations, biomass concentration, and algal assemblage were monitored during the kinetic study.

Semi-continuous algal cultivation in the pilot photobioreactor

The PBR has been running in a semi-continuous mode since April 2018. Cultivation data was collected from April 2018 to March 2019. The twelve case scenarios in Table 1correspond to optimization tests conducted during this time period. The following cultivation conditions were modified during the study: harvest amount (30%, 40%, 50%, 60%, 70% or 100% of the PBR volume), light cycle (12 h and 24 h illumination), and with and without the addition of NaOH and SO_2. The 100% harvesting amount refers to 50% harvesting performed twice in a 24 h period. Liquid broth was collected daily at the specified amount (30, 40, 50, 60, 70 or 100% v/v). Algal biomass concentrations were left to stabilize for at least 2 days and the data collected from this point on were used for analysis. The culture temperature was kept at 20 ± 2 °C. Fresh water was used to refill the PBR reactor after harvesting and nutrients and trace metals were added according to the modified TAP medium to maintain N/P molar ratio at 6.65. Among the twelve case scenarios, three scenarios (1, 8, and 9) were first selected to study the effects of sulfur supplement and pH adjustment on algae cultivation. Consequently, eleven scenarios (2, 3, 4, 5, 6, 7, 8, 9, 10, 11, and 12) were compared to elucidate the effects of harvesting amount and light cycle on algae cultivation. In addition, data from the eleven scenarios were also used to study the effects of cultivation on the stability of algae assemblage.

Table 1. Twelve case scenarios during the test period.

Scenarios	**Harvesting amount (L/day)**	**Sulfur supplement [a]**	**Light cycle [b]**	**pH stabilization [c]**	**Data collection period**
1[d]	30	No	No	NaOH	April 12 – April 20, 2018
2	50	No	No	NaOH	May 9 – May 20, 2018
3	100	No	No	NaOH	May 26 – June 15, 2018
4	50	Yes	No	NaOH	June 16 – July 5, 2018
5	60	Yes	No	NH_4NO_3	July 6 – August 6, 2018
6	70	Yes	No	NH_4NO_3	August 10 – September 5, 2018
7	30	Yes	Yes	NH_4NO_3	September 25 – October 31, 2018

Table 1 (cont'd)

8	30	Yes	No	NH_4NO_3	November 4 – November 17, 2018
9	30	No	No	NH_4NO_3	November 21 – December 10, 2018
10	50	No	Yes	NH_4NO_3	December 14 – December 30, 2018
11	40	No	Yes	NH_4NO_3	January 5 – January 20, 2019
12	40	Yes	Yes	NH_4NO_3	January 25 – March 9, 2019

a. 15-20 mg/L Na2SO3 were maintained in the cultivation medium for the "Yes" sulfur supplement.
b. The "Yes" light cycle was run on 12-hour light on and 12-hour light off. The "No" light cycle was run on 24-hour light on.
c. pH stabilization of "NaOH" was that NaOH was used to adjust pH and NH4Cl was used as the nitrogen source. pH stabilization of "NH4NO3" was that NH4NO3 was used for both pH adjustment and nitrogen source.
d. The culture was from a pre-test before the long-term continuous cultivation.

Chemical analysis

Samples were analyzed for dry biomass weight, pH and nutrient (total nitrogen (TN), total phosphorus (TP), nitrate (NO_3-N) and ammonia (NH_3-N)) concentrations. Consumption data is calculated as the difference in nutrients over 24 h using concentration data measured before and after harvesting. Algal biomass was concentrated for dry weight measurement using a Thermo Electron Corporation IEC Centra CL2 Centrifuge at 3800 rpm for 5 m. Biomass was washed once and resuspended using deionized water, and then dried at 105°C for 24 hours. Sample pH was measured using a pH meter (Fisherbrand™ accumet™ AB15 + Basic, Fisher Scientific Co., Pittsburgh, PA). Nutrient concentrations were tested in the liquid supernatant using nutrient test kits (HACH Company, Loveland, Colorado) equivalent to EPA methods [71]. Algal biomass composition was analyzed using the standard forage analysis method [72].

Microbial analysis

DNA extraction

Samples (1 mL) collected for DNA analysis were kept frozen at -20°C until their use. To remove nutrient media, algae sample was centrifuged using an Eppendorf 5416R centrifuge at 10,000 rpm for 5 min and the supernatant was discarded. The remaining pellet was used for

DNA extraction using the DNeasy® PowerSoil® Kit (Qiagen, Germany). DNA was eluted with 100 μL of 10 mM Tris-HCl (pH 8.5) and the concentration and purity determined using a NanoDrop Lite spectrophotometer (Thermo Fisher Scientific, USA). The DNA extracts were stored at -80°C and then used for polymerase chain reaction (PCR) and Illumina DNA sequencing.

Illumina preparation and sequencing

Illumina sequencing was performed for the 16S rRNA gene region to assess the bacterial community. Prior to PCR, extracted DNA samples were diluted 10x due to high DNA concentrations. The PCR conditions were as follows: 1.0 mL DNA template (10x diluted), 0.5 mL of 100 mM forward primer (IDT, Pro341F 5'-CCTACGGGNBGCASCAG-3'), 0.5 mL of 100 mM reverse primer (IDT, Pro805R 3'-GACTACNVGGGTATCTAATCC-5'), 12.5 mL 2x Supermix (Invitrogen, USA), and 10.5 mL PCR grade water. The PCR program used for all assays is as follows: 96°C for 2 min, followed by 30 cycles of 95°C for 20 s, 52°C for 30 s, and 72°C for 1 min, and a final elongation period of 72°C for 10 min. After PCR, samples were diluted to normalize DNA concentrations within a range of 5-10 ng mL^{-1}. DNA concentration was determined using the PicoGreen dsDNA quantitation assay (Invitrogen, USA) and Fluostar Optima microplate reader (BMG Labtech, Germany). The PicoGreen conditions were as follows: 95 mL 1x TE buffer solution, 100 mL 1:200 diluted PicoGreen reagent, 5 mL DNA template. Samples with known DNA concentrations were also prepared for standard curve generation. The normalized PCR products were then sequenced at the Michigan State University (MSU) Research Technology Support Facility (RTSF). Illumina MiSeq (pair-end 250 bp) targeting on V3_V4 hypervariable regions was used to carry out the sequencing. Fastq files from the high-

throughput sequencing were analyzed using QIIME2 database to generate the taxonomic and phylogenetic data for statistical analysis [73].

Statistical analysis

All data collected were analyzed using the statistical tools of R (version 3.6.3). In order to determine whether a parametric or non-parametric test was necessary, the data were first tested for normality and equal variance using a Shapiro-Wilk's test and an F-test, respectively. Those data that were normal with equal variance were tested using a one-way analysis of variance (ANOVA) and a Tukey test was used when applicable to compare individual factors. Data with non-normal distribution and unequal variance were tested using the Kruskal-Wallis test by ranks. All tests were performed with a significance value of α=0.05. Microbial community analysis was completed using Vegan, ggplot2, phyloseq, and MASS R libraries. Taxonomic/phylogenetic data was analyzed in order to graph relative abundances of algae and bacteria in the sample.

Results and discussion

Kinetics of the algal assemblage

The growth kinetics of algal assemblage is important to determine harvesting rate, which inherently controls substrate loading rate and pH stability, under the fixed CO_2 (g) and light supply. The kinetics of algae growth has been studied in the PBR (100 L) operated in a batch mode. During the 108-hour cultivation, 18 samples were taken in order to monitor biomass concentration (g dry weight algae/L), nutrient concentration and pH were monitored. The initial concentration of microalgae in PBR was 0.081 g/L after adding a 1% v/v inoculum. The results from the measurements during the kinetics study are depicted in Figure 2 (a, b, c, and d). In

addition, the changes in relative abundance of microbial communities in PBR over the course growth kinetics experiment are shown at domain, phylum, and class levels in Figure 3

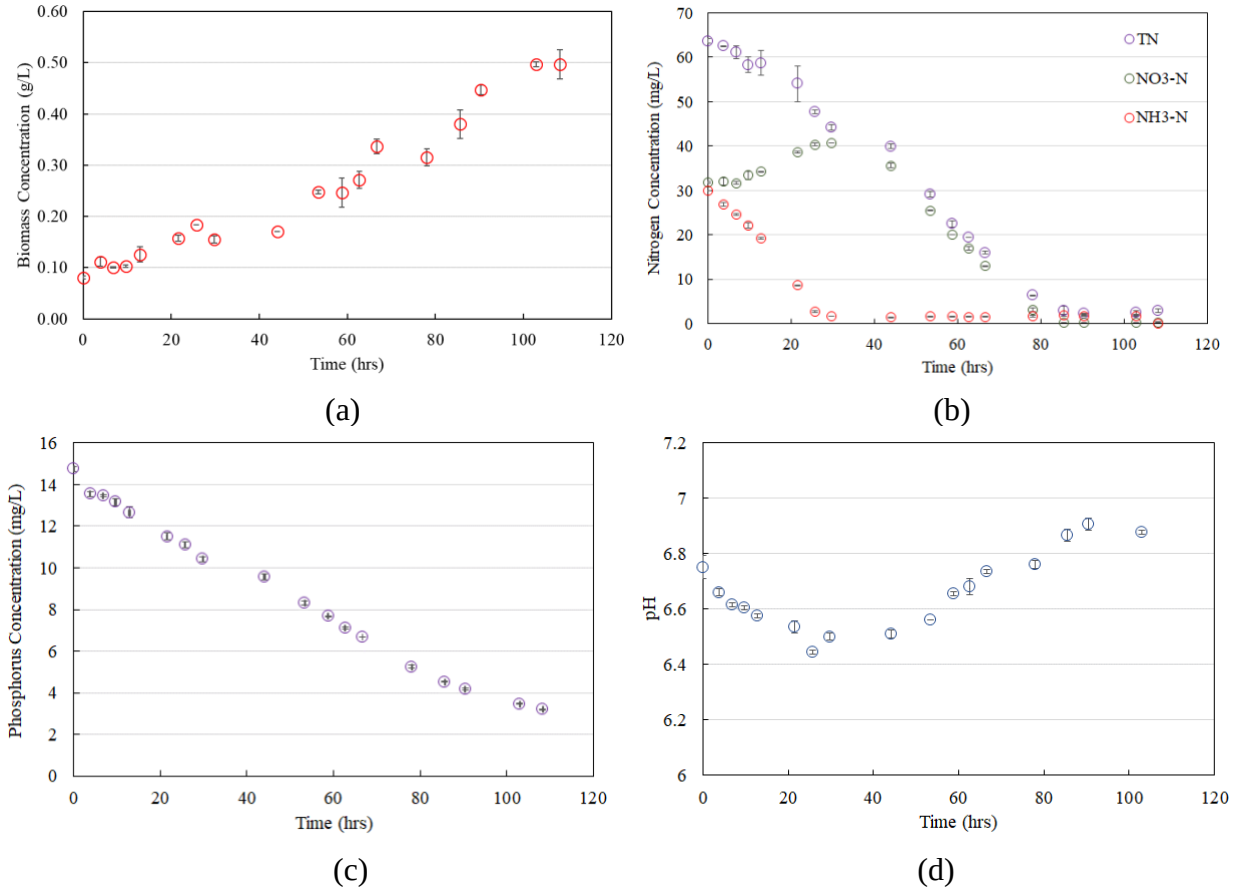

Figure 2. Kinetics of the algal assemblage growth in the pilot unit. (a) Biomass concentration; (b) TN, NH3-N, and NO3-N concentrations; (c) PO4-P concentration; (d) pH. Data are the mean of two replicates with standard deviation.

Biomass concentration increased from 0.081 g/L to 0.500 g/L over the course of the experiment (Figure 2a). The observed increase in dry biomass correlates with TN and TP uptake as shown in Figure 2b and c, respectively, indicating none was limiting the growth at 7.5% CO_2 (g). The nutrient concentrations were measured as 2.88 ± 0.37 mg N/L and 3.2 ± 0.04 mg P/L at the end of kinetics study. The observed increase in dry biomass concentration in PBR can be modeled as the log (exponential) growth (1^{st} order) since there are no limiting nutrients and CO_2 was supplied continuously. The equation for the log phase growth is as follows, where $\frac{dX}{dt}=$

growth rate of algae assemblage (g/L/hr), X=concentration of dry biomass (g/L), and μ=specific growth rate constant (hr^{-1}) [74]:

$$\frac{dX}{dt} = \mu X \qquad \textit{Equation 1}$$

The Matlab® curve fitting toolbox was used to calculate the specific growth rate constants (μ) of the algal assemblage based on the $dXdt = \mu X$ Equation 1 and the data in Figure 2a. The overall specific growth rate constant was 0.01782/hr (0.43/day) with R^2 = 0.9408, which is similar to growth rate constants observed in a range of 0.2-0.9/day in autotrophic, heterotrophic, and mixotrophic algae cultivation studies [75]. A closer examination of changes in biomass concentration over time reveals that there are potentially two different growth rates. These growth rates correspond to the use of NH_4-N (between 0 and 30 hr) and NO_3-N (between 40 and 108 hr) as a nitrogen source by the algal culture (Figure 2a and b). The growth rate constant when NH_4-N consumption was dominant was higher (0.53/day, R^2 = 0.8294) than the growth rate when NO_3-N consumption took over (0.34/day, R^2 = 0.9364). This is an expected result as NH_4-N can be used directly as the nitrogen source, where NO_3-N must first be reduced to NH_4-N in order to be assimilated by the algal culture [76]. Despite this difference in growth rate, using NH_4-N as the sole nitrogen source is undesirable since it will decrease the pH over time and put the culture stability at risk (Figure 2d).

Different consumption patterns of NH_4^+ and NO_3^- also enlightened that both forms of nitrogen can be used to stabilize the pH without the use of acid/base. Analysis of Figure 2b and d detail the relationship between nitrogen consumption and pH stabilization. Figure 2b shows that NH_4-N was first to be consumed, followed by NO_3-N approximately 40 hours after inoculation. The consumption pattern of NH_4-N and NO_3-N helped to maintain the pH above 6.5 (Figure 2d). At hour 40, the pH begins to recover from its initial decrease. This increase in pH, from hour 40

until approximately hour 90, corresponds to the decrease in NO_3-N concentration during the same period (Figure 2d). Thus, it is confirmed that NH_4NO_3 is an effective pH stabilization agent to prevent the low pH inhibition in addition to providing sufficient nitrogen for algal growth.

DNAs from all 18 samples collected during the 5-day period were extracted to determine the bacterial-algal assemblage. The results from amplicon sequencing show a high abundance of cyanobacteria, which is known to have 85-93% of 16s rRNA gene sequence similarity with *C. sorokiniana* [77]. Microscopic imaging analysis of the samples did not indicate the presence of cyanobacteria, which are characterized by blue-green color and various shape and size, unlike *C. sorokiniana* [78]. Thus, the cyanobacteria sequence was interpreted as microalga *C. sorokiniana* for all samples.

The relative abundance (ratio of frequency of a gene or a group of genes to total frequency of all genes in a community) was first determined at the domain and phylum levels. The dominating domain and phylum are Eukarya and Chlorophyta, which correspond to the *C. sorokiniana* inoculum (Figure 3a and b) [77]. This is complemented by a relatively stable bacterial abundance. However, at the phylum and class level, there are changes in the relative abundance of certain bacteria.

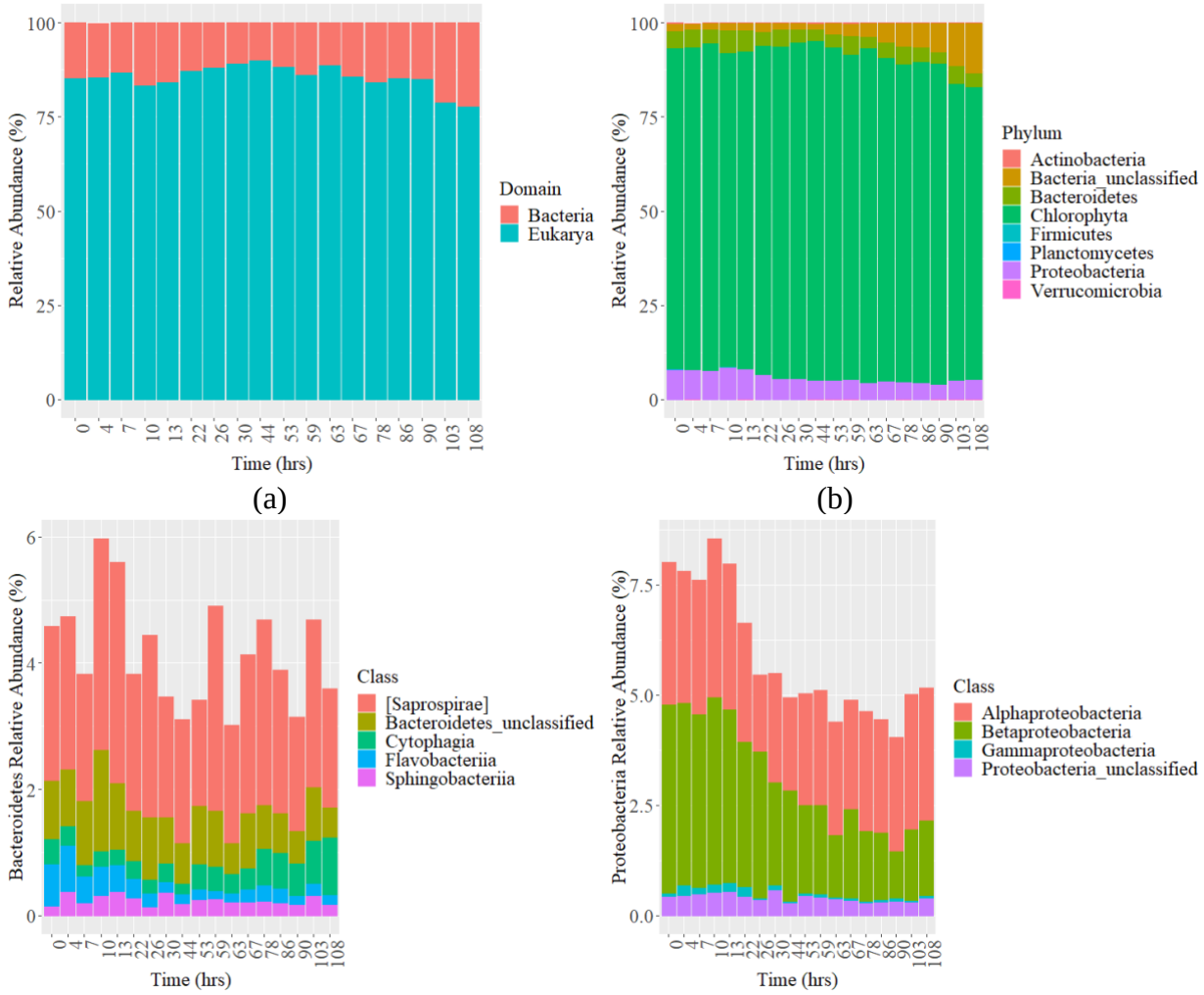

Figure 3. Relative abundance of microbial communities in the algal assemblage during the kinetic study. (a). Relative abundance at the domain level; (b). Relative abundance at the phylum level; (c). Bacteroidetes relative abundance at the class level; (d). Proteobacteria relative abundance at the class level. Relative abundance data are from a sample at each time point during the kinetics study.

Proteobacteria and *Bacteroidetes* are the dominating bacterial phyla in the microalgae co-culture system (Figure 3b). This is consistent with literature on large-scale microalgae cultivation systems [79]. At the class level, communities within the *Bacteroidetes* phylum remained stable throughout the kinetics study (Figure 3c), while communities within *Proteobacteria* changed over increasing time (Figure 3d). Many species belonging to the β subdivision of *Proteobacteria* (*Nitrosomonas, Nitrosospira, Nitrococcus*) are ammonium oxidizing bacteria (AOB), capable of

oxidizing ammonium to nitrite, and their prevalence in NH_4^+ rich culture medium is expected, especially in freshwater systems [80-82]. The relative abundance of *Betaproteobacteria* decreased as algal assemblage growth continued exponentially (Figure 3d). The observed population dynamics of *Betaproteobacteria* follow a trend similar to NH_4^+ concentration (Figure 2b), addressing their role as AOB in the PBR. On the other hand, certain species of the α subdivision of *Proteobacteria*, such as those in the Nitrobacter genus, are able to oxidize nitrite to nitrate and are therefore referred to as nitrite oxidizing bacteria (NOB) [83]. During the first 30 hours of growth, *Alphaproteobacteria* abundance was stable and ammonia was still present within the system, however, increasing NO_3^- levels were observed (Figure 2b). This observation confirms the role of the *Alphaproteobacteria* as NOB in the algal-bacterial assemblage. Another noteworthy observation regarding the presence of *Alphaproteobacteria*, is their ability to non-photoautotrophically fix nitrogen (N_2 (g)) in symbiosis with plants [84-86]. The significant, and stable, relative abundance of *Alphaproteobacteria* may indicate an established mechanism to use N_2 (g) as a nutrient in microalgae growth reactors, which needs to be further studied. Overall, microbial community analysis suggests that *Proteobacteria* played an important role in nitrification and fixation within the algal assemblage, thus influencing nitrogen consumption and pH patterns of the cultivation.

Effects of culture conditions on algal biomass accumulation and nutrient consumption

Figure 4 shows all the data that was collected from April 2018 to March 2019. Figure 4a and c indicate both biomass concentration and total phosphorous concentration respond to the changes introduced during the different case scenarios. Figure 4b and d show the stability of total nitrogen concentration and pH throughout the year-long study.

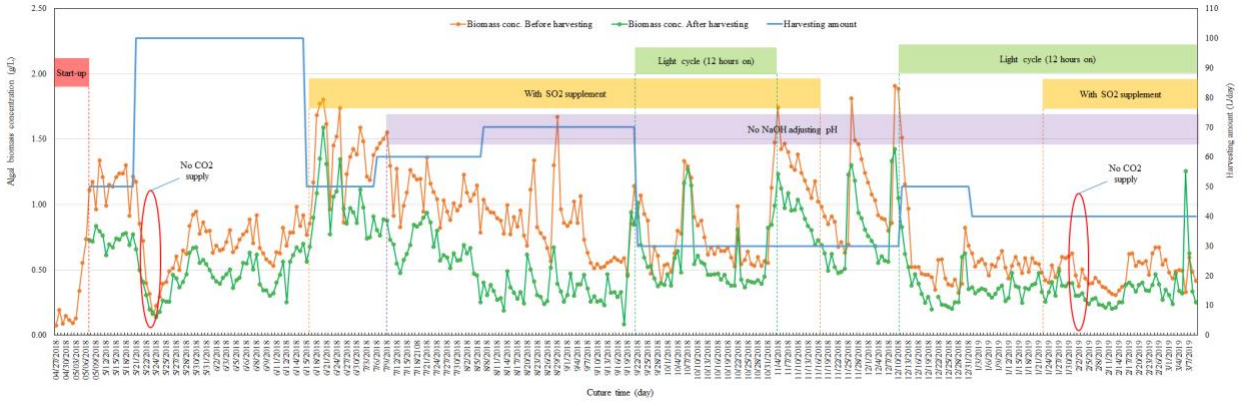

(a)

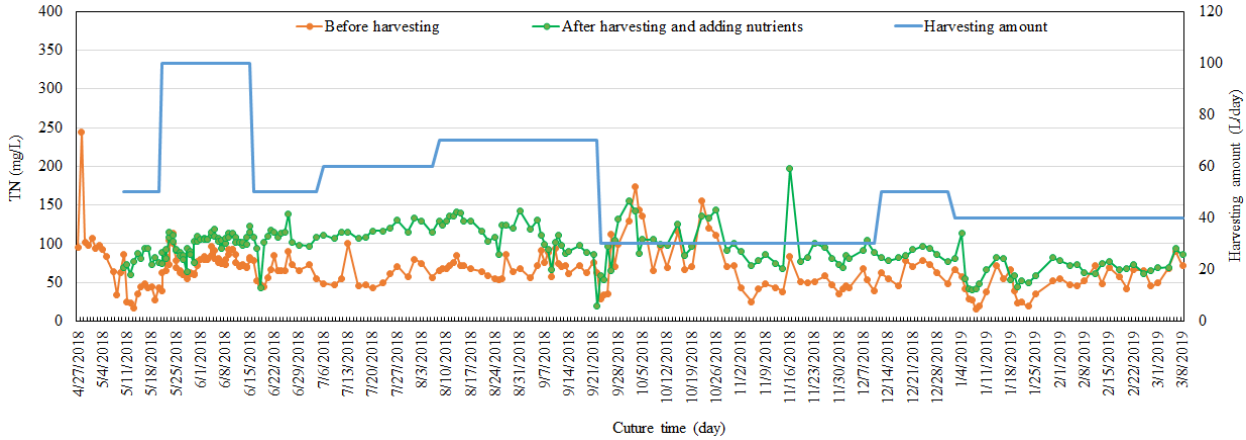

(b)

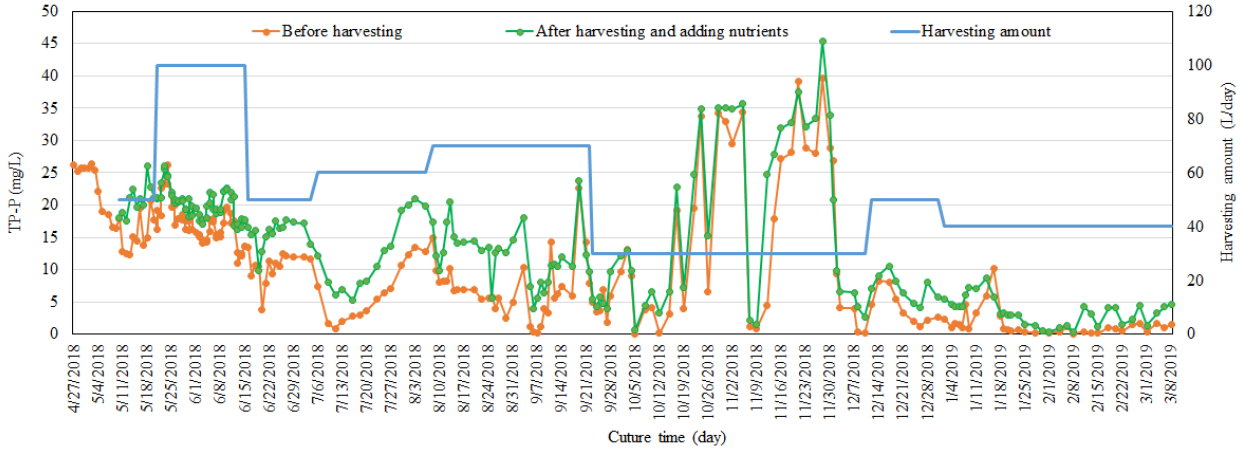

(c)

Figure 4. Long-term algal cultivation on the flue gas from a power plant. (a). Biomass concentration before and after harvesting and operational conditions; (b). TN content in the medium before and after harvesting (adding the nutrient after harvesting): (c). TP content in the medium before and after harvesting; (d). pH of the medium before and after harvesting. Data are the mean of two technical replicates.

Figure 4 (cont'd)

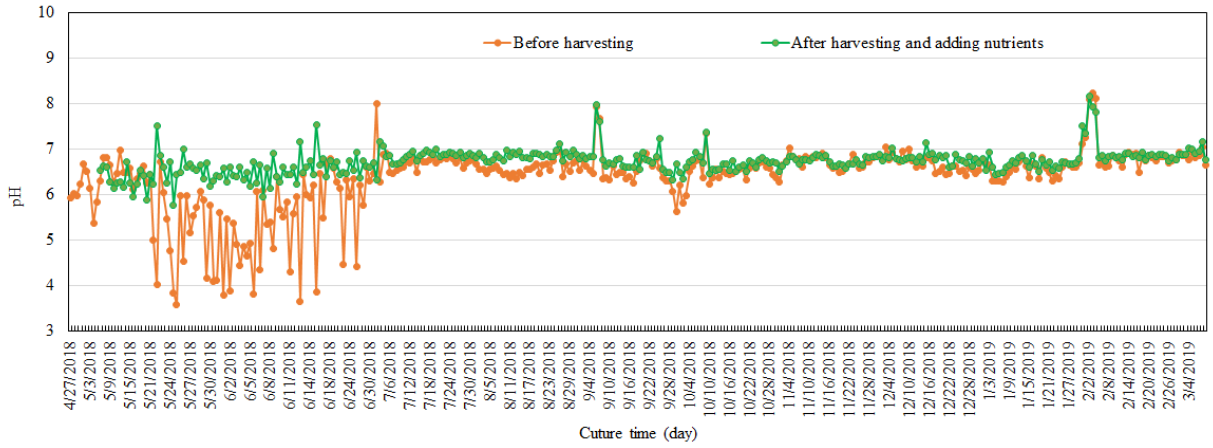

(d)

Effects of sulfur addition and pH stabilization

Case scenarios (1, 8, 9) were used to demonstrate the effects of sulfur addition and pH stabilization on the algal biomass production and nutrient consumption (Table 2). Figures corresponding to Table 2 can be found in Appendix B (Figure 28, Figure 29).

Table 2. Effects of sulfur addition and pH stabilization on cultivation parameters.

Factors and levels		Sulfur addition		pH stabilization	
		Yes [a]	No [b]	NaOH [c]	NH_4NO_3 [d]
Biomass concentration	Biomass concentration (g/L)	1.22±0.17	1.10±0.33	1.05±0.20	1.10±0.33
	Influence on biomass concentration	P=0.433		P=0.655	
Biomass productivity	Biomass productivity (g/L/day)	0.29±0.02	0.34±0.08	0.31±0.08	0.33±0.08
	Influence on biomass productivity	P=0.061		P=0.556	
pH	pH	6.81±0.08	6.81±0.15	6.62±0.10	6.81±0.15
	Influence on pH	P=0.920		P=0.005	
TN consumed	TN consumed (mg/L)	36.38±6.51	37.09±8.47	27.59±6.68	37.09±8.47
	Influence on TN consumed	P=0.873		P=0.387	
TP consumed	TP consumed (mg/L)	3.50±3.97	3.50±1.72	3.06±2.43	3.50±1.72
	Influence on TP consumed	P=0.999		P=0.672	

a. Data are reported as the mean of 6 replicates with standard deviation.
b. Data are reported as the mean of 9 replicates with standard deviation.
c. Data are reported as the mean of 9 replicates with standard deviation.

Table 2 (cont'd)

d. Data are reported as the mean of 10 replicates with standard deviation.

Sulfur addition was achieved by supplementing sodium sulfite (Na_2SO_3) in the culture medium, since SO_2, the most dominant and harmful form of sulfur oxide in flue gas, is soluble in water and forms sulfite under alkaline conditions [87]. To determine the cultures response to sulfur addition, the sulfur content in the algal biomass (% w/w) was measured during each case scenario (Table 31). Under the condition of no light-cycle, average sulfur content of the algal biomass with sulfur addition (0.54 ± 0.06%) is slightly higher than the average sulfur content without sulfur supplement (0.50 ± 0.03%), which shows capability of the algal assemblage to utilize sulfur originating from the supplemented SO_2. However, the sulfur addition had no significant impact on the biomass concentration or stability of the culture (Table 2). These results indicate that the studied algal assemblage cultured in the PBR is able to capture CO_2 without adverse effects from potential SO_2 present in flue gas.

When comparing pH stabilization of the culture using NaOH or NH_4NO_3, pH was the only parameter among the five (biomass concentration, biomass productivity, pH, TN consumed, and TP consumed) that was significantly ($P = 0.005$) influenced. This is an expected outcome and is a result of the mechanism through which each chemical stabilizes the pH. As seen in Figure 2b and d, NH_4NO_3 does not force an immediate pH change but gradually shifts the pH as a result of algal metabolism of nitrogen. On the other hand, NaOH forced pH change via acid-base chemistry. Although NaOH and NH_4NO_3 had a significant impact on pH, both chemicals were able to maintain a desirable pH range of 6-7.5 for *C. sorokiniana* growth. This result indicates that NH_4NO_3 can be used to replace NaOH and stabilize pH of the algal cultivation. In addition, the lack of significance of the pH stabilization on all other parameters indicates that NH_4NO_3 can effectively stabilize the culture pH while not significantly impacting any other growth outcomes.

Effects of harvesting amount and light-cycle

Figure 5 compares the effects of different harvesting amounts on the five cultivation parameters. In addition, the effects of a 12-hour light-cycle can be seen across three harvesting amounts (30%, 40% and 50%). To determine the effects of different culture conditions on the cultivation parameters, three comparisons were made: different harvesting amounts with no light cycle, different harvesting amounts with light cycle, and matching harvesting amounts with light-cycle and without light-cycle. A complete summary of the statistical analysis is presented in Table 28, Table 29, and Table 30 in Appendix B.

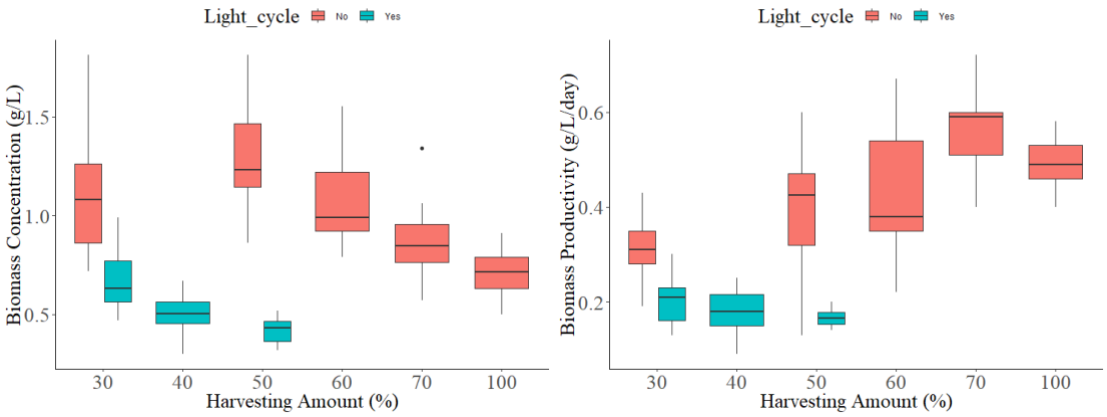

(a) (b)

Figure 5. Effects of harvesting amount and light cycle on algal cultivation. (a). Biomass concentration; (b). Biomass productivity; (c). pH; (d). TN consumed; (e). TP consumed.*

Figure 5 (cont'd)

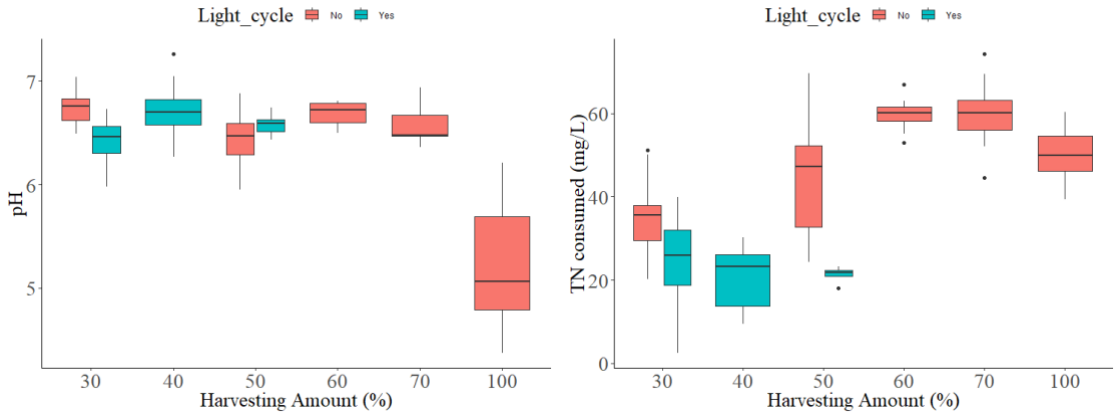

(c)

(d)

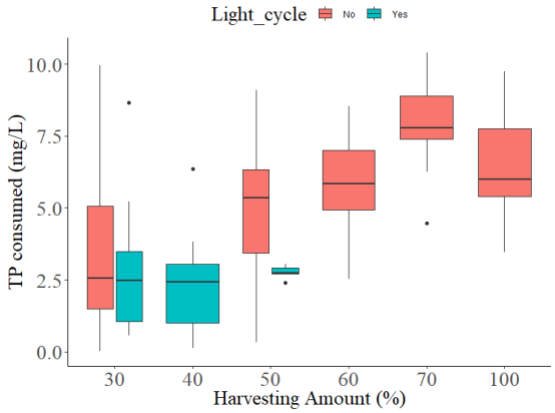

(e)

*: Data for 30% harvesting amount and light cycle off are the mean of 25 replicates with standard deviation. Data for 30% harvesting amount and light cycle on are the mean of 18 replicates with standard deviation. Data for 40% harvesting amount and light cycle on are the mean of 27 replicates with standard deviation. Data for 50% harvesting amount and light cycle off are the mean of 25 replicates with standard deviation. Data for 50% harvesting amount and light cycle on are the mean of 7 replicates with standard deviation. Data for 60% harvesting amount and light cycle off are the mean of 14 replicates with standard deviation. Data for 70% harvesting amount and light cycle off are the mean of 15 replicates with standard deviation. Data for 100% harvesting amount and light cycle off are the mean of 20 replicates with standard deviation.

Statistical analysis of the data collected under no light-cycle condition was applied such that all harvesting amounts were compared pairwise. A collection of 10 comparisons are presented in Table 28 in Appendix B. The harvesting amounts of 30%, 50%, and 60% had biomass concentrations of 1.11 ± 0.26, 1.28 ± 0.28, and 1.07 ± 0.23 g/L, respectively (Figure 5a) and a pair-wise comparison concluded that there were no significant ($P > 0.05$) differences between the three harvesting amounts. However, these three harvesting amounts had significantly ($P < 0.05$)

higher biomass concentrations than the harvesting amounts of 70% and 100% (0.86 ± 0.12 and 0.72 ± 0.12 g/L). As for the biomass productivity, the harvesting amount of 70% showed the best performance at 0.56 ± 0.09 g/L/day (Figure 5b), with significant ($P < 0.05$) differences from the harvesting amounts of 30%, 50%, and 100%. Biomass productivity of the harvesting amount of 60% (0.43 ± 0.14 g/L/day) showed no significant differences ($P > 0.05$) from the harvesting amounts of 50%, 70%, and 100%, likely due to its large standard deviation. Generally, with increasing harvesting amount, biomass concentration decreased and biomass productivity increased. For example, a 70% harvesting amount resulted in the highest productivity but led to one of the lowest biomass concentrations when compared to 30%, 50%, and 60%. When the culture is diluted to a higher degree (70% harvested versus 30% harvested), it is able to respond with a higher productivity level but it is unable to regrow and replenish to a high biomass concentration.

As for pH, the harvesting amounts of 30%, 50%, 60%, and 70% were in a narrow range around 6.7 even though most of them had significant ($P < 0.05$) differences between each other except two pairs of 30%/60% and 50%/70% (Figure 5c). The harvesting amount of 100% had the lowest pH of 5.20 ± 0.55, which was significantly ($P < 0.05$) different from all other harvesting amounts. TN and TP consumption further show the effects of different harvesting amounts on the cultivation. The harvesting amounts of 60% and 70% had similar ($P > 0.05$) TN consumption (59.80 ± 3.64 and 60.02 ± 7.29 g/L/day, respectively), which were significantly ($P < 0.05$) higher than other harvesting amounts (Figure 5d). The harvesting amount of 70% had the highest TP consumption of 7.99 ± 1.51 g/L/day, which are significantly ($P < 0.05$) different from other harvesting amounts except 100%. The harvesting amounts of 50%, 60%, and 100% had TP

consumption of 5.03 ± 2.19, 5.88 ± 1.58, and 6.50 ± 1.85 mg/L/day, respectively, with no significant ($P > 0.05$) difference among each other.

When comparing all harvesting amounts with a 12-hour on/off light-cycle, there were significant ($P < 0.05$) differences in biomass concentration when comparing 30% harvesting to 40% and 50%, where 30% harvesting resulted in a higher biomass concentration (0.67 ± 0.14 g/L) (Figure 5 and Table 29). Biomass productivity of the three harvesting amounts (30%, 40%, and 50%) were 0.20 ± 0.05, 0.18 ± 0.05, and 0.17 ± 0.02 g/L/day respectively (Figure 5), none of which were significantly ($P > 0.05$) different from each other. In addition, pH of the three harvesting amounts were in a narrow range around 6.5. Nutrient consumptions (TN and TP) were not significantly ($P > 0.05$) different among the three harvesting amounts (30%, 40% and 50%). Unlike the results when no light-cycle condition was applied, the biomass productivity remained fairly stable across the three harvesting amounts, indicating biomass productivity is limited by light exposure. This can be confirmed in current literature, where *C. sorokiniana* showed decreased specific growth rates with intermittent lighting [88]. Lower growth rates and productivity are thought to be a result of inability to store ample light energy to maintain productivity and respiration losses during subsequent dark periods. These statistics confirm that, although there were significant differences in biomass concentration, the algae maintained consistent productivity and nutrient consumption across different harvesting amounts under a 12-hour on/off light-cycle.

The analysis comparing light cycle to no light cycle confirms that the 12-hour light-cycle has significant ($P < 0.05$) effects on all factors measured, and led to inferior cultivation performance (Figure 5 and Table 30). The only exception is TP consumption for 30% harvesting; there is no significance for this factor when comparing light cycle to no light cycle for the same harvesting

amount (P = 0.470). This may be a result of the spread of the data (30% average = 2.74 ± 2.01, 40% average = 3.34 ± 2.48) and its non-normal distribution.

Overall, the harvesting amount of 60% with no light-cycle proved to be the preferred operational conditions, resulting in the highest average biomass concentration, sustainable pH levels and good nutrient consumption. With an average biomass concentration of 1.07 ± 0.23 g/L, 60% harvesting results in a starting concentration of approximately 0.64 g/L. The increase of approximately 0.43 g/L/day reflects the calculated growth rate constant of 0.43/day.

Effects of cultivation conditions on algal biomass composition

Microalgae can adapt to cultivation conditions with varying nutrient concentrations, light intensity, and duration [89]. This behavior is reflected in the composition of microalgal biomass at the elemental (C, H, N, P, S) and macromolecular (carbohydrates, protein, lipid) levels. Elemental analysis of microalgal biomass collected during individual case scenarios tested in this study was conducted to show changes in biomass composition between different culture conditions (Table 31). The statistical analysis concluded that there was not a significant (P > 0.05) variance in the composition of biomass in terms of their C, H, N, S, and P contents (% dry matter). This confirms the robustness of algae assemblage and demonstrates its ability to adapt to different cultivation conditions. The average contents of elements are given in Table 3 along with coefficient of variation (COV) values. Major elements in the algae assemblage are measured as C (48.4%), H (7.29%), and N (9.08%), with S and P contents in trace amounts. The slightly higher COV values (greater than 0.10) for S and P contents of the biomass were attributed to their low concentrations resulting in higher variance in measurements. This composition is typical for chlorophyte alga, such as *Chlorella* species that are composed of 44.33%, 7.09%, 8.53%, 0.84% dry matter of C, H, N, and S respectively [90].

Table 3. Element contents of algal biomass and corresponding coefficients of variation [a,b,c].

	C (% dry matter)	H (% dry matter)	N (% dry matter)	S (% dry matter)	P (% dry matter)
Algal biomass	48.40±1.56	7.29±0.15	9.08±0.42	0.56±0.09	1.53±0.21
Coefficient of variation [b]	0.03	0.02	0.05	0.15	0.13

a. Element contents of individual algal biomass under different cultivation conditions are listed in Table 31.
b. Element contents are reported as the mean of 15 replicates with standard deviation.
c. Coefficient of variation is the ratio of the standard deviation to the mean. It shows the extent of variability regarding the mean of the sample population.

There are four major types of biochemical molecules in microalgae: carbohydrates, proteins, lipids and nucleic acids [91]. Nucleic acids make up a relatively small amount of the total biomass and were thus excluded from the biochemical analysis in this study. Carbohydrate, protein, and lipid contents of the algae assemblage cultivated in NH_4NO_3 containing culture media without S are listed in Table 4 under the operation conditions of 50% harvesting amount and no light-cycle. The Chlorophyte alga has been reported as a rich source of protein, between 40% to 51.45%, which agrees with the results obtained in this study [39, 40]. The protein content (58.60% dry matter) was much higher than that of carbohydrates (19.70%) and lipids (9.70%) of dry algal biomass.

Table 4. Macromolecules in algal biomass [a,c].

	Carbohydrate [b] (% dry matter)	Lipid (% dry matter)	Protein (% dry matter)	Ash (% dry matter)
Algal biomass	19.5±2.44	9.70±1.68	58.60±2.41	12.20±1.52

a. The data is from the cultivation with 50% harvesting amount, NH_4NO_3 as pH stabilization, light-cycle off, and no sulfur addition.
b. Carbohydrates includes NFC (non-fiber carbohydrate) and NDF (neutral detergent fiber), i.e. lignin, hemicellulose and cellulose.
c. Data are reported as the mean of 3 replicates with standard deviation.

Changes of microbial communities during the long-term algal cultivation

Microbial community analysis was also conducted on the eleven samples (scenarios 2, 3, 4, 5, 6, 7, 8, 9, 10, 11 and 12) to elucidate the interaction between algae and bacteria during different operational conditions. The dataset of 16S rRNA gene sequences was rarified at 25,000

reads. The rarefaction analysis indicates sufficient sample coverage (Figure 30a). A rank abundance curve with a relatively gentle slope between 10 and 160 species shows that the gene sequences were evenly distributed (Figure 30b). Shannon's (H) and Pielou's (J) indices were determined to assess alpha-diversity and evenness, respectively, within the microbial community of the case scenarios (Table 32). Microbial communities were stable within samples, as harvesting amount, SO_2 supplement, light cycle and pH stabilization did not significantly ($P > 0.05$) affect alpha-diversity or evenness ($P > 0.05$) (Table 5). However, light cycle and pH stabilization were shown to significantly ($P < 0.05$) affect beta-diversity, which is an indicator of microbial community differences between samples (Table 6). Light-cycle had a significant effect on biomass accumulation and may have created an opportunity for the microbial component of the assemblage to flourish. In addition, different methods of pH stabilization, and consequently nitrogen sources, may have influenced microbial growth. Other factors (harvesting amount and SO_2 supplement) showed no effect ($P > 0.05$) on beta-diversity.

Table 5. One-way analysis of variance of harvesting amount, SO_2 supplement, light cycle, and pH stabilization on alpha-diversity and evenness of microbial communities.

Parameter	Statistic	Harvesting amount	SO_2 supplement	Light cycle	pH stabilization
H [a]	Degree of freedom	4	1	1	1
	Sum squared	0.0896	0.0267	0.0082	0.0052
	P	0.34	0.254	0.542	0.627
J [b]	Degree of freedom	4	1	1	1
	Sum squared	0.00756	0.00258	0.00038	0.00188
	P	0.502	0.27	0.684	0.353

a. H: Shannon's index which indicates the diversity of the microbial community.
b. J: Pielou's index which indicates the evenness of the microbial community.

Table 6. Permutational analysis of variance of harvesting amount, SO_2 supplement, light cycle, and pH stabilization on beta-diversity of microbial communities.

Parameter	Statistic	Harvesting amount	SO_2 supplement	Light cycle	pH stabilization
Beta-diversity	Degree of freedom	4	1	1	1
	Sum squared	0.16619	0.01622	0.1098	0.14096

Table 6 (cont'd)

Beta-diversity	P	0.34	0.7811	0.04478	0.01493

The average relative abundances of algae and bacteria at the domain level were 88 ± 4% and 12 ± 4%, respectively, with no significant ($P > 0.05$) differences between individual case scenarios at either the domain or phylum level (Figure 6a and b). The result demonstrates the robustness of *C. sorokiniana* over a wide range of culturing conditions. However, several bacterial communities (Betaproteobacteria and Alphaproteobacteria) were significantly ($P < 0.05$) affected by culture condition at the class level (Figure 6c). Light-cycle significantly affected several microbial classes within the Proteobacteria phylum. The Proteobacteria phylum is a large and physiologically diverse group and includes many phototrophic bacteria [92]. Both Alphaproteobacteria and Betaproteobacteria classes were affected by light-cycle conditions. Although, whereas Alphaproteobacteria comprise numerous phototrophic genera, Betaproteobacteria is composed of many chemolithotrophic genera, which may better suit Betaproteobacteria for survival under periods of darkness [93].

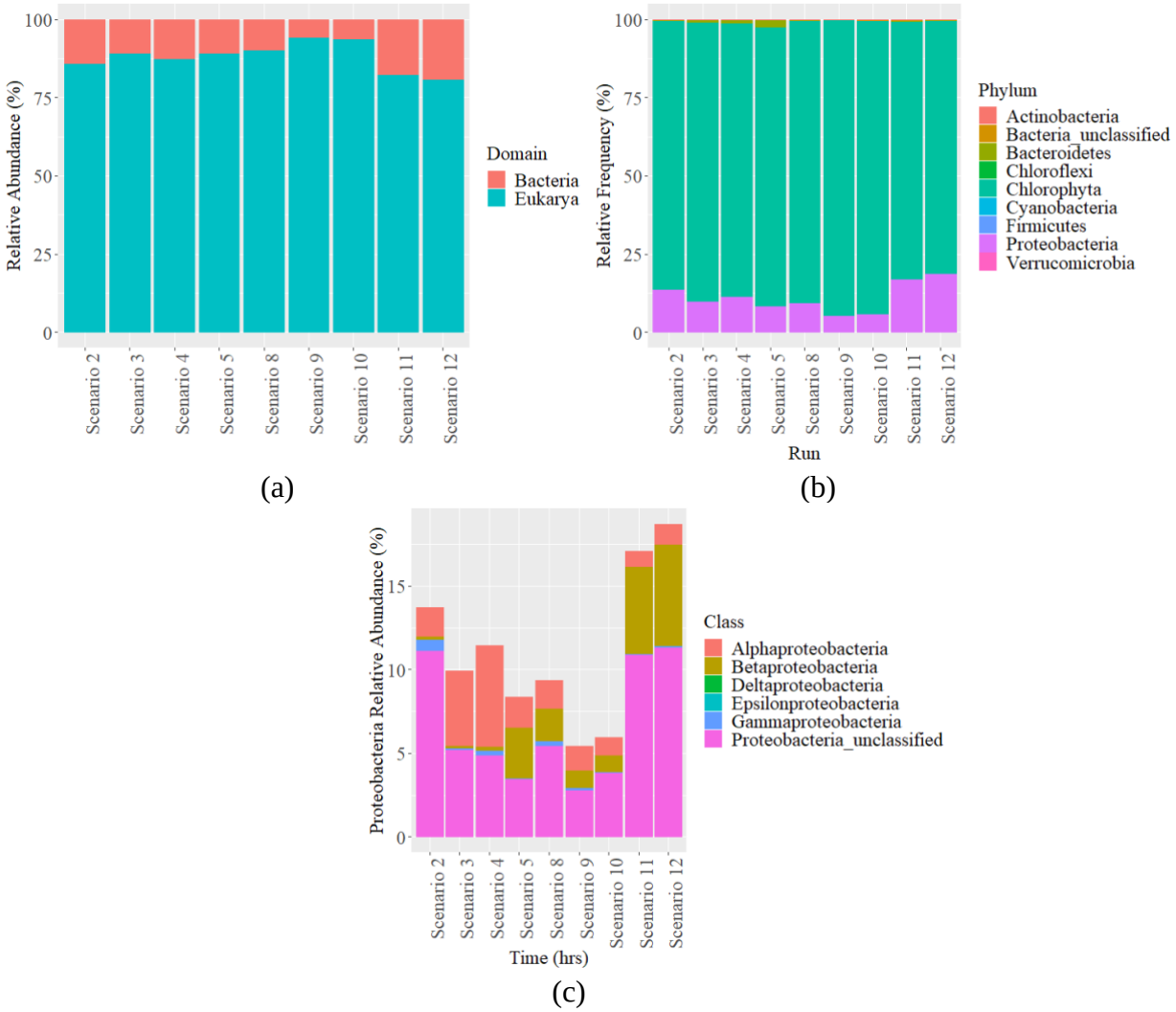

Figure 6. Relative abundance of microbial communities in the algal assemblage during the long-term pilot cultivation. (a). Relative abundance at the domain level; (b). Relative abundance at the phylum level; (c). Proteobacteria relative abundance at the class level. Relative abundance data are from a sample during each scenario.

Additionally, Alphaproteobacteria and Betaproteobacteria were significantly influenced by pH stabilization and harvesting ratio, respectively. Both Alphaproteobacteria and Betaproteobacteria are frequently reported in proximity to microalgae, therefore the observed differences in their abundance may be related to microalgal productivity and concentration [31, 94-96]. As previously discussed, Alphaproteobacteria and Betaproteobacteria are known to play key roles in nitrogen cycles, thus the nitrogen source under various conditions may also influence their abundance. However, due to limited knowledge on microalgae-bacteria

relationships under specific culturing conditions, only generalized statements can be inferred from the obtained results. In-depth analysis of microbial community such as functioning genome is an important research topic on large-scale microalgae cultivation and requires future work. Overall, microbial community of the long-term pilot-scale operation under different operational conditions was stable, with only some differences detected at the class level. Additional information on the effects of culturing conditions on key microbial communities are presented in Table 33.

Conclusion

The culture performance and microbial community analyses concluded that a long-term, stable culture on power plant flow gas was achieved using a selected freshwater microalgal assemblage. The assemblage was stable with average relative abundances of 88 ± 4% and 12 ± 4% for algae and bacteria domains during a 12-month continuous operation despite different operational conditions. The daily harvesting amount of 60% with no light-cycle and NH_4NO_3 as the nitrogen source and pH stabilization reagent resulted in optimal cultivation performance. The tested operational conditions had no significant influence on algal biomass composition. A protein-rich biomass was produced from the long-term pilot-scale operation.

This chapter represents published work:
Cutshaw, A., et al., *A long-term pilot-scale algal cultivation on power plant flue gas – Cultivation stability and biomass accumulation*. Algal Research, 2020. **52**: p. 102115.

CHAPTER 2: PROTEIN EXTRACTION, PRECIPITATION, AND RECOVERY FROM *CHLORELLA SOROKINIANA* USING MECHANOCHEMICAL METHODS

Introduction

Atmospheric carbon dioxide emissions reached 4.75 million metric tons (Gt) in the U.S. and 36.4 Gt globally in 2018 [97]. More than 85% of all global CO_2 emissions are from energy-related processes, such as construction, transportation, and electricity. Of these energy-related processes, electricity generation accounts for approximately 45% of all energy-related global CO_2 emissions. Thus, comprehensive carbon capture technologies and mitigation strategies are critical for reducing CO_2 emissions from the electricity sector. Co-located microalgal cultivation is an attractive post-combustion carbon capture strategy. The biological sequestration of CO_2 using microalgae yields profitable biomass, rich in valuable metabolites, with the potential for low environmental and economic burdens. *Chlorella sorokiniana*, a freshwater species of green microalgae, is a good candidate for this application due to its demonstrated resilience against acidifying gases, such as SO_x and NO_x, that can be present in flue gas [98]. In addition, *C. sorokiniana* have a high protein content, recorded as being 58.6% of the dry matter [30].

Despite the potential of biological CO_2 sequestration, there are ongoing challenges that must be addressed before its widespread implementation and successful adoption. Namely, the cost and energy demands associated with cultivation must be offset during downstream processing. The manufacture of products from high-value cellular components and development of co-product systems has the potential to address these challenges. However, current microalgal processing technologies demand improvements that will lower the overall cost and energy required to obtain value-added products. Developing low-energy, low-cost processing technologies is a critical step towards the success of microalgal technologies.

Following the cultivation of microalgae, biomass in suspension must be harvested from the reactor or pond, and dewatered. Once the biomass has been harvested and dewatered, the next

step in converting biomass into value-added products is typically cell disruption. Downstream products receive their value from intracellular components, like lipids, proteins, and pigments, that are transformed into goods like biofuels or nutraceuticals. Several different techniques have been explored to achieve different degrees of disruption, including alkali/acid treatment, enzymatic treatment, microwave, sonication, high pressure homogenizers, thermochemical conversion, pulsed electric field treatment, and milling with beads or balls [37, 42, 43]. Several reports indicate that despite the high energy demands of mechanical methods, like homogenizers and mills, they are the most efficient techniques for cell disruption and offer the best opportunities for scalability [43]. Notably, reports of imbalances in the energy and cost of these techniques are based on data from microalgal suspensions that have low biomass concentrations (w/w) [43]. Increasing the solids content of the microalgal suspensions and scaling up the cell disruption process has been shown to reduce the overall energy demand [44]. Research efforts should be focused on developing methods capable of handling suspensions with high biomass concentrations and evaluating these techniques on a process scale.

Following cell disruption, the component, or components, of interest can be isolated and recovered. There are several techniques for recovery of microalgal metabolites, including the use of alkali or organic solvents, ionic liquids, and aqueous two-phase extraction [15, 48]. Until recently, component recovery from microalgal biomass was focused on lipids and, subsequently, the development of biofuels. However, efforts have started to shift towards other valuable cellular components such as protein, pigments, and antioxidants. Protein is especially valuable for its use in nutraceuticals and food products, however, methods for protein extraction and recovery from microalgal biomass are scarce and under-developed [15].

The goal of this study was to develop a low energy, mechanochemical cell disruption process for protein extraction from concentrated microalgal biomass suspensions. *Chlorella sorokiniana* biomass was first characterized using gel electrophoresis and macromolecular analysis. Dewatered biomass was used for cell disruption using ball mills and, to increase the efficiency of cell disruption and reduce the overall energy demand, simultaneous alkali treatment was performed. Additionally, this study developed a protocol for protein recovery from fractionated biomass using the isoelectric point of microalgal proteins. Finally, a mass balance and energy analysis were performed to demonstrate the scalable nature and energetic viability of these processing technologies.

Methods and Materials

Microalgal strain and cultivation techniques

Chlorella sorokiniana MSU biomass was collected from an indoor photobioreactor (PBR) at the T.B. Simon Power Plant on Michigan State University's campus. *C. sorokiniana MSU* is a microalgal strain native to the Great Lakes region [69]. The PBR used in this study was installed by PHYCO$_2$ LLC in the T.B. Simon Power Plant and has been described previously [65]. The 118 L PBR (100 L working volume) is comprised of a helical coil accompanied by a vertical up-tube and LED light sources. Light is provided to the PBR with 12, 8-foot LED light bars (Independence LED Lighting LLC, USA), with 4 bars in the center of the coil and 8 around the up-tube. Each light bar contains forty-four red and twelve blue diodes, providing light at 660 nm and 450 nm, respectively. Combined, the light bars deliver a continuous photosynthetic photon flux density (PPFD) of approximately 407 μmol m^2/s, as measured by a LI-190R Quantum Sensor paired with a LI-250A light meter (LI-COR, Lincoln, Nebraska).

Flue gas, generated by natural gas fired combustion, is pumped directly from the stack into the PBR. A gas sparger at the bottom of the up-tube delivers the flue gas at a rate of 12 L/min and drives flow throughout the reactor. A continuous emissions monitoring system (CEMS), as regulated by the United States Environmental Protection Agency (EPA), was used to determine the CO_2 and NO_x emissions in the flue gas to be 7.2 ± 0.06% v/v and 76.9 ± 0.4 ppmv, respectively. Modified Tris-Acetate-Phosphate media containing the following nutrients was used for cultivation: 3.75 mmol/L of NH_4NO_3, 0.34 mmol/L of $CaCl_2 \cdot 2H_2O$, 0.4 mmol/L of $MgSO_4 \cdot 7H_2O$, 0.68 mmol/L of K_2HPO_4 (anhydrous), 0.45 mmol/L of KH_2PO_4 (anhydrous), and 0.09 mmol/L $FeCl_3 \cdot 6H_2O$. All nutrient solutions and media were prepared using deionized water and tap water (fresh water) from the power plant was used for cultivation. No sterilization was performed.

Microalgal biomass and protein characterization

Untreated, whole *C. sorokiniana* biomass was characterized using standard forage analysis methods [72]. In addition, gel electrophoresis was performed to characterize the proteins present in the untreated biomass. The Mini-PROTEAN® Tetra Cell System (Bio-Rad Laboratories Inc., Hercules, CA) was used to perform SDS-PAGE. 2x Laemmli sample buffer, 10x Tris/Glycine/SDS buffer and Bio-Safe™ Coomassie stain were also obtained from Bio-Rad Laboratories. A working 2x Laemmli sample buffer was obtained by adding 50 uL of 2-mercaptoethanol per 950 uL of sample buffer. A sample of biomass, previously frozen at 4°C, was thawed and the microalgal cells were lysed using a mortar and pestle. The sample was ground for approximately 5 minutes to achieve total lysis. To maintain protein integrity, liquid nitrogen was added incrementally during grinding and the lysed cells were immediately put in pre-chilled 2x Laemmli buffer. Lysed cells were then heated at 80°C for 10 min and allowed to

cool to room temperature. Proteins were then precipitated using acetone following a protocol adapted from Pierce Protein Biology TR0049.0 (Thermo Fisher Scientific Inc., Waltham, MA). Samples were incubated overnight at -20°C and a centrifuge speed of 14,000 rpm was used to collect the precipitated proteins. Following precipitation, residual acetone was allowed to evaporate off and all samples were resuspended in 2x Laemmli sample buffer. To encourage solubilization, samples were then heated for another 10 min at 80°C. Any lingering insoluble material was isolated with a final centrifuge step for 5 min at 14,000 rpm. All samples were loaded onto 10% polyacrylamide, 10-well Mini-PROTEAN® TGX™ Precast Protein Gels and run at 150V for approximately 40 min. Empty wells were loaded with 2x Laemmli sample buffer

Mechanochemical protein extraction and recovery

Ball milling optimization

Microalgal biomass was harvested from the PBR previously described and dewatered using centrifugation. The dewatered microalgal biomass had a total solids content of 20% w/w (0.2 g dry biomass/g wet biomass) and was frozen at 0°C immediately after harvest. For cell disruption, biomass was thawed and used directly without additional drying. Optimization of the ball milling process was completed in a lab-scale planetary ball mill with a power rating of 100W (Figure 7) (Tencan, China). Five milling parameters were varied to induce different cell disruption conditions, including the type of milling media, rotational speed, run time, ball to biomass ratio, and the amount of potassium hydroxide (KOH) added. Agate (SiO_2) and zirconia (ZrO_2 and Y_2O_3) milling media were selected to evaluate the effectiveness of the two characteristically different materials. Agate is relatively soft, according to Mohs scale, while zirconia is quite hard. Additionally, agate is, on average, much less expensive than zirconia. The agate media was a heterogeneous mix of four 12 mm, ten 10 mm, and ten 8 mm balls. Likewise, the zirconia media

was made up of two 12 mm, three 10 mm, and four 8 mm balls. Ball sizes and quantity were determined based on mass, therefore, the denser media (zirconia) had fewer overall balls. The ball to biomass ratio was varied between 2:1 and 4:1 to determine the most effective mass loading conditions of the planetary ball mill.

The selected milling vessels can hold approximately 25 mL and are made of the corresponding milling material. The rotational speed of the ball mill was varied between 400, 500, and 600 rpm, and run time was varied between 30 and 60 minutes. The milling speed and milling time, and their respective values, represent the mechanical intensity of the cell disruption. Finally, the KOH to algae ratio was based on mole ratio of KOH and nitrogen (N), and varied between 1 mol KOH/2 mol N (1:2) and 1 mol KOH/1 mol N (1:1) to determine the preferred chemical intensity of the cell disruption (Equation 1). A protein content of 58.6% w/w for *C. sorokiniana* biomass was previously determined using standard forage analysis methods [30]. A protein-to-nitrogen conversion factor of 6.25 was selected for this study [99]. Equation 1 was used with the molecular weight of KOH (56.11 g/mol KOH) to determine the KOH loading required for each ratio.

$$\frac{\text{Dry biomass}}{\text{mol N}} = \frac{1\text{ g dry biomass}}{0.586\text{ g protein}} \times \frac{6.25\text{ g protein}}{1\text{ g N}} \times \frac{14\text{ g N}}{1\text{ mol N}} = \frac{149\text{ g dry biomass}}{1\text{ mol N}} \quad \text{Eq. 1}$$

The metric used to compare treatments and to determine the most effective milling conditions was the percent of protein extracted. This was calculated as the amount of protein in the fractionated biomass, or microalgal slurry, divided by the expected protein the untreated biomass. The expected protein was calculated using a previously determined protein content of 58.6% of the dry matter. The protein content of the microalgal slurry was determined by measuring the total nitrogen and converting the nitrogen to protein. Total nitrogen was used in place of a protein assay due to its ease of measurement and conversion, and thus, measurements

were completed in duplicate. The total nitrogen concentration (mg/L) of the microalgal slurry was measured using nutrient test kits (HACH Company, Loveland, Colorado) following an appropriate dilution and in reference to EPA methods [71]. The minimum data point from each data pair was selected to use for statistical analysis to underestimate the protein extraction efficacy of the milling process. The milling conditions that yielded the highest percentage of protein extracted were used for all scaled up experiments.

Figure 7. Left & middle: Lab scale planetary ball mill used for the optimization of milling for microalgal biomass. Zirconia (white) and agate (grey) milling vessels are pictured next to the ball mill. Right: Microalgal slurry after cell disruption in the planetary ball mill using agate milling media.

Protein precipitation by pH shifting

Following the optimization of cell disruption, the process was scaled up to a 2 L (1.5 working volume), 100 W stirred ball mill (Tencan, China) (Figure 8). Because of its larger capacity, the amount of microalgal slurry acquired from the 2 L ball mill will be sufficient to evaluate the efficacy of pH shifting to the isoelectric point to precipitate the extracted proteins. To remove insoluble cell matter and isolate a protein-rich supernatant prior to pH adjustment, the microalgal slurry was centrifuged at 3,000 rpm for 15 min in 50 mL centrifuge tubes (Alkali Scientific, Fort Lauderdale, FL) using an Allegra® X-12R centrifuge (Beckman Coulter, Brea, CA). This centrifugation step was identified as key pre-treatment to obtain a protein-rich supernatant, thus

this separation process needed to be optimized. The total solids content of the microalgal slurry was ~20% w/w, which can lead to poor separation during centrifuging. Therefore, dilution factors of 0 (no dilution), 2, 5, and 10 were applied to the microalgal slurry prior to centrifugation to optimize the total solids content of the slurry.

Figure 8. Stirred 2 L ball mill for cell disruption and protein recovery.

Following the initial centrifugation, the microalgal slurry was separated into protein-rich supernatant and settled solids. The protein-rich supernatant was removed from the settled solids for pH adjustment to the isoelectric point of microalgal proteins which, according to previous examination, is approximately a pH of 4 [100, 101]. The pH of the protein-rich supernatant was adjusted using 1M sulfuric acid (H_2SO_4) in 1 mL intervals and 0.1 mL intervals close to the p*I* while being stirred consistently. Once the p*I* was reached, the protein-rich supernatant was centrifuged at 3,000 rpm for 15 min to obtain a supernatant and precipitated proteins. The supernatant, containing mostly K_2SO_4 as a result of the reaction between KOH added for cell disruption and H_2SO_4 added for pH adjustment, was referred to as the salt supernatant.

The applied dilution factors were evaluated based on net recovered protein isolate (dry, g), percent recovered protein (w/w %) and relative protein content (w/w %). The protein content (g/L) of all samples were determined by measuring the TN, using nutrient test kits (HACH Company, Loveland, Colorado) in duplicate, and the stoichiometric conversion. The net recovered protein was determined by calculating the dry weight of the protein in a sample using the protein content measurements. Percent recovered protein was calculated as the mass of recovered protein per mass of expected protein. The net mass of recovered protein was determined as previously mentioned and expected protein was estimated using the protein content of the untreated dry biomass and the calculated protein extraction following optimization of cell disruption. Relative protein content was calculated as the dry mass of recovered protein divided by the total dry mass of the sample. The relative protein content was used as an indicator of the purity of the protein isolate. The dry mass of the samples was determined by drying in duplicate at 105°C for 24 hours.

Mass balance and energy analysis

Mass and energy balances of the mechanochemical process (mechanochemical cell disruption and protein recovery) at a process scale were completed to identify key mass flows and estimate the energy intensity. The current mechanochemical cell disruption was scaled to process 10,000 kg of wet biomass (2,000 kg dry biomass) per batch. An envisioned cylindrical ball mill with a diameter and height of 1.2 m and 2.4 m, respectively, and an effective volume of 10 m^3 was assumed to carry out the mechanochemical cell disruption. The agitation power was calculated according to Equation 2 [102].

$$P = N_P' \rho N_i^3 D_i^5 \qquad \text{Eq. 2}$$

The agitation power P (W) was calculated based on the following coefficients and values: N_P' is the power number (0.35) for rod impeller in the turbulent regime, ρ is the density of the biomass slurry (kg/m^3), N_i is the agitator speed (rotation per second), and D_i is the impeller diameter of 1.18 m. Centrifugation is used to remove solids from the protein-rich supernatant and to recover the isolated proteins (Alfa Laval WHPX 513 TGD 24-60, Dolphin Centrifuge, Warren, MI). The selected centrifuge has a processing capacity of 14 m^3/hr with a power requirement of 11.24 kW. The resulting protein yield was based on a 58.6% protein content of the dry biomass, and the calculated protein extraction and protein recovery efficiencies. Finally, it was assumed that 5% of the total microalgal slurry would be lost during the cell disruption process due to the high solids content and resulting high viscosity.

Statistical analysis

R (version 4.0.3) and R Studio were used to analyze the data collected for this study. A Shapiro-Wilk's test was applied to check for normality and an F-test was applied to confirm equal variances. Data with normal distributions and equal variances were tested using parametric, analysis of variance (ANOVA) statistical tests. To determine if there were any statistically significant interactions between treatments during milling optimization, a factorial ANOVA was used followed by Tukey's test for post hoc multiple comparison. A one-way ANOVA and Tukey's test were used to determine optimal pH shifting conditions. Data with non-normal distributions and unequal variances were tested using the non-parametric Kruskal-Wallis test. All tests were performed with α=0.05 and statistical significance was determined as a p-value $\leq$ 0.05.

Results and discussion

C. sorokiniana characterization

The results from forage analysis of the original biomass used for cell disruption and protein recovery are shown in Table 7. The crude protein content of the untreated biomass, at 58.3 ± 1.84%, is expected based on a previously recorded value of 58.6% [30]. Lipid, carbohydrate, and ash contents are also consistent with previous analysis.

Table 7. Forage analysis characterization of C. sorokiniana biomass. Samples were freeze dried prior to analysis. Values represent the average of two samples.

Component	Value (% dry matter)
Crude Protein	58.3 ± 1.84
ADF	3.70 ± 0.141
NDF	6.70 ± 2.55
Lignin	2.45 ± 0.0707
Starch	2.60 ± 1.98
ESC	4.95 ± 0.636
TFA	9.42 ± 0.184
Ash	9.52 ± 1.05
TDN	82.5 ± 0.707

SDS-PAGE was performed to characterize the proteins present in the untreated biomass. Figure 9 shows the proteins present in untreated biomass loaded at 10, 20, 25, 30, 40, and 50 uL. The observed bands A-I, and their estimated molecular weights, are detailed in Table 8. Bands C, G, and I, at approximately 50, 25, and 15 kD, were observed to have the darkest staining and thus, the highest protein concentration. A related study of *Chlorella sorokiniana* identified proteins with similar molecular weights [103]. Using nanoLC-nanoESI MS/MS, researchers were able to accurately characterize proteins such as Phosphoglycerate Kinase (49.13 kD), ATP Synthase Subunit Beta (Chloroplast) (51.83 kD), 50S Ribosomal Protein L7/L12 (Chloroplast) (13.58 kD), and Fe-superoxide Dismutase (26.41 kD). Although these observed bands may be

used to estimate the identity of the proteins observed in bands C, G and I, further analysis with a method such as MS/MS is needed to confirm.

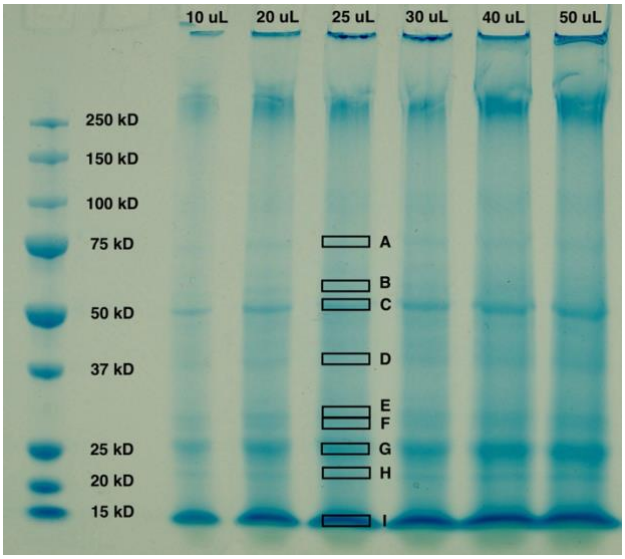

Figure 9. SDS-PAGE characterization of untreated biomass under different loading volumes.

Table 8. Observed molecular weights of the proteins present in C. sorokiniana biomass.

ID	Observed MW (kD)
A	75
B	55
C	50
D	37
E	30
F	29
G	25
H	22
I	19

Mechanochemical cell disruption

A total of 48 experiments were conducted in duplicate, producing 96 data points that were analyzed with a factorial ANOVA (Table 9). These results indicate that milling speed and ball to biomass ratio have no significant effect on protein extraction as measured by percent of protein extracted. However, the milling time, milling media, and KOH to biomass ratio have a

significant effect on protein extraction. Due to the complexity created by having several independent variables, the results from the factorial ANOVA also show multiple significant interactions between variables. Notably, there is no significant interaction between all five parameters, indicating that there is a synergistic effect resulting in similar protein extraction efficiencies. A post-hoc comparison with Tukey's test detailed nearly 1,400 significant interactions between factors and the levels within those factors. A summary of the results from the factorial ANOVA can be seen in Table 9.

Table 9. Results of the factorial ANOVA for optimization of mechanochemical cell disruption. More than one variable indicates the presence of a significant interaction between variables.

Variable	df	Sum Squared	Mean Squared	Statistic	P Value
Milling media	1	3355	3355	162.7	0.0000
Ball to biomass ratio	1	4.402	4.402	0.2135	0.6461
Milling speed	2	39.36	19.68	0.9546	0.3923
Milling time	1	422.4	422.4	20.49	0.0000
KOH to biomass ratio	1	14545	14545	705.5	0.0000
Milling media x Ball to biomass ratio	1	20.93	20.93	1.015	0.3189
Milling media x Milling speed	2	170.9	85.47	4.146	0.0220
Ball to biomass ratio x Milling speed	2	232.0	116.0	5.627	0.0064
Milling media x Milling time	1	2.991	2.991	0.1451	0.7050
Ball to biomass ratio x Milling time	1	0.1044	0.1044	0.0051	0.9436
Milling speed x Milling time	2	34.28	17.14	0.8312	0.4418
Milling media x KOH to biomass ratio	1	578.1	578.1	28.04	0.0000
Ball to biomass ratio x KOH to biomass ratio	1	121.9	121.9	5.912	0.0189
Milling speed x KOH to biomass ratio	2	66.51	33.26	1.613	0.2101
Milling time x KOH to biomass ratio	1	212.5	212.5	10.31	0.0024
Milling media x Ball to biomass ratio x Milling speed	2	18.88	9.440	0.4578	0.6354
Milling media x Ball to biomass ratio x Milling time	1	34.34	34.34	1.666	0.2032
Milling media x Milling speed x Milling time	2	44.38	22.19	1.076	0.3491
Ball to biomass ratio x Milling speed x Milling time	2	309.4	154.7	7.504	0.0015

Table 9 (cont'd)

Milling media x Ball to biomass ratio x KOH to biomass ratio	1	20.77	20.77	1.008	0.3206
Milling media x Milling speed x KOH to biomass ratio	2	217.8	108.9	5.281	0.0085
Ball to biomass ratio x Milling speed x KOH to biomass ratio	2	193.9	96.95	4.702	0.0138
Milling media x Milling time x KOH to biomass ratio	1	8.764	8.764	0.4251	0.5176
Ball to biomass ratio x Milling time x KOH to biomass ratio	1	114.5	114.5	5.552	0.0227
Milling speed x Milling time x KOH to biomass ratio	2	38.35	19.17	0.9300	0.4017
Milling media x Ball to biomass ratio x Milling speed x Milling time	2	16.63	8.313	0.4032	0.6705
Milling media x Ball to biomass ratio x Milling speed x KOH to biomass ratio	2	4.721	2.361	0.1145	0.8921
Milling media x Ball to biomass ratio x Milling time x KOH to biomass ratio	1	7.546	7.546	0.3660	0.5481
Milling media x Milling speed x Milling time x KOH to biomass ratio	2	32.38	16.19	0.7853	0.4619
Ball to biomass ratio x Milling speed x Milling time x KOH to biomass ratio	2	283.4	141.7	6.873	0.0024
Milling media x Ball to biomass ratio x Milling speed x Milling time x KOH to biomass ratio	2	6.848	3.424	0.1661	0.8475

There are only three significant individual factors: milling media, milling time and KOH to biomass ratio. The optimal milling conditions for these factors are 60 minutes, zirconia media and a 1:1 ratio. It's clear that the most significant parameter is the KOH to biomass ratio (Figure 10a), with the 1:1 ratio resulting in better protein extraction at 54.0 ± 11.1% compared to 31.0 ± 4.63% with the 1:2 ratio. This is followed by milling media (Figure 10b), where zirconia performed better than agate, extracting 48.0 ± 15.1% of protein compared to 36.9 ± 11.2%. Finally, Figure 10c shows mean protein extraction grouped by milling times of 30 and 60 minutes. The data seem to indicate that there is no significant difference between 30 and 60 minutes, with protein extraction of 40.3 ± 13.2% and 44.4 ± 15.2%, respectively. However, the

results from the factorial ANOVA indicate a significant difference between the two milling times. This significance is likely due to the statistical test's ability to detect the dependent nature of seemingly independent variables, such as milling time. The complexity of the system, its variables, and their interactions is further confirmed with the results from the Tukey's test.

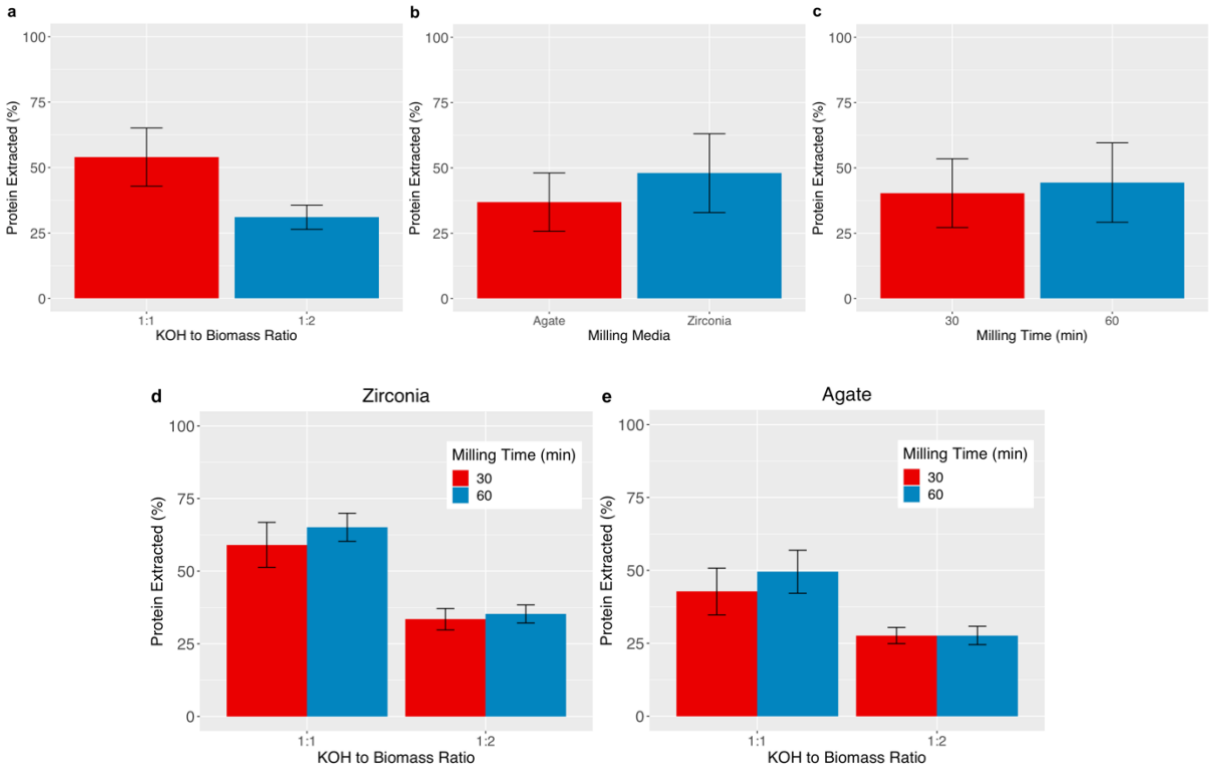

Figure 10. Average protein extraction based on KOH to biomass ratio (a), milling media (b), milling time (c), KOH to biomass ratio and milling time for zirconia media (d), and KOH to biomass ratio and milling time for agate media. Error bars are equal to the standard deviation.

Figure 10d and e show the means of these factors when grouped together and separated by milling media. The data clearly show that there is a significant interaction between milling media and KOH to biomass ratio, and KOH to biomass ratio and milling time. The 1:1 KOH to biomass ratio results in significantly higher protein extraction across milling medias and milling times. Looking at the means with a 1:1 KOH to biomass ratio and zirconia for milling media, 30 minutes resulted in 59.1 ± 7.75% and 60 minutes resulted in 65.1 ± 4.83% protein extracted.

Comparatively, agate media with a 1:1 KOH to biomass ratio resulted in 42.8 ± 8.01% and 49.5 ± 7.37% protein extracted from 30- and 60-minute milling times, respectively.

Due to the complexity of the results from the factorial ANOVA and corresponding Tukey's test, decisions regarding milling conditions for scale up were made based on both statistical significance and practical considerations. A KOH to biomass ratio of 1:1 proved to be significantly more effective for protein extraction on several levels, and thus was used for scaled up experiments. Although there was no significant difference between the ball to biomass ratios, a 4:1 ratio is preferred for scaling purposes to address clogging and cleaning issues. Additionally, a rotational speed of 400 rpm will require less energy and is thus the optimal speed. Due to the significance resulting from interactions between milling time and other factors, a 60-minute milling time was selected. The results from the factorial ANOVA revealed that zirconia was significantly better than agate in terms of protein extraction efficiency using the planetary ball mill. However, the density of zirconia (5.68 g/cm^3) is much higher than agate (2.62 g/cm^3) and it has been observed that microalgal biomass and zirconia media do not mix well in a stirred tank ball mill. This can cause high energy demand and may impact protein extraction efficiency as well. This reason, in addition to the cost difference between the two materials, resulted in agate being the selected milling media for scale up. Under these selected milling the conditions, the mean protein extraction was 52.7 ± 6.45%.

Protein precipitation

Following cell disruption, a total of 18 samples were produced using the precipitation protocol. The samples were then tested for total nitrogen to determine the protein content. A total of 18 data points were collected for statistical analysis using the three metrics previously described: net recovered protein, percent protein recovered, and relative protein content. Figure

11 shows the mean of each metric for 0 (no dilution), 2, 5, and 10 times diluted microalgal slurry.

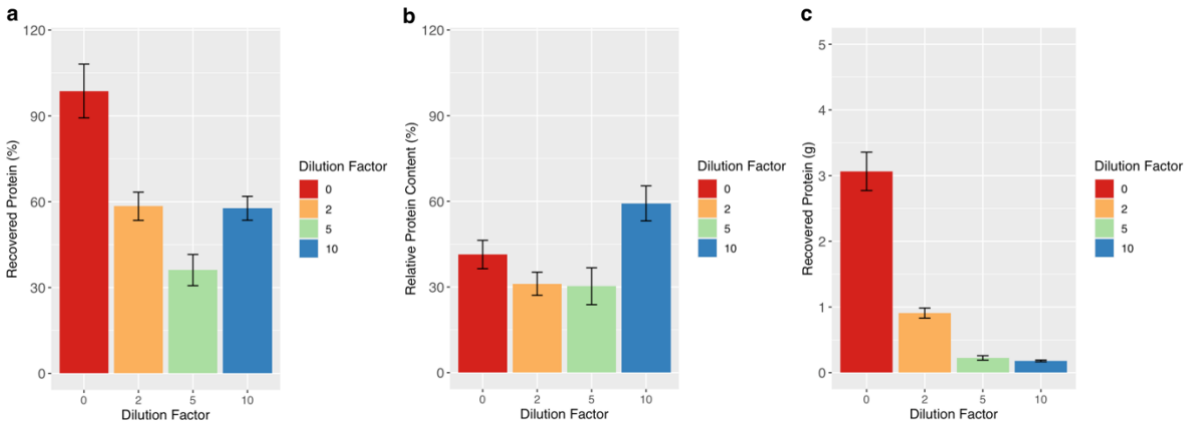

Figure 11. Mean protein recovery (a), relative protein content (b), and net recovered protein (c) and are representative of 5, 4, 6, and 3 replicates for 0, 2, 5, and 10 times dilution factors, respectively. Error bars are equal to the standard deviation.

Percent of protein recovered, shown in Figure 11a, was calculated using the net mass of protein recovered and the starting mass of protein in the microalgal slurry after mechanochemical cell disruption. The starting mass of protein was determined using the dry mass of the microalgal slurry used for precipitation, a mean protein extraction of 52.7%, and a protein content of 58.6% of the dry matter. The sample that received no dilution performed significantly better than those samples that were diluted 2, 5, and 10 times, with a mean protein recovery of 98.7 ± 9.40%. The lower recovery for the 2, 5, and 10 times diluted samples is likely due to the lower starting mass and the larger effect that any mass losses had on recovery. Figure 11b shows the relative protein content, or the purity, of the samples. The 10 times diluted samples had a significantly higher relative protein content than all other dilution factors, with a mean of 59.3 ± 6.13%. The samples that received no dilution had a mean relative protein content of 41.4 ± 4.97%, which was significantly higher than the samples diluted 5 times but not significantly higher than those that were only diluted 2 times.

Figure 11c shows the net dry mass of recovered protein, which was significantly higher for the samples that received no dilution when compared to all other dilution factors, with means equal to 3.07 ± 0.292 g, 0.910 ± 0.077 g, 0.224 ± 0.034 g, and 0.179 ± 0.013 g for the 0, 2, 5, and 10 times diluted samples, respectively. This result is expected due to the fact that the starting biomass for the 2 times diluted sample is half that of the sample that was not diluted, and likewise for the 5 and 10 times diluted samples. The descending order of net recovered protein correlating with the increasing dilution factors indicates that, though not exact, the precipitation method can recover protein that is proportional to the starting biomass. The results detailed in Figure 11 indicate that while the precipitation method is successful at recovering nearly all the protein extracting during the milling process, its unable to successfully remove all non-protein solids.

Mass balance and energy analysis

The mass and energy balance analyses were based on processing 2,000 kg dry microalgal biomass for protein production (Table 10). Parameters used to calculate the power required for cell disruption were based on the optimal milling conditions selected in this study. The ball mill was assumed to have a zirconia vessel and rod impeller, however, agate balls were selected as the milling media. Using a 1:4 mass ratio of wet biomass to agate, the density of the microalgal slurry was estimated to be 1,857 kg/m^3. The agitator speed was set as 6.67 rps (400 rpm) and milling time was set to 60 min. The extraction efficiency of cell disruption was assumed to be 52.7%, a dilution factor of 0, and corresponding protein recovery of 97.8% were used for this analysis.

The consumption of 5,959 kg of 1M H_2SO_4 is equivalent to the consumption of 540 kg of 99.9% H_2SO_4 and 5,419 kg of water. The mechanochemical cell disruption and protein recovery

process generated 618 kg dry protein isolate from 2,000 kg dry algal biomass per batch. Meanwhile, the energy demands for the ball mill and centrifuge were 0.79 and 0.036 MJ/kg dry algal biomass. The energy required for centrifugation reflects the two stages in the protein recovery method and a processing capacity of 14 m^3/hr. Yap et al. found that *Nannochloropsis* sp. suspensions with 25% w/w solids can be processed by high-pressure homogenization with an energy consumption of about 1.00 MJ/kg dry [44]. Safi et al. achieved 49% protein yield from 10% w/w solids suspensions of *Nannochloropsis* sp. with an energy input of 1.58 MJ/kg dry [104]. The total energy consumed by the mechanochemical process was 0.83 MJ/kg dry biomass at the envisioned commercial scale in this study. With a solids content of approximately 20% w/w and a 52.7% protein extraction efficiency, this study was able to achieve protein recovery from a high total solids biomass with a much lower energy consumption than other reported mechanical disruption methods.

Table 10. Key mass and energy flows from the mass and energy balance analyses.

Parameter	**Value**
Microalgal biomass (wet, kg)	10,000
Microalgal biomass (dry, kg)	2,000
KOH (kg)	760
1M H_2SO_4 (kg)	5,959
Protein (kg)	618
Ball mill (MJ/kg dry biomass)	0.79
Centrifuge (MJ/kg dry biomass)	0.036
Total energy demand (MJ/kg dry algal biomass)	0.83

Conclusion

The goal of this study was to evaluate the developed protein extraction, precipitation, and recovery methods. Optimization of the ball milling process resulted in a set of milling conditions that achieved protein extraction of 52.7 ± 6.45%. These conditions were successfully scaled up from a bench-top planetary mill to a standing stirred mill, which represents a 100-fold increase in

scale. The acid precipitation method was optimized to determine that 98.7% recovery of proteins from the microalgal slurry can be achieved at a solids content of 20% w/w. However, the measured protein content of the protein isolate remained relatively low, at 41.4% w/w for the same solids concentration. These results indicate that the precipitation method is successful at recovering the extracted proteins in the algal slurry, however, the removal of non-protein solids during centrifugation and pH adjustment is not complete. Future work should address these challenges by modifying the method for removal of solids. The energy analysis elucidated that the energy demand of the protein extraction and recovery operation, at 0.83 MJ/kg dry algal biomass, is much lower than previous studies using high-pressure homogenization and membrane filtration. Collectively, this study suggests that mechanochemical protein extraction and recovery is an effective, low-energy processing method. The goal of future work should be to improve the richness and integrity of the protein isolate, and to further evaluate the viability of this method on a process scale.

CHAPTER 3: EVALUATION OF BIOBASED POLYOLS FROM MICROALGAL BIOMASS USING TECHNO-ECONOMIC AND LIFE CYCLE FRAMEWORKS

Introduction

Global production of plastics totaled 367 million metric tons (Mt) in 2020 [105]. This includes the production of thermoplastics, including polyethylene (PE) and polypropylene (PP), and thermosets like polyurethane (PU) and epoxy resin. While thermoplastics like PP and PE make up a majority of the global plastics market, nearly 10% of all plastics are PU polymers [106]. Polyurethanes are chemically defined as a polymer whose monomer units are joined by urethane linkages [49]. All polyurethanes are created using the same chemical reaction between an organic isocyanate and a polyol. A polyol is a liquid substance that will react with isocyanate and is generally classified as hydroxyl-terminated or amino-terminated [49]. Although global production of plastics saw a slight decrease in recent years, the polyurethane market is expected to grow significantly in coming years due to its continuing use in adhesives and foams [22, 51, 105]. This growth is expected to be accompanied by a shift towards using renewable sources of nitrogen and carbon, namely to alleviate the reliance on petrochemicals for polyol production [50].

There are several feedstocks currently being researched for use in biobased polyols, ranging from natural sugars, like sucrose and glucose, to lignin [50]. One of the most common starting materials is unsaturated oils, like those found in soybean and castor plants, that have characteristic double bonds that can be chemically transformed into hydroxyl groups. While these polyols are well documented and even commercially utilized, competition with vegetable oils used in the food industry and the use of arable land for non-food products represent challenges for long-term sustainability [52]. More recently, microalgae oil has been explored as an alternative that does not currently compete as a food source [19-21]. Although these oil feedstocks have established themselves as viable alternatives, other feedstocks still need to be

explored. Amino acids and proteins represent an alternate polyol synthesis pathway [50]. Studies using proteins extracted from microalgae biomass and soymeal, after oil extraction, have demonstrated the feasibility of these protein polyols [22, 107]. Biomass feedstocks, that require little to no additional processing after harvest, have the potential to be more energy efficient and thus, have better environmental and economic outcomes. However, no work has been done to evaluate microalgal biomass as a polyol feedstock.

The goal of this work is to evaluate the use of whole microalgal biomass and extracted protein for polyol synthesis. A previously established one-pot method was adapted to microalgae feedstocks and synthesized microalgal polyols were characterized by amine value, hydroxyl value, viscosity, and specific gravity [107]. Further characterization was completed using ATR-FTIR and TGA methodologies, and results were compared to similar biomass polyols. While the physical and chemical properties of the synthesized polyols may demonstrate their feasibility, the environmental and economic benefits, or tradeoffs, are critical to evaluating any sustainable alternative. Thus, the most viable microalgal polyols, as determined through characterization, were selected to perform gate-to-gate life cycle and techno-economic assessments. A comparative life cycle assessment (LCA) was used to determine the environmental impacts of these microalgal polyols in contrast to conventional polyols. A techno-economic assessment (TEA) was conducted to determine the minimum polyol selling price (MPSP) using a discounted cash flow rate of return (DCFROR).

Methods and Materials

Feedstocks and Chemicals

The green microalgae *Chlorella sorokiniana MSU* was cultivated in a 100 L indoor photobioreactor (PBR) under previously studied conditions [30]. The biomass used in this study was harvested from the PBR using 50% (50 L) or 60% (60 L) daily harvesting and the resulting protein, lipid and carbohydrate contents were 58.60 ± 2.41%, 9.70 ± 1.68%, and 19.5 ± 2.44%, respectively. The microalgal polyols in this study were synthesized using whole, untreated biomass or a protein isolate. The extraction and isolation method to prepare the protein isolate has been previously described in Chapter 3. Both biomass and protein feedstocks averaged 20% w/w solids content. Monoethanolamine (≥98%) and propylene carbonate (anhydrous, 99.7%) were obtained from Sigma Aldrich (MilliporeSigma, Burlington, MA).

Polyol synthesis

A one-pot, two-step polyol synthesis method, previously tested on de-oiled soymeal, was adapted for this study [107]. The previously described method consists of a transamidation reaction using monoethanolamine (MEA) (Figure 12a), followed by a ring-opening reaction with propylene carbonate (PC) for polyol synthesis (Figure 12b). Both MEA and PC exhibit desirable qualities, such as existing as liquids at room temperature and having high solubility in water. The microalgae-MEA mixture was combined in a round bottom flask, purged with nitrogen gas, and reacted at 100°C for 2 hours, forming amine derivatives (AD) (Step 1). When applied to soymeal, a 1:3 feedstock to MEA mass ratio produced the best performing polyols [107]. Thus, based on the similarity between soymeal and microalgae biomass, a 1:3 MEA ratio was also used in this study. The AD were then reacted in the same round bottom flask with PC at 10% molar excess for 2 hours at 70°C (Step 2).

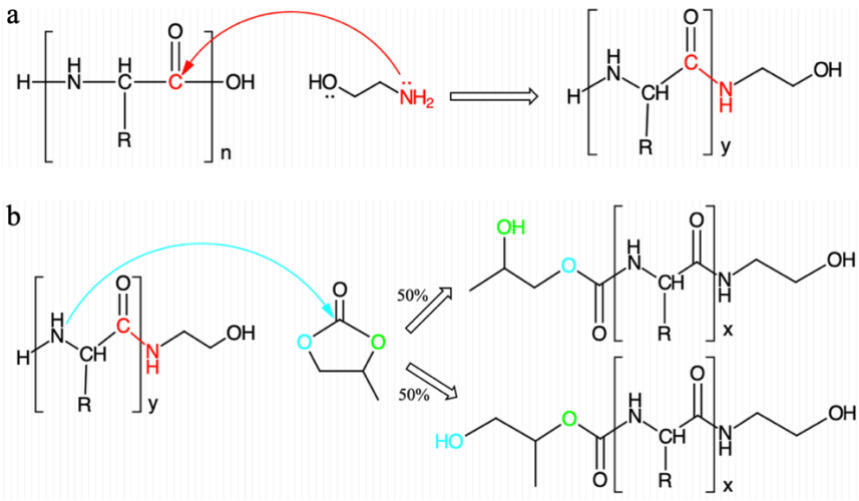

Figure 12. Chemical synthesis of amine derivatives (a) and microalgal polyols (b).

Microalgae and soymeal have similar biomass compositions, making microalgae a good candidate for adapting this synthesis method (Figure 13). However, compared to soymeal with a water content of ~20% w/w, the microalgae feedstocks in this study have a much higher water content at ~80% w/w. Thus, to provide a basis for comparison, biomass and protein feedstocks were dried to reach a water content of 20% w/w. The feedstocks were also used in their "wet" form (80% w/w water) to determine the difference in characteristics when no additional energy for drying is used. Biomass and protein feedstocks will be referred to as such, while feedstocks with a 20% water content will be referred to as "dry" and 80% as "wet".

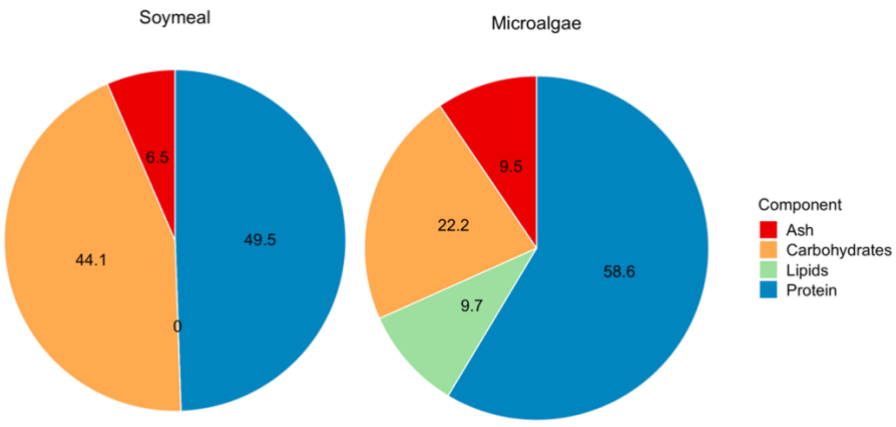

Figure 13. Soymeal (de-oiled) and microalgal biomass cell composition. Numbers represent the percent of dry weight.

Polyol characterization

The resulting AD, from Step 1 of synthesis, and polyols, from Step 2 of synthesis, were characterized for amine value using ASTM D2073-92. Polyols were also characterized for hydroxyl value using ASTM E1899-16. In addition, viscosity was measured using a HAAKE™ Viscotester™ 550 and the MV/MV DIN cup/sensor system (DIN 53019) (Thermo Fisher Scientific, Waltham, MA). Tests were performed in duplicate and at room temperature (22°C).

Thermogravimetric analysis (TGA) was performed using a TGA/DSC 1 STAR^{e} System (Mettler Toledo, Columbus, OH). To determine the degradation temperatures of the original feedstock, amine derivatives, and polyol, the weight loss (%) was recorded as the temperature of the samples was increased from 37°C to 550°C using a heating rate of 10°C/min. Finally, attenuated total reflection Fourier transformed infrared spectroscopy (ATR-FTIR) was performed on the original feedstocks, amine derivatives, and polyols using a Spectrum One FTIR with a single reflection ATR accessory (PerkinElmer, Waltham, MA). Spectra for the original biomass, amine derivatives, and polyol were each collected from 4 accumulated scans in a range

of 4000 cm^{-1} to 550 cm^{-1}. The transmittance (%) per wave number (cm^{-1}) was used to identify characteristic bonds in each sample.

Life cycle assessment

Scope

The goal of this LCA was to compare the environmental impacts of microalgal polyols to petrochemical, or polyether, polyols. To evaluate the life cycle impacts of the synthesized microalgal polyols, a wet and dry version of the same feedstock were selected based on characteristics. A functional unit of 1 kg of polyol was selected and allocation was avoided during the inventory phase. The process model for microalgal polyol production is shown in Figure 14 and the system boundary for this analysis is represented by the dark grey box. The unit processes within this system boundary are identical for the two polyols, however the dry biomass feedstock requires the use of a dryer to reach a lower water content. This results in additional material and energy flows for the harvesting and dewatering step, specifically. Outside of this unit process, the material and energy flows through the wet and dry systems differ only in values due to the requirements needed to produce 1 kg of polyol from wet versus dry biomass. In particular, the different amine values of each polyol indicate varying amounts of PC are needed to achieve a 10% molar excess, thus changing the mass requirements for polyol synthesis.

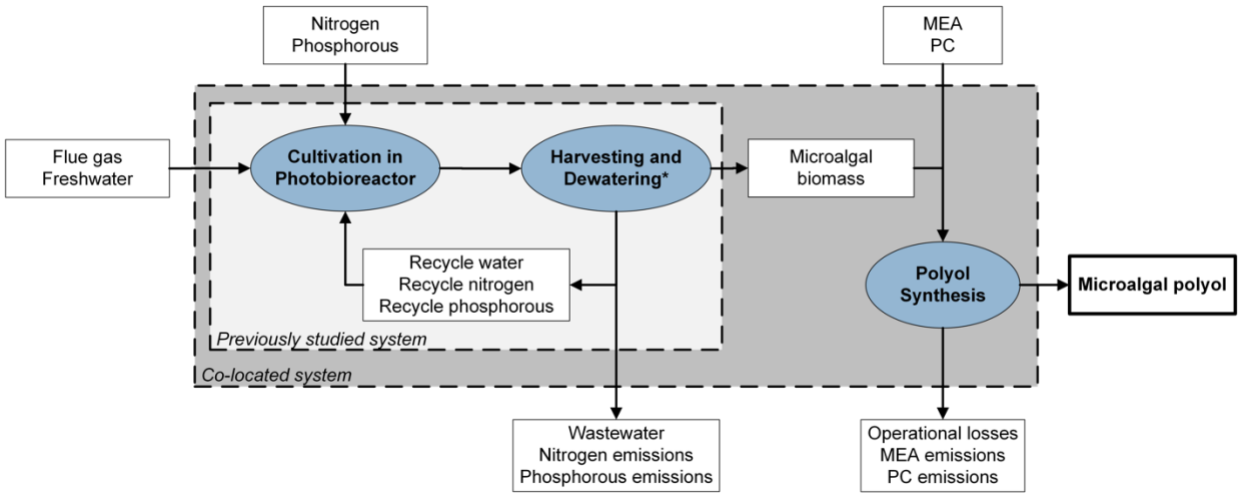

*Figure 14. System flow diagram of the microalgal polyol production system. *: The dry feedstock requires additional energy and equipment to reach the desired water content.*

Inventory

The inventories for the unit processes in Figure 14 (represented in blue) were constructed using empirical data that underwent mass and energy balances. A process scale cultivation system was modelled for the purposes of this study using productivity and water recycle data from previous reports on *C. sorokiniana* cultivation using flue gas [30, 108]. A summary of the PBR operation and assumptions is represented in Table 11. The envisioned 1000 m^3 PBR uses a horizontal tubular PBR set up that has been previously characterized [14, 109, 110]. The details of this configuration have been summarized such that the PBR area per volume ratio was calculated to be 4.13 m^2/m^3, meaning the 1000 m^3 PBR would occupy 4,130 m^2 or approximately 1 acre of land. The PBR was modelled using a harvest rate of 50% daily (500 m^3/day) and a water recycle system that has been previously studied [108]. Due to the scope of this analysis, the impacts of a system without water and nutrient recycle were not evaluated.

Table 11. Assumptions made for microalgal cultivation using a horizontal tubular PBR configuration.

Assumption	Value	Unit
PBR volume	1,000	m^3
PBR area	4,130	m^2
Biomass productivity	0.17	g/L/day
Density (at harvest)	0.50	g/L
Harvest rate	50	%
CO_2 consumption	0.30	kg/kg wet biomass

Nitrogen and phosphorous addition, in the form of NH_4NO_3 and K_2HPO_4, were modeled using data from the recirculation study. Micronutrients were assumed to have a negligible effect on life cycle and techno-economic outcomes and were therefore not included in this study. The co-located nature of the production facility means CO_2 is delivered to the PBR in the form of flue gas. The natural gas combustion required to produce the flue gas that's used for cultivation was considered outside the system boundary. The process scale reactor for polyol synthesis was assumed to be the same configuration used for a similar synthesis method at process scale [12].

Nitrogen and phosphorous emissions from the system were calculated using a mass balance and previously collected empirical data [108]. MEA and PC air emissions were calculated as 0.2% of the total input, in addition to a 5% operational loss. Any waterborne emissions were assumed to be treated by the power plant's water treatment system prior to exiting the facility. The co-located nature of the system under study negated the use of transportation between cultivation, harvesting, and polyol synthesis. Commercial polyol production relies solely on fossil-derived materials, and while the production of microalgal polyols uses biomass, a renewable source of carbon, this method of synthesis still requires the use of petrochemicals. To determine the impact of this reliance, and the replacement of fossil carbon, the renewable carbon content was determined from the results of the mass balance.

A complete life cycle inventory for polyether polyol, including a detailed description of the data and its sources, was completed by a third party and published in the U.S. Life Cycle Inventory (USLCI) Database provided by the National Renewable Energy Laboratory (NREL) [111, 112]. In addition to the full cradle-to-gate life cycle inventory, this report also provided data for a gate-to-gate life cycle inventory. To directly compare the microalgal polyols to the polyether polyol, the gate-to-gate data was used for this LCA. Transport for the delivery of raw materials, transport of the polyol product from the facility, and end use of the polyols was considered outside the scope of this assessment.

Data quality

Data quality goals and indicators were set using guidelines published by the U.S. Environmental Protection Agency [113]. These guidelines suggest goals for temporal and geographical scale, as well as technological representativeness and data completeness. Because this LCA uses both empirical and secondary data, the temporal and geographical data quality goals should reflect this. The temporal data quality goal was set at 5 years to include more sources for secondary data collection, and the United States was selected as the geographical scale for this study. The EPA has subdivided technological representativeness into four categories: process design, operating conditions, material quality, and process scale. This study aims to fulfill these goals by providing as much transparency as possible regarding modelling, assumptions, and data sourcing. Finally, the data completeness goal aims to include all flows entering and exiting the system boundary. However, this study recognizes there are limitations present when evaluating an emerging technology. While the goal is to identify every flow into and out of the system, we recognize that future investigation will be required to elucidate all

system flows. The updated data quality indicators and scoring matrix provided by the EPA will be used to evaluate the data quality of the two microalgal polyol inventories [113].

Impact assessment

The Tool for the Reduction and Assessment of Chemical and Other Environmental Impacts (TRACI) (v2.1, 2014) was selected for impact assessment. This impact assessment method was chosen over ReCiPe, a popular method in the field of LCA, because of the availability of characterization factors for chemicals like MEA and PC. The characterization factors were used to quantify the impacts in the following categories: ecotoxicity (urban air, CTUeco), freshwater eutrophication (kg N eq.), global warming (kg CO_2 eq.), and smog formation (kg O_3 eq.). Greenhouse gas emissions from electricity use were characterized using the Greenhouse Gas Equivalencies Calculator provided by the U.S. Environmental Protection Agency (EPA) [114]. The energy demand (kWh) and water consumption (m^3) of each system were also evaluated for each polyol.

Techno-economic assessment

The cost per unit volume for the horizontal tubular PBR, calculated using the area per volume ratio of 4.13 m^2/m^3, was \$44.65/m^3 in 2021 dollars [14, 109, 110]. Based on the small cultivation area of approximately 1 acre, it was assumed that the land requirements would be met by the existing power plant, thus land purchase costs were not considered in this analysis. The energy requirements of this PBR configuration have also been previously summarized and were adapted for this study [14]. The purchase price of the centrifuge and dryer models were obtained from a previous report and linearly scaled [65]. Ten cone bottom plastic tanks were selected for short term storage of the algal suspension and recycle water [115]. The equipment costs associated with polyol synthesis were obtained from a recent report that evaluated the cost of a

similar reactor system [12]. The processing capacity of this reactor unit is approximately 1,200 kg/hr, thus only one unit was required, and the associated energy demand was calculated to be 0.54 MWh/metric ton (t) [12]. The capital cost of all required equipment was reported in 2018 dollars and was indexed to 2021 dollars for this study using the Plant Cost Index from *Chemical Engineering* [116]. Based on reports from NREL and Pacific Northwest National Laboratory (PNNL), an installation factor of 1.2 was applied to the PBR and an installation factor of 3 was used for the plastic storage tanks [14, 117, 118]. The installation factors for the centrifuge, dryer, and polyol synthesis reactor represent average values from a range of installation factors, at 1.5, 1.7 and 1.7, respectively [119].

The microalgal polyol production system is assumed to be co-located with a natural gas fired power plant and a portion of the flue gas emissions are directed to the PBR as a source of CO_2. Using previously determined estimates, the cost of CO_2 delivery was assumed to be $45/t [14]. The cost of the infrastructure required for CO_2 delivery, including piping and storage, is included in the unit cost of the PBR. Nitrogen and phosphorous were assumed to be purchased as bulk fertilizer and prices were obtained from the USDA Economic Research Service Fertilizer Use and Price dataset [120]. This dataset only provided purchase price up to the year 2014, thus the BLS Data Finder provided by the U.S. Bureau of Labor Statistics was used to identify price indexes for the two chemicals.

The most up to date prices for monoethanolamine were obtained from ICIS Chemical Business for the region of Europe and it was assumed that U.S. prices would be comparable [121]. A price range of 1,240-1,270 EUR/t was obtained for the year 2020 and, in order to overestimate the cost of the system, 1,270 EUR/t was selected as the purchase price of MEA. The price was adjusted to 2021 dollars using the average exchange rate in 2021 of 0.8458

EUR/USD. Prices for PC varied significantly based on quantity and a representative value was difficult to obtain. An average price of $1.00/kg was obtained from a bulk chemical distributor [122]. Based on the scale of the system, it was assumed that a lead chemical engineer and four technicians would manage the operation. Salary data was collected from the U.S. Bureau of Labor Statistics Occupational Outlook Handbook [123].

Table 12. Assumptions made based on n^{th} plant economics for a DFROR analysis.

Assumptions	
Working Capital (% of FCI)	5%
Equity	40%
Loan Interest	8%
Loan Term (Years)	10
Salvage Value	$0
Depreciation Period (Years)	7
Construction Period (Years)	1
Start-up Time (Years)	0.5
Revenue (% of Normal)	50%
Variable Costs (% of Normal)	75%
Fixed Cost (% of Normal)	100%
Discount Rate (Internal Rate of Return)	10%
Income Tax Rate	35%
Cost Year for Analysis	2021

A discounted cash flow rate of return (DCFROR) analysis was selected to determine the minimum polyol selling price (MPSP). The assumptions for this analysis were based on n^{th} plant economics (Table 12) [36]. In addition to the assumptions listed in Table 12, it was assumed that a year of operation was 329 days, or 90% of a full year. The calculated minimum selling price will be compared to the average price of polyether polyols, which was $1,931/t ($1.93/kg) in 2018 dollars or $2.19/kg in 2021 dollars [124].

Sensitivity analysis

A sensitivity analysis of each microalgal system, for both LCA and TEA, was completed to determine the most sensitive material and energy flows. Each flow was varied by ± 30%, while all other flows were held constant, and the subsequent change in impact was recorded.

Results and discussion

Polyol characterization

The characteristics of amine derivatives and polyols are reported in Table 13. The dry feedstocks were found to have higher amine values than the wet feedstocks, likely due to the total biomass content of the starting biomass, with the dry feedstocks containing more biomass (w/w) than the wet feedstocks. Amine values were measured for the final polyol product to confirm 100% of the amine derivatives were reacted. This is verified by the negligible amine values for all microalgal polyols. The hydroxyl values of the microalgal polyols were slightly elevated compared to the reference feedstock, soymeal. This may be due to the higher protein content of microalgae and subsequently, more available hydroxyl groups. Higher hydroxyl values, greater than 360 mg KOH/g polyol, represent polyols that will form rigid PU foams [50]. Thus, all the evaluated microalgal polyols would form rigid PU foams. The dry feedstocks resulted in significantly higher viscosities than the wet feedstocks. The higher water content of 80%, compared to 20% in the dry feedstocks, caused the final polyol products to have viscosities much closer to that of water at 1 centipoise (cP). Viscosity of a polyol is a key characteristic because of the mixing that is required to achieve a homogenous blend of polyol and additives before reacting with an isocyanate. The lower viscosity values of the wet feedstocks would allow

for better mixing and homogeneity would be more easily achievable. Finally, the specific gravity of the microalgal polyols is comparable to the soymeal polyol and water at a value of 1.

Table 13. Amine derivative and polyol characterization of dry biomass (DB), dry protein (DP), wet biomass (WB), wet protein (WP). Soymeal polyol (SP) and Jeffol SG-360 characteristics were obtained from literature reports [107, 125].

Polyol	Amine Value-AD (mg KOH/g)	Amine Value-Polyol (mg KOH/g)	Hydroxyl Value (mg KOH/g)	Viscosity (cP)	Specific Gravity
DB	1099	-	628	826	1.23
DP	1077	-	558	1404	1.05
WB	481	-	601	275	1.26
WP	573	-	620	314	1.19
SP	772	6	568	37000	1.18
Jeffol SG-360	NA	NA	360	3500	NA

The results of TGA analysis of microalgal biomass, amine derivatives (WB) and microalgal polyol (WB) are shown in Figure 15 as the percent of original weight as a function of temperature. All phases are marked on the figure with grey dotted lines for clarity. The amine derivatives appear to have three distinct degradation phases at 37-75°C, 75-130°C and 130-550°C. These three stages are likely due to loss of water and volatile MEA, followed by low and high molecular weight amines, respectively [107]. The microalgal polyol sample appeared to have two distinct phases, from 37-200°C and 200-260°C. These two phases may represent the existence of two different polymers that can form as a result of this unique synthesis pathway. At approximately 260°C the untreated biomass sample slows a slight change in degradation, likely reflecting the torrefaction of cellulose and hemicellulose present in the microalgal cell wall. Future analysis should include the explicit determination of the identities of off gases using mass spectrometry.

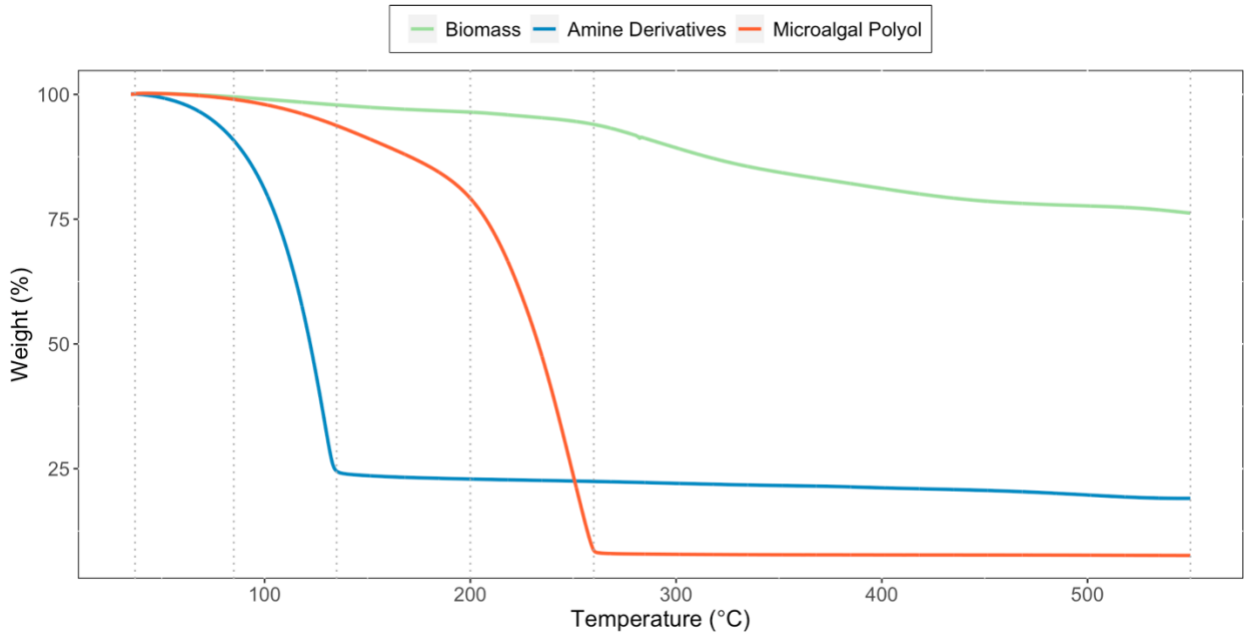

Figure 15. Weight (w/w) from microalgal samples at a heating rate of 10 ℃/min to reach 550 ℃.

Microalgae have documented, characteristic wavenumbers for bonds within compounds like proteins (1650 cm^{-1}), carbohydrates (1010 cm^{-1}), and lipids (1745 cm^{-1}) [126]. The spectrum collected from the sample of untreated biomass shows the presence of proteins and carbohydrates (Figure 16). The lack of a bond corresponding to the presence of lipids is likely due to the low lipid content of the microalgae strain relative to the protein and carbohydrate content. The ATR-FTIR spectra of all three samples show a characteristic OH stretch at approximately 3300 cm^{-1} [127]. In the AD spectrum, the OH stretch is followed closely by the NH stretch at 3200 cm^{-1} that is present in amines, like MEA. All three spectra show a -C-H stretch from ~2900 to 3000 cm^{-1}. The urethane linkages, characterized by a C=O bond, can be seen in the microalgal polyol spectrum at approximately 1750 cm^{-1}. A summary of all identified bonds and wavenumbers can be found in Table 14. The complexity of the spectra can be attributed to the biological nature of the samples. Both TGA and ATR-FTIR data show close similarity to the reference feedstock of soymeal [107]. Based on the summary of all microalgal

polyol characteristics and taking into consideration the energy and cost implications of protein extraction (detailed in Chapter 3), the wet and dry biomass feedstocks were selected for life cycle and techno-economic assessment.

Table 14. Bonds and corresponding wavenumbers identified in the ATR-FTIR spectra of microalgal biomass, amine derivatives (WB), and microalgal polyol (WB).

Bond/Compound	Wavenumber (cm^{-1})
OH stretch	3300
NH stretch	3200
-C-H stretch	2900-3000
C=O bond	1750
Proteins	1650
Carbohydrates	1010

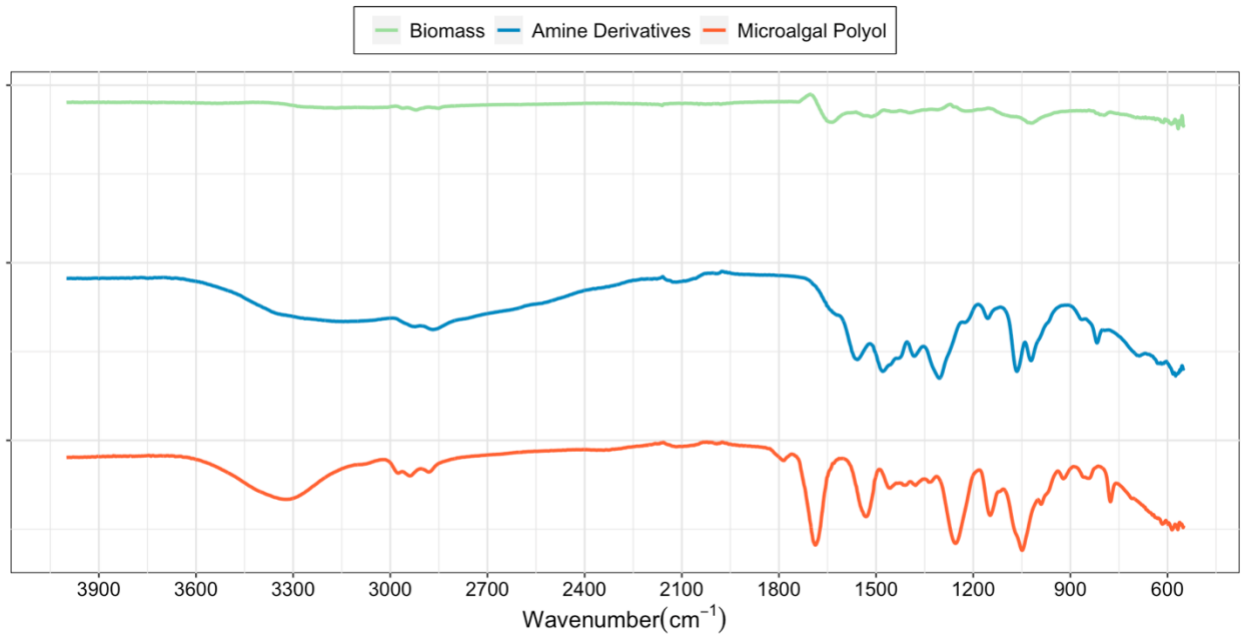

Figure 16. ATR-FTIR spectra of microalgal biomass, amine derivatives (WB), and microalgal polyol (WB) from four accumulated scans.

Life cycle assessment

Data quality

Data quality was assessed for each unit process in the microalgal polyol production systems and Table 15 shows the scores for each data quality category as defined by the EPA's pedigree

matrix [113]. Scores of 1 and 2 represent high quality data and make up most of the scores for the microalgal systems. However, to address those less satisfactory scores of 3 and 4, rationale will be provided. A flow reliability score of 3 was given to the polyol synthesis unit process because the data used in the mass and energy balances, and subsequently in the inventories, were based primarily on calculations. This was due to the scaling required to use the empirical data collected in this study at a process scale. A technological score of 3 for cultivation and polyol synthesis indicates that two of the four sub-categories previously mentioned were equivalent. The adopted PBR configuration maintained its original process design and material quality, while the process scale and operating conditions were modified for this assessment. Compared to the original configuration, the scale was decreased, and the operating conditions were varied to match the selected algal strain. The polyol reactor unit selected for analysis shared the same process design and process scale as the unit modelled for this LCA, however, the operating conditions and material quality differ. The operating conditions of the model reactor unit were selected for production of microalgal oil instead of microalgal biomass, thus the operation was modified to account for the change in material being processed. The data collection methods of all three unit processes received lower scores because of the narrow scope of the selected studies and their lack of representativeness of the total market. Finally, process review scores of 3 were given to all unit processes due to their lack of additional third-party reviews. Overall, the quality of the data collected for this LCA was considered satisfactory despite the identified data gaps.

Table 15. Data quality indicators and scores for the unit processes within the microalgal polyol system boundary. These scores are representative of both dry and wet feedstocks.

Data Quality Indicator	Cultivation	Harvest & Dewatering	Polyol Synthesis
Flow reliability	2	2	3
Temporal correlation	1	1	2
Geographical correlation	1	1	1
Technological correlation	3	2	3

Table 15 (cont'd)

Data collection methods	4	4	3
Process review	3	3	3
Process completeness	1	2	1

Inventory

The key inputs and outputs from the mass and energy balances of the microalgal polyol production systems can be seen in Table 16. Because the cultivation systems for the two microalgal polyols are identical, their daily inputs are identical as well. However, the daily production of biomass differs between the two systems due to the water content goals. The dry biomass feedstock is dried after dewatering to reach moisture content of ~20%, while the wet biomass has a moisture content of ~80% after dewatering and receives no additional drying. Therefore, although the inputs to each PBR are identical, the daily production of the dry biomass feedstock is less than that of the wet biomass feedstock. Downstream, this leads to a significantly lower daily production of polyol than the wet biomass system. This effect is compounded by the different amine values of each polyol's amine derivatives and the resulting difference in PC requirements. Based on a 10% molar excess, the mass ratios of PC to biomass are approximately 8:1 and 4:1 for dry and wet feedstocks, respectively.

Table 16. Key flows for microalgal polyol inventories, including the daily production of biomass that is ultimately consumed during polyol synthesis. All -e notations represent electricity consumption.

Input Flow	Dry	Wet	Unit
Freshwater	3	3	m^3/day
Nitrogen	28	28	kg/day
Phosphorous	7	7	kg/day
Carbon dioxide	375	375	kg/day
Cultivation	77	77	kWh-e/day
Centrifuge	280	280	kWh-e/day
Dryer	503	-	kWh-e/day
Monoethanolamine	938	3750	kg/day

Table 16 (cont'd)

Propylene carbonate	2523	5045	kg/day
Polyol reactor	2129	5670	kWh-e/day
Output Flow	Dry	Wet	Unit
Microalgal biomass	313	1250	kg/day
Microalgal polyol	3577	9525	kg/day

For both biomass polyols, all the carbon in the original biomass, less the losses experienced during production, is retained in the final product. However, based on the mass ratios in the final polyol product and the carbon content of each component, the renewable carbon content is 7% and 3% for dry and wet microalgal polyols, respectively. The majority of the carbon in the final polyol product is from PC, which is derived from propylene, a common petrochemical. Although this is a relatively small amount of fossil carbon being replaced, it is not insignificant and should still be regarded as a reduction in fossil reliance.

Impact assessment

Figure 17 shows a summary of the impacts from the dry microalgal, wet microalgal and polyether polyols. The ecotoxicity impacts of the microalgal polyols were significantly higher compared to the polyether polyol. This difference is likely due to the emissions assumptions made for the mass balance and the resulting inventory. This is also likely the case for freshwater eutrophication, where the assumption was made that the emissions of nitrogen and phosphorous were equal to 100% of the nitrogen and phosphorous present in the wastewater that did not get recycled during cultivation. In addition to a slightly higher ecotoxicity impact than the wet feedstock, the dry feedstock also resulted in much higher eutrophication. As was previously noted, these differences are due to each polyols characteristics, and biomass and polyol production rates. While the eutrophication impact of the microalgal systems was anticipated to

be higher, the significant difference for both eutrophication and ecotoxicity could be reduced with more accurate assumptions and more data.

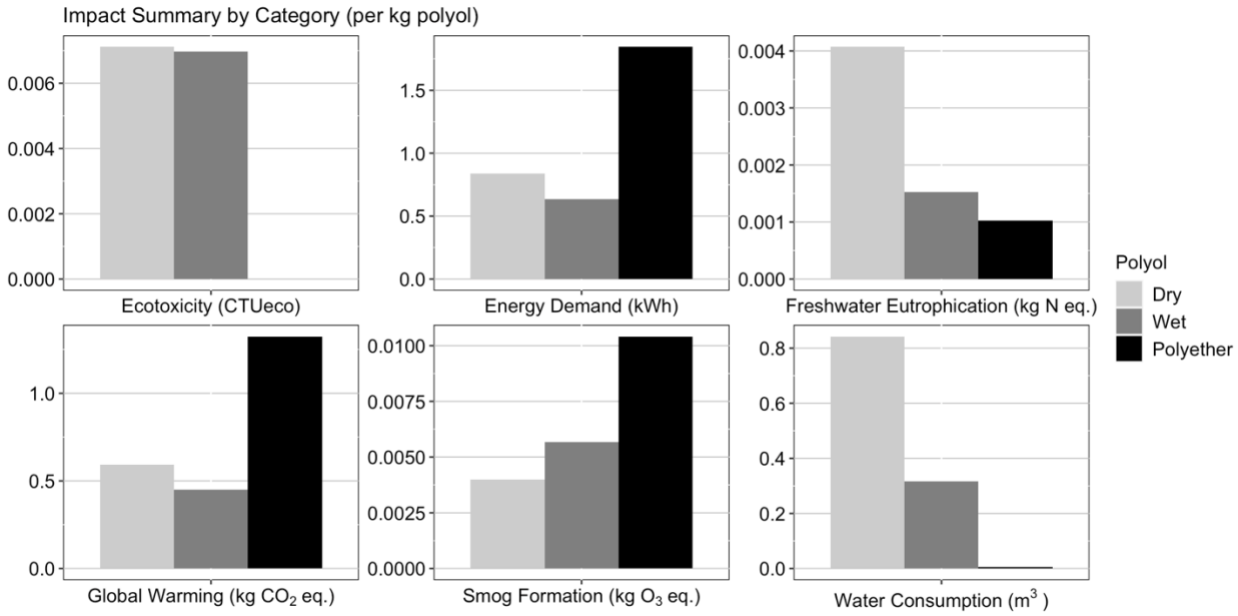

Figure 17. Impact assessment summary of dry and wet microalgal polyols compared to a conventional polyether polyol. Results are shown relative to the production of a functional unit (1 kg polyol).

The global warming impacts of the dry and wet microalgal polyols were 2-3 times less than the polyether polyol. This result directly coincides with the energy demand of the polyether system being 2-3 times higher than the microalgal systems. This difference in energy demand is substantial when considering the cultivation and production of biomass carbon is included in the microalgal systems. When comparing the microalgal polyols, the dry feedstock resulted in a higher energy demand and global warming impact than the wet feedstock. On the other hand, the smog formation impact from the wet polyol was slightly higher than the impact from the dry polyol. This is a result of the differences in MEA and PC inputs. The polyether polyols smog formation impact was also 2-3 times higher than dry and wet microalgal polyols. Finally, the water consumption of the microalgal polyols was found to be significantly larger than the

polyether polyol. This result was to be expected, considering the water requirements of microalgal cultivation.

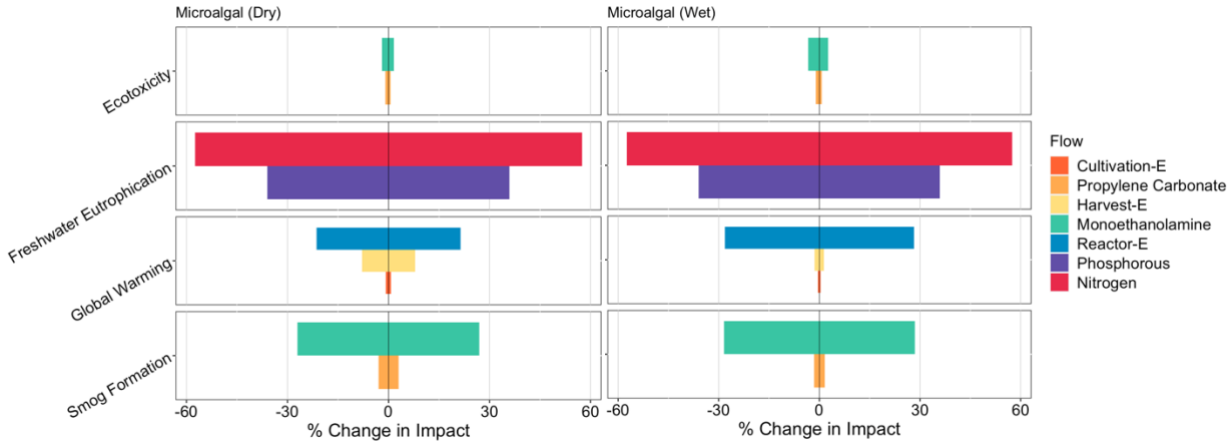

Figure 18. Life cycle impact sensitivity analysis of dry and wet microalgal polyols. Results show the percent change in each impact category when the original flows were varied ±30%.

Figure 18 shows the sensitivity analysis of the impact results for the microalgal polyols. For all categories and flows, a -30% change corresponds to a negative change in impact and a +30% corresponds to a positive change. For both polyols, the ecotoxicity impacts were more sensitive to changes in the flow MEA than the flow of PC. The wet feedstock was more sensitive to changes in the flows of MEA and PC than the dry feedstock. The eutrophication impacts of both microalgal polyols showed the same response to changes in nitrogen and phosphorous flows. This is a result of the identical operating conditions during cultivation, despite different daily production values for each feedstock. These large responses in eutrophication impacts only reiterate the importance of the emission assumptions made during the mass balance of the cultivation system.

Despite having a lower energy demand per kg of polyol, the wet polyol was found to be more sensitive to a change in the polyol reactor electricity consumption, and associated greenhouse gas emissions, than the dry polyol. Varying the cultivation and harvest electricity consumption

resulted in larger changes in the global warming impact for the dry polyol than the wet polyol. Both microalgal polyols resulted in a much lower impact when compared to the polyether polyol and improvements in the overall electricity consumption of microalgal polyol production would further reduce the global warming impact. While this reliance on grid electricity should still be of concern, recent shifts towards renewable energy sources, such as wind, suggest the global warming impacts from electricity generation will be reduced in the near future. Finally, both microalgal polyols showed similar changes in smog formation when varying MEA and PC. Notably, the sensitivity of PC was slightly larger in the dry polyol than in the wet. This is another demonstration of the effects that varying amine values and feedstocks can have on the overall life cycle impacts of the microalgal polyols.

Techno-economic assessment

Using n^{th} plant economic assumptions and a DCFROR analysis on the polyol production process based on 1,000 m^3 horizontal tubular PBR, the MPSP was estimated to be $1.73/kg and $1.39/kg for dry and wet microalgal polyols, respectively (Table 17). The difference in capital investment between the two polyols is due to the addition of drying during the harvest and dewatering process of the dry polyol. The two systems were assumed to require the same amount of labor for operation and thus, share the same fixed operational expenses. The significant increase in variable operational expenses for the wet polyol is a result of the higher annual polyol production and the associated increase in chemical inputs. Both MPSP's were found to be lower than the price of polyether polyol at $2.19/kg. This result is noteworthy when considering the cultivation, harvest, and dewatering unit processes were included in both microalgal system boundaries. On the other hand, the equivalent feedstock production and processing steps were not considered in the system boundary for the polyether polyol. While both microalgal polyols

have the potential to compete with current petrochemical-based polyols based on their respective MPSP's, the wet feedstock would be the preferable selection for a process scale facility. The low annual production rate and higher selling price make the dry feedstock less advantageous.

Table 17. TEA results and MPSP as determined through DCFROR analysis.

Metric	Microalgal (Dry)	Microalgal (Wet)
Total capital investment	$2,164,904	$1,688,106
Fixed operational expenses	$307,820	$307,820
Variable operational expenses	$1,433,067	$3,774,372
Annual loan payment	$184,363	$143,759
Polyol production rate (t/year)	1,177	3,133
Minimum polyol selling price ($/kg)	$1.73	$1.39

Figure 19 shows the results of the sensitivity analysis where each variable was varied ± 30%. PC was found to be more sensitive for the dry feedstock and this is likely due to the lower polyol production rate and the higher PC to biomass ratio compared to the wet feedstock. on the other hand, MEA was found to be the most sensitive variable for the wet feedstock. While both polyols were synthesized with a 1:3 MEA to biomass ratio, the lower PC to biomass ratio for the wet feedstock resulted in a higher proportion of MEA per kg of synthesized polyol when compared to the dry feedstock. This higher MEA to synthesized polyol ratio is likely the cause of the sensitivity of the flow of MEA for the wet feedstock. MEA and PC were found to be the second most sensitive variables for the dry and wet feedstocks, respectively. Overall, these chemical inputs were most sensitive due to the baseline magnitude of the flows accounting for over 90% of the final mass of synthesized polyol. The fixed capital investment was the next sensitive flow for the dry polyol and this is due to the higher capital investment, compared to the wet polyol. Alternatively, the next sensitive flow for the wet polyol was the total electricity

demand of the production process. Again, this can be owed to the higher production rate and subsequently, the higher energy consumption during polyol synthesis.

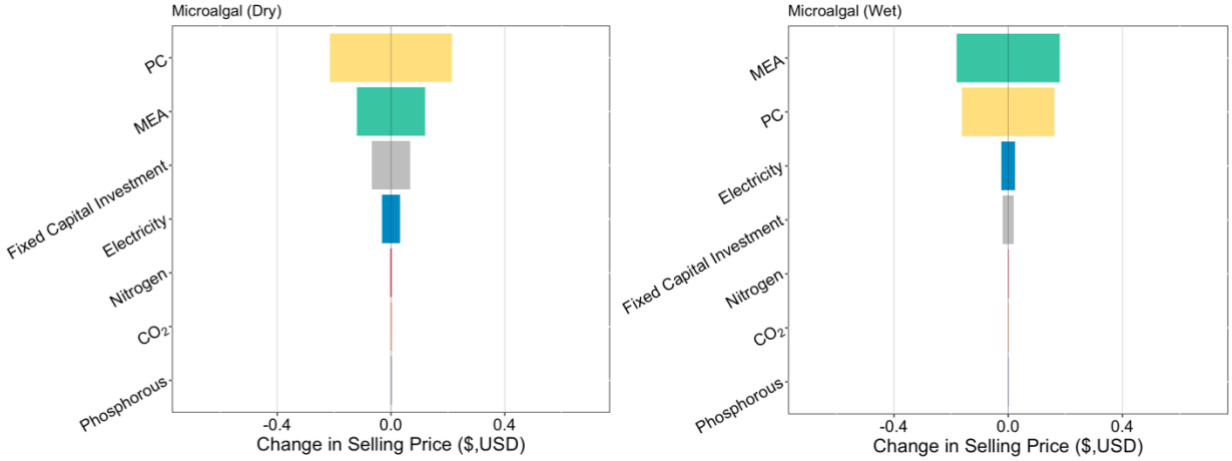

Figure 19. Techno-economic sensitivity analysis of dry and wet microalgal polyols. Results show the percent change in each polyols MPSP when the original flows were varied ±30%.

Conclusion

Polyols were successfully synthesized from microalgal biomass using a one-pot synthesis method. The characterization of the polyols from biomass and protein feedstocks, at 20% and 80% water content, show a close similarity to the characteristics from reference polyols. These likenesses strongly suggest that microalgal polyols have the potential to be a viable alternative to polyether polyols to produce rigid polyurethane foams. The results of the LCA indicate that microalgal polyols have environmental benefits, including lower global warming and smog formation impacts, and less energy demand compared to polyether polyols. On the other hand, the ecotoxicity, freshwater eutrophication and water consumption impacts of the microalgal polyols were greater than those from the polyether polyol. Notably, the results of the TEA conclude that the MPSP's of both dry and wet microalgal polyols were lower than the polyether polyol at $1.73/kg and $1.39/kg, respectively. Sensitivity analyses of both life cycle and techno-economic flows indicate that reducing the flow of MEA and PC would have the biggest impact

on both the overall environmental impact and the MPSP. Decreasing the flows of MEA and PC has the potential to reduce the MPSP by up to $0.36 and $0.42, respectively. This would increase the gap in selling prices between the microalgal polyols and polyether polyol, and further incentivize the use of microalgal biomass as a sustainable, renewable feedstock for polyol production. Despite these significant results, future work should focus on developing microalgal polyols with lower MEA to biomass ratios. The MEA to biomass ratio should be varied to optimize both hydroxyl value and viscosity, while prioritizing lower amine values which will result in a decreased flow of PC. Ultimately, decreasing reliance on MEA and PC will lead to better life cycle outcomes and will further reduce the MPSP of microalgal polyols.

CHAPTER 4: TECHNO-ECONOMIC AND LIFE CYCLE ASSESSMENT OF A COMBINED BIOLOGICAL AND CHEMICAL CARBON CAPTURE SYSTEM FOR THE POWER INDUSTRY

Introduction

Despite a recent dip in global greenhouse gas emissions, atmospheric carbon dioxide (CO_2) levels remain high and continue to pose a threat to our climate and planet [97]. With nearly 45% of global CO_2 emissions originating from power generation, there is an ongoing focus on the development of post-combustion carbon capture technologies. Technologies such as adsorption, membrane absorption and separation, and chemical absorption have long histories and have been studied extensively [2]. In particular, chemical absorption with alkanolamines, or amines, is a commercially accepted technology that has become the standard post-combustion capture method for electricity generation [24]. Of this class of chemical, monoethanolamine (MEA) is the most commonly used solvent for this application due to its ability to react readily with CO_2, with an absorption capacity of approximately 0.5 mol CO_2/mol amine and its low cost [25]. However, the primary amine has a limited capture, or loading, capacity and requires significant energy for regeneration that ultimately puts a strain on the host plants energy generation [128]. Regeneration, and the associated energy demands, are key factors when considering post-combustion carbon capture. To avoid unnecessary consumption and waste, a solvent must be regenerated and recycled for multiple capture cycles. If the regeneration energy of the solvent is too high, the solvent cannot be considered viable. Thus, recent research efforts on amine-based capture have been focused on the development of highly reactive, low-cost solvents that have low regeneration energy requirements.

In addition to concerns regarding the energy demand of conventional amines, there are also issues with corrosion, volatility, and oxidative degradation during scrubbing [2]. Amino acid salt solutions (AASS) have been explored as an alternative to amines because of their resistance to thermal and oxidative degradation, low volatility, low corrosion rates, and low toxicity [63,

129]. Although precipitation of amino acid salts may occur at high CO_2 loading, studies indicate that this may increase the overall loading capacity and will lead to lower regeneration energies [60]. There are limited studies evaluating the economics of AASS scrubbing systems, however, recent data indicate that they have the potential to be more cost effective than MEA scrubbing [130]. In particular, the initial cost of the AASS was found to be significantly higher compared to MEA, despite the annualized total makeup cost of the MEA solvent being larger overall. This difference in initial cost represents an opportunity to improve the overall economics of AASS capture systems.

In an effort to reduce the reliance on synthetic amino acids and decrease the initial solvent cost, biological sources should be explored. It has been reported that certain strains of microalgae have high protein content and, in some cases, protein accounts for over 50% of the dry matter [30]. Some of these protein-rich strains have complete amino acid profiles and represent a good source of amino acids [131]. However, microalgae have resilient cell walls that make cell disruption and total hydrolysis energy intensive processes [17, 132]. A recent study investigated the hydrolysis of the green microalgae *Chlorella sorokiniana* using a thermochemical treatment (paper under review). In addition, this study evaluated the effectiveness of the hydrolyzed biomass, or slurry, to act as a microalgal amino acid salt solution (MAASS). Results indicated that the MAASS had a cyclic absorption capacity of 1.27 mol CO_2/mol amine, which is over twice the capacity of conventional MEA solvents and synthetic AASS [25, 63]. A preliminary mass and energy balance indicated that the recyclability of the MAASS will be critical to the feasibility of this technology on a process scale.

The goal of this study was to evaluate this novel MAASS as a solvent and its' ability to capture 90% of the CO_2 emissions from a 100 MW, natural gas fired power plant. Life cycle and

techno-economic frameworks were applied to assess the viability of this technology. To compare the MAASS to commercial systems, an MEA post-combustion carbon capture system was also modelled for the same reference plant.

Materials and Methods

Microalgal amino acid salt solution preparation

Chlorella sorokiniana, a strain of green microalgae, was cultivated in a 100 L photobioreactor (PBR) under previously studied conditions [30, 108]. The biomass used for MAASS synthesis had a protein, lipid and carbohydrate content of 58.60 ± 2.41%, 9.70 ± 1.68%, and 19.5 ± 2.44%, respectively. The full methodology of solvent optimization and preparation has been previously reported (paper under review). Potassium hydroxide (KOH) is added to microalgal biomass with 20% solids (w/w) at a protein to KOH mole ratio of 1:5 using a stoichiometric relationship between nitrogen, protein and KOH. The mixture is then reacted at 134°C for 3 hours at atmospheric pressure to hydrolyze proteins, yielding an amino acid concentration of 67.19 g/L as detected by liquid chromatography mass spectrometry-mass spectrometry (LC/MS/MS). The hydrolyzed solution must be further processed to remove impurities and improve the final performance of the MAASS. Solids in the solution are first removed with centrifugation, followed by acidification with CO_2 to neutralize additional KOH and avoid the formation of potassium carbonate during absorption. Finally, the solution undergoes desorption and, subsequently, activation of the microalgal amino acids. The prepared solvent was found to have a cyclic absorption capacity of 1.27 mol CO_2/mol amine with a CO_2 concentration of 10% v/v. The time for absorption and desorption were recorded to be 120 and 100 minutes, respectively.

MAASS system operation

The studied system includes microalgal cultivation, MAASS production, and MAASS post-combustion CO_2 capture from flue gas (Figure 20). The T.B. Simon power plant on Michigan State University's campus was selected as the reference plant for this study. T.B. Simon is a natural gas fired system that generates approximately 100 MW of power and 1,000 metric tons (t) of CO_2 daily. Operating parameters of the capture system were based on the bench-scale MAASS study and then scaled to capture the daily CO_2 emissions from the reference power plant. Due to the co-located production facility, there is dual carbon capture by the microalgal cultivation system and MAASS scrubbing. The original bench-scale MAASS study tested recirculation of the MAASS up to 10 cycles and the data showed no degradation or decrease in absorption over that time. Additional analysis from this study showed that there is a log-like relationship between the number of cycles the MAASS can be used and the size of the PBR required to produce the solvent. That analysis indicates that the PBR required when the MAASS is recycled 2,000 or more times is of a realistic scale. Thus, this study assumes the maximum recyclability to be 2,000 cycles. Because the MAASS is non-volatile, it was assumed that any losses from the system would be negligible.

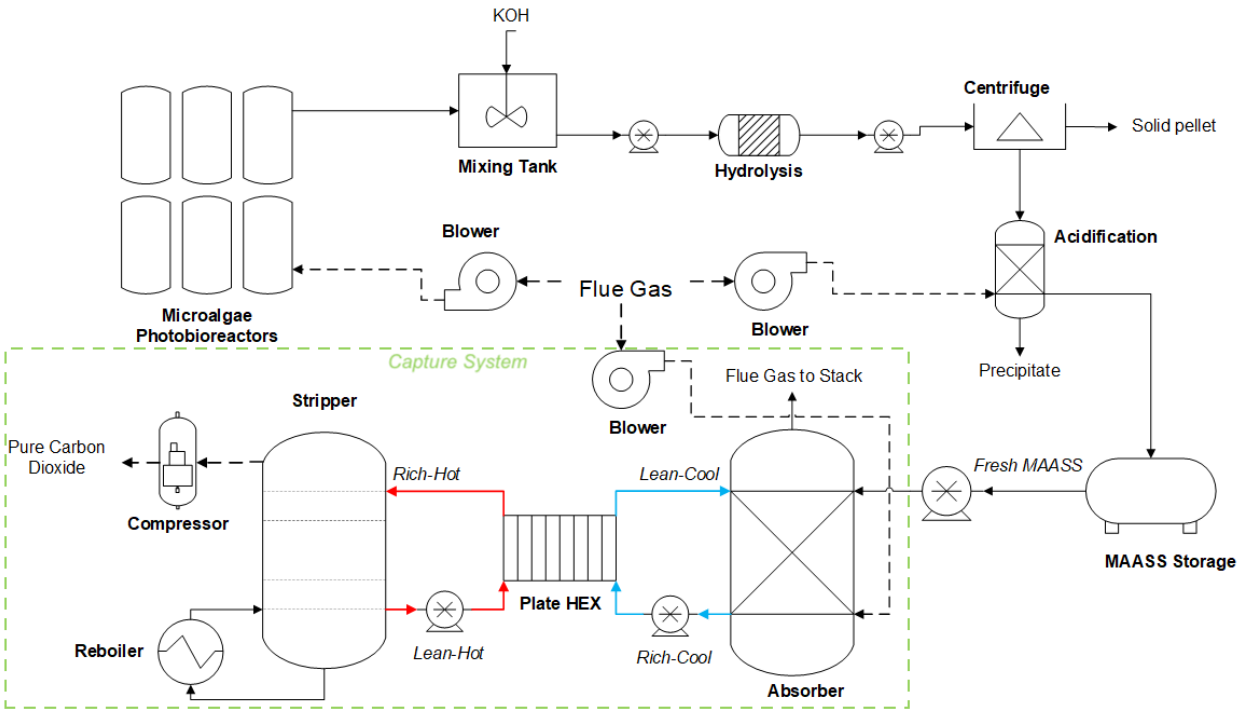

Figure 20. Process flow diagram of the MAASS production and capture system.

In addition to the empirical data and assumptions mentioned above, a calculated CO_2 consumption of 0.3 kg per kg wet biomass (20% solids w/w), a MAASS conversion efficiency of 0.44 kg MAASS per kg wet biomass and a CO_2 content of 10% v/v were all used in this analysis. To maintain the high productivity seen in previous studies cultivating *C. sorokiniana* in PBRs, an outdoor PBR system was selected for this study [30, 108]. The envisioned PBR uses a horizontal tubular set up that has been previously described [14, 109, 110]. The PBR was modelled using a productivity of 0.17 g/L/day, a harvest rate of 50% daily, and a water recycle system [30, 108]. This PBR configuration is estimated to have an area per volume ratio of 4.13 m^2/m^3. Collectively, these parameters were used to calculate the scale of the cultivation and production processes, as well as the scrubbing operation. A summary of the data and assumptions used can be seen in Table 18.

Table 18. Data and assumptions used to determine the scale and capacity of the MAASS production and capture system.

Parameter	Value	Unit
Absorption time	120	min
MAASS recyclability	2,000	cycles
Operating/production cycle	167	days
Microalgae CO2 consumption	0.30	kg CO_2/kg biomass
Biomass to MAASS conversion	0.44	kg MAASS/kg biomass
CO_2 content of flue gas	10	% v/v
CO_2 flow	1,000,000	kg/day
Absorption capacity	1.27	mol CO_2/mol amine
Biomass productivity	0.17	g/L/day
Daily harvest	50	% v/v
PBR area to volume ratio	4.13	m^2/m^3

Based on the bench-scale MAASS study, the temperature required for hydrolysis of microalgal biomass is 134°C and the starting temperature is assumed to be room temperature, or 25°C. The energy required for hydrolysis was calculated as heat energy using the heat equation (Equation 2) and then converted to electricity equivalents using a conversion factor of 3.6 MJ/kWh.

$$Q = c_p m \Delta T \qquad \textit{Equation 2}$$

The specific heat capacity of the hydrolyzed biomass, or microalgal slurry (biomass + KOH), was estimated to be 3.6 kJ/kg·K. Following solvent preparation and the removal of excess potassium salts, the heat capacity was assumed to increase to 3.8 kJ/kg·K. Heat is assumed to be supplied by the reference plant in the form of low-pressure steam. The density of the MAASS is 1,230 kg/m^3. The desorption required for MAASS preparation after acidification is assumed to be completed with a run of desorption in the stripper prior to the first cycle through the capture system.

MEA control system operation

A control system using MEA as a solvent was studied to evaluate the performance of the MAASS system. The capture process can be seen in the green boundary seen in Figure 20. A 30% w/w MEA solvent was selected for this study as it is one of the most commonly used concentrations [24]. A liquid solvent to flue gas (L/G) ratio of 3.7 kg/m^3 and an absorption capacity of 0.5 mol CO_2/mol amine were used for modelling [133-135]. A loading capacity of 0.5 mol CO_2/mol is based on both the theoretical chemical reaction between CO_2 and MEA, and empirical capture data for a 30% MEA solvent. Like the MAASS system, the MEA system was also modelled for 90% CO_2 capture at a 10% w/w CO_2 concentration in the flue gas. The density of a 30% MEA solvent is 1,003 kg/m^3 at 40°C and the specific heat capacity was assumed to be 3.734 kJ/kg·K before CO_2 capture and 3.359 kJ/kg·K after capture at 0.5 mol CO_2/mol amine loading [136, 137]. A degradation rate of 1.6 kg MEA/t CO_2 was used to model MEA loss from the system [55]. Unlike the MAASS system, where the number and time of each capture cycle was used, the MEA system used the degradation rate to determine the recyclability and addition of fresh solvent. A summary of the emissions produced because of the oxidative and thermal degradation of MEA can be seen in Table 19 [138-141]. Disposal of solid, hazardous reclaimer bottoms has been shown to account for a large portion of the waste and emissions created by MEA degradation and can cause significant negative impacts in human toxicity and ecotoxicity LCA impact categories [140, 142]. Although this study did not evaluate the impact of waste disposal practices, this finding is an important consideration when comparing the MAAS and MEA systems. Additional studies will be required to investigate the degradation and waste products of the MAASS under realistic flue gas flow and operating conditions.

Table 19. Emissions from the MEA capture system from degradation of the MEA solvent.

Emission	Value (kg/t CO_2)
Acetaldehyde	0.167
Ammonia	0.035
Formaldehyde	0.262
MEA	0.063

CO_2 capture parameters

The operational parameters of CO_2 scrubbing systems using amines have been previously documented and studied in detail [133, 138, 143, 144]. Due to the novelty of a MAASS capture system and the limited data on process parameters, the standard operating conditions of an MEA capture system were adopted for this study. The L/G ratio of the MAASS system was determined using a ratio of the absorption capacities of the two solvents, and the L/G ratio of 3.7 kg/m^3 for the MEA system. This resulted in a L/G ratio of 1.46 kg/m^3 for the MAASS system. The scrubbing operation is based on 90% carbon capture from the 100 MW reference plant that emits 1000 t CO_2 daily. The energy lost to heat was assumed to be 65% of the total energy capacity of the plant, yielding 2,400 MWh of electricity and 4,457 MWh-e of heat daily. The flue gas inlet temperature to absorber column and CO_2 rich MAASS outlet temperature from the absorber column were set at 40°C. Flue gas desulphurization and pre-cooling was not considered within the scope of this assessment. The CO_2 rich MAASS temperature exiting the plate and frame heat exchanger to desorption was set to 90°C and the temperature required for regeneration was set at 100°C and 110°C for MAASS and MEA solvents, respectively [133, 138] (paper under review). Finally, the CO_2 lean MAASS exiting the desorption column was assumed to be 100°C entering the heat exchanger and 40°C exiting the heat exchanger back to the absorption column. The energy required by the heat exchanger was determined by first calculating the heat loss from the lean-hot stream as the temperature decreased from 90°C to 60°C. The calculated heat energy was

used to find the resulting temperature increase in the rich-cool stream from a starting temperature of 40°C. Finally, the additional heat energy required to take the rich-cool stream from the calculated temperature to 90°C was determined and assigned as the energy demand of the counter flow, plate and frame heat exchanger.

The size and dimensions of the absorber, stripper and compression equipment can be determined using operating conditions and design equations in concert with mass and energy balance results [145]. However, due to the limitations of this study and cost data availability, equipment sizing was based on a similar report assessing the economic implications of different system configurations for the promising water-lean solvent technology [146]. The absorber diameter and height were assumed to be 20 m and 21 m, respectively, with an approximate volume of 6,600 m^3. Stripper height and diameter were assumed to be 10 m and 21 m, respectively, with an approximate volume of 1,650 m^3. Sulzer Mellapak™ 250Y (Winterthur, Switzerland) were used for packing the absorber and Koch-Glitsch Cascade Mini Rings® were used in the stripper. These dimensions were not considered in the performance analysis for this study, however the cost data for the capture system equipment was scaled accordingly for the TEA. The energy required for regeneration was calculated using the heat equation (Equation 2) and then converted to electricity equivalents. It is well known that using steam from the host plant for regeneration significantly reduces the efficiency of power generation and it's important to note that the steam required by the hydrolysis process will put additional strain on power generation.

Cooling water used during the capture and compression processes is estimated to be consumed at a rate of 0.8 $m^3/t\ CO_2$ for an MEA system [54]. Due to the lower temperature required for regeneration, the rate of water consumption for the MAASS system was assumed to

be 90% of that for the MEA system, or 0.72 m^3/t CO_2. The purpose of this study was not to optimize the process parameters and performance, but rather to provide a foundation for those future studies on the MAASS by evaluating its feasibility in a preliminary manner. Thus, despite the assumptions made to conduct this analysis, the results will provide rationale for further research projects in this area of study.

Life cycle assessment

Goal and scope

An LCA was conducted to compare the environmental impacts of a novel MAASS post-combustion carbon capture system to a conventional MEA system. A functional unit of 1 t CO_2 captured was selected to evaluate the two systems. The process flow diagram for the MAASS system is shown in Figure 20, with the capture process outlined in green. This green boundary represents the entirety of the MEA system is and fresh solvent is assumed to be added to the system with a pump to the lean-cool stream. Although the MAASS system has mass flows exiting the system that potentially have value-added components, further studies are needed to evaluate their economic value. Thus, no co-products were considered in this study and allocation was avoided.

The impacts of installing an MEA capture system at an operating power plant have been previously characterized [54, 138, 140, 147]. The data from these studies indicate that there are several tradeoffs to using amine solvents for carbon capture. While these carbon capture systems reduce the overall greenhouse gas emissions, and subsequently the global warming potential, they may cause greater impacts in categories such as acidification and ecotoxicity. The goal of this LCA was not to compare the impacts of a MAASS capture system and a reference plant with no capture system, but rather to identify the differences between MAASS and MEA solvents. A

functional unit of 1 t CO_2 captured will allow more cohesion between LCA and TEA results, and will highlight the environmental impact and economic cost of capture. Once the feasibility of this technology is established, future work should investigate the penalties associated with implementation compared to a no-capture scenario.

Data quality

Guidelines for data quality published by the U.S. Environmental Protection Agency were used to inform the data quality goals of this study [113]. Based on these guidelines, goals for temporal and geographical scale, as well as technological representativeness and data completeness, were chosen. The temporal data quality goal was set at 10 years due to the age of amine capture technologies, and the United States was selected as the geographical scale. These temporal and geographical targets were set to reflect the use of both primary and secondary data sources from locations around the U.S. The four categories within technological representativeness (process design, operating conditions, material quality, and process scale) allow the LCA practitioner to be diligent about process modelling, scale up, and assumptions. This study set goals in regards to technological representativeness based on transparency and clear data sourcing. Lastly, data completeness goals are based on an effort to include all flows within and crossing the system boundary. Due to the innovative nature of this study, and its foundation, accounting for 100% of the system flows becomes more challenging. Future work will be required to complete an analysis that fully meets this data completeness goal. In addition to the guidelines, updated data quality indicators and a scoring matrix were provided by the EPA [113].

Impact assessment

Although impact assessment methods such as ReCiPe are popular in the field of LCA, it does not contain characterization factors for chemicals like MEA. Therefore, the Tool for the Reduction and Assessment of Chemical and Other Environmental Impacts (TRACI) (v2.1, 2014) was selected for impact assessment. The following categories were used to evaluate the two systems: acidification (kg SO_2 eq.), ecotoxicity (CTUeco), freshwater eutrophication (kg N eq.), and smog formation (kg O_3 eq.). The upstream and downstream processes associated with each system have been identified as key contributors to the total global warming impact and should be assessed in future work. On the other hand, the processes within the system boundary were hypothesized to only contribute to the global warming impact in the form of energy use and were characterized as such. In lieu of evaluating the global warming impacts of the two systems, a carbon balance was performed by characterizing the electricity usage as CO_2 equivalent emissions. Greenhouse gas emissions from electricity use were characterized using the Greenhouse Gas Equivalencies Calculator provided by the U.S. Environmental Protection Agency (EPA) [114]. The energy demand (kWh) and water consumption (m^3) of each system were also evaluated.

Techno-economic assessment

In several amine-based capture reports, the Aspen Process Economic Analyzer, or similar software, is used to estimate the capital cost of the required equipment. Despite the validity of these results, there is little transparency associated with this type of software-based estimation and, without identical software access, repeatability may be an issue. Cost data used in this study will be explicitly cited and, where assumptions had to be made, rationale will be provided. It is important to acknowledge the limitations of techno-economic analysis in general, and even more

so in the case of innovative technologies like the foundational study that motivated this work. Cost data not reported in 2021 dollars were converted using the Plant Cost Index from *Chemical Engineering* [116]. Installation factors were applied to the purchase cost of all equipment to determine the final installed cost [119].

The capital cost of the horizontal tubular PBR was calculated in 2014 dollars using an area per volume ratio of 4.13 m^2/m^3 and a cost per volume ratio of \$44.65/m^3 [14, 109, 110]. The energy requirements of this PBR configuration were adapted for this study [14]. Cost data for the solvent storage tank, absorber, stripper, plate and frame heat exchanger, and flue gas blower were obtained from a previous report with similar operational parameters [146]. The cost data for all capture equipment was used directly for the MEA system, after converting to 2021 dollars, while the costs of the absorber, stripper, and plate and frame heat exchanger were scaled based on the reduced flow rate of the MAASS system. Capital cost scaling was done using a cost to capacity scaling method and an exponent of 0.61 [148]. All other equipment costs were estimated using current vendor prices and cost estimation curves [149]. Facility and site development costs were assumed to be 4% and 9% of the installed equipment cost, respectively. Indirect costs included construction fees, proratable expenses, field expenses, and project contingency. Construction fees were set at 20% of the total direct cost and the remaining expenses were set at 10% of the total direct cost. Finally, working capital was assumed to be 5% of the fixed capital investment.

The CO_2 used to feed the PBR was presumed to be provided at no additional cost, however, the delivery of the flue gas to the reactor was assumed to have a cost of \$45/t [14]. The capital cost of the infrastructure required for CO_2 delivery was included in the cost of the PBR. Nitrogen and phosphorous for cultivation were assumed to be purchased as bulk fertilizer. Prices

were obtained from the USDA Economic Research Service Fertilizer Use and Price dataset, however, purchase prices were only available up to 2014 [120]. Price indexes for the two chemicals were obtained from the BLS Data Finder, provided by the U.S. Bureau of Labor Statistics, and applied to the 2014 prices to determine the price in 2021 dollars. The cost of KOH was obtained from *Chemical Weekly* as $0.04/kg [150]. For the MEA system, the cost of MEA was obtained from ICIS Chemical Business [121]. For both solvent systems, the cost of electricity was assumed to be $0.12/kWh.

Labor costs for the MAASS system included the salaries of two chemical engineers, ten power plant operators, and four chemical technicians. The MEA system retained the same number of power plant operators and chemical technicians. The chemical engineers employed for the MAASS system were assumed to handle microalgal cultivation and solvent production and were therefore not needed for the operation of the MEA capture system. Salary data was obtained from the U.S. Bureau of Labor Statistics Occupational Outlook Handbook [123]. The analysis selected for this study was discounted cash flow rate of return (DCFROR). The DCFROR analysis used n^{th} plant economics assumptions to determine the cost of capture for both MAASS and MEA systems (Table 20) [36]. An annual operating time of 329 days was applied to calculate the annual carbon capture for each system.

Table 20. Assumptions made based on n^{th} plant economics for a DFROR analysis.

Assumptions	
Working Capital (% of FCI)	5%
Equity	40%
Loan Interest	8%
Loan Term (Years)	10
Salvage Value	$0
Depreciation Period (Years)	7
Construction Period (Years)	2
Capital Spent in Year -1 (% of Total)	50%

Table 20 (cont'd)

Capital Spent in Year 0 (% of Total)	50%
Start-up Time (Years)	0.5
Revenue (% of Normal)	50%
Variable Costs (% of Normal)	75%
Fixed Cost (% of Normal)	100%
Discount Rate (Internal Rate of Return)	10%
Income Tax Rate	35%
Cost Year for Analysis	2021

Current policies, such as Cap-and-Trade and carbon credits, have the potential to improve the economic feasibility of post-combustion carbon capture. To evaluate the efficacy of these programs, a policy scenario was applied and reductions in the cost of carbon capture were analyzed. The policy scenario included an assumed carbon credit of \$31/t CO_2 abated (captured) based on the most recent data from California's Air Resources Board Cap-and-Trade program [151]. In addition, it was assumed that a capital grant of \$25,000,000 was received and applied to the capital costs during the first year of construction for each capture system.

Sensitivity analysis

The results from the LCA and TEA were used to perform a sensitivity analysis. Individual flows were varied by ± 30%, while all other flows were kept constant, and the resulting change in LCA or TEA indicators was recorded. Key mass and energy flows were identified by comparing the magnitude of change across all flows.

Results and Discussion

Capture system operation

The analysis completed for the production and implementation of the MAASS was unique due to the need to balance the biological and chemical capture components in the system.

Using the recorded time for absorption and 2000 cycles, a batch of MAASS can be used for 167 days before it needs to be replaced with fresh solvent. Likewise, the production system has 167 days to produce the volume required to replace the wasted solvent. Based on this production cycle and the calculated solvent flow rate, approximately 38 kg of MAASS solvent would need to be produced daily. Applying a 0.43 kg MAASS/kg wet biomass conversion efficiency, daily biomass production was calculated to be 87.16 kg wet (17.43 kg dry). The microalgal culture was estimated to consume 26.15 kg CO_2/day and the MAASS solvent was estimated to capture 899,976 kg CO_2/day under 90% capture efficiency. As hypothesized, the biological capture makes up a small fraction, less than 0.01%, of the total carbon capture. Table 21 shows the key parameters of the MAASS system.

Table 21. MAASS system parameters.

Parameter	Value	Unit
Biomass production	87.16	wet kg/day
	17.43	dry kg/day
MAASS production	37.91	kg/day
MAASS flow	7,786	t/day
Flue gas flow	5,347,453	m^3/day
Biological CO_2 capture	26.15	kg/day
Chemical CO_2 capture (90% eff.)	899,976	kg/day

The operating conditions of the MEA system are quite different from the MAASS system as a result of the increased absorption capacity and the lower L/G ratio for the MAASS solvent. In addition, the analysis of the two systems differs due to the assumed degradation of the MEA solvent. In contrast to the batch-style and cyclic operation of the MAASS system, the MEA system experiences solvent loss that requires daily replacement. Using the estimated degradation rate of 1.6 kg MEA/t CO_2 produced, the system loses, and thus needs to replace, 1,600 kg of MEA daily. This difference in the stability of the two solvents will be a key variable in the life

cycle and techno-economic comparisons. Overall, the flow of MEA is over 2.5 times higher than MAASS when both systems are operating at 90% efficiency.

Table 22. MEA system parameters.

Parameter	Value	Unit
Fresh MEA	1,600	kg/day
MEA flow	19,778	t/day
Flue gas flow	5,347,594	m^3/day
Chemical CO_2 capture (90% eff.)	900,000	kg/day

Using the heat equation and the respective heat capacities of the two solvents, the regeneration energy was calculated to be 33.4 MWh-e/day and 154 MWh-e/day for MAASS and MEA, respectively. This significant difference in the regeneration energy was due to the lower flow rate of the MAASS solvent and the elevated stripper temperature of 110°C versus 100 °C for the MAASS solvent. This is a clear demonstration of the advantage of using the MAASS as an alternative to MEA. The temperature conditions of solvent heat exchange were identical for the two systems, however, the heat energy demand of the plate and frame heat exchanger to heat the rich MAASS was significantly lower than for MEA, at 187 MWh-e/day and 345 MWh-e/day, respectively. In addition to heat transfer and regeneration, the MAASS required further heat energy for hydrolysis of the microalgal biomass during solvent preparation. However, at 0.66 kWh-e/day, the additional energy demand was negligible. Overall, the total heat demand of the MEA system was found to be significantly higher than the MAASS system. Based on the total heat energy requirements of the two systems, it was assumed that the thermal energy from electricity generation at the natural gas-fired power plant would be more than sufficient to supply heat to the two system. Thus, no additional natural gas was required to provide heat energy for hydrolysis or stripping. A summary of the energy demands of the two systems can be seen in

Table 23. Although several assumptions were made during the course of this analysis in the absence of more specific data, the results are of reasonable accuracy for the purposes of comparing the MAASS and MEA systems.

Table 23. Energy demand of the unit processes for the MAASS and MEA systems.

Process	MAASS (MWh-e/day)	MEA (MWh-e/day)
Cultivation	$8.14x10^{-3}$	-
Solvent preparation	$3.80x10^{-3}$	-
Absorption[a]	3.72	4.53
Solvent heat exchange	187	345
Desorption[b]	33.9	155
Compression	41.7	41.7
Total energy demand	**266**	**546**

a. Absorption is the sum of the energy required for the flue gas blower and solvent pumping.
b. Desorption is the sum of the regeneration energy and the energy required for solvent pumping.

Life cycle assessment

Data quality

Data quality was assessed for each unit process in the microalgal and MEA capture systems and Table 24 shows the scores for each data quality category [113]. Scores of 1 and 2 represent quality data and were accepted as satisfactory. However, in order to address those less satisfactory scores of 3 and 4, rationale will be provided. A flow reliability score of 3 was given to MAASS production and carbon capture because the data used in the inventories were based on assumptions and calculations, rather than empirical data and measurements. A technological score of 3 for cultivation and carbon capture shows that two of the four sub-categories were equivalent, while the remaining two were modified. The modelled PBR maintained the original process design and material quality, however, the process scale and operating conditions were modified for this assessment. The carbon capture process modelled for analysis shared the same process design and process scale as the original system, however, the operating conditions and material quality varied. The MAASS production unit process received a technological correlation

score of 4 because 3 of the 4 sub-categories, process scale, process design, and operating conditions, were not equivalent. The data collection methods of cultivation and MAASS production unit processes received lower scores because of the scope of the selected studies was not representative of the market majority. Process review scores of 3 were given to all unit processes due to their lack of additional third-party reviews. Finally, MAASS production and carbon capture received process completeness scores of 3 due to the scarcity of data regarding the degradation products of the MAASS solvent. Overall, the quality of the data collected for this LCA was considered satisfactory considering the novelty of the MAASS production and capture process.

Table 24. Data quality indicators and scores for the unit processes within the MAASS and MEA system boundaries.

Data Quality Indicator	Cultivation	MAASS Production	Carbon Capture
Flow reliability	2	3	3
Temporal correlation	1	1	2
Geographical correlation	1	1	2
Technological correlation	3	4	3
Data collection methods	4	4	2
Process review	3	3	3
Process completeness	1	3	3

Impact assessment

Based on the results of mass and energy analysis, and the TRACI characterization factors, life cycle impacts were evaluated. Due to the scope of this assessment, the global warming impacts from both systems were exclusively the result of electricity usage and capture efficiency, and the resulting carbon emissions. Thus, the CO_2 emissions from the reference power plant, with and without a capture system, were evaluated using a carbon balance approach (Figure 21). Without carbon capture, emissions from the reference plant are 1,000 t CO_2/day.

Both MAASS and MEA solvents capture approximately 90% of the daily emissions, with the MAASS capturing an additional 2.62 kg CO_2/day. This additional capture is a result of the biological capture during microalgal cultivation, and it represents another slight advantage the MAASS system has over the traditional amine system. While both systems captured nearly the same amount of carbon, it's important to note that the MEA system "generated" slightly more native system emissions than the MAASS system due to a higher electricity demand. Additional value could be garnered from a cradle-to-grave LCA of the MAASS system that can more comprehensively evaluate the global warming impact of this alternative solvent.

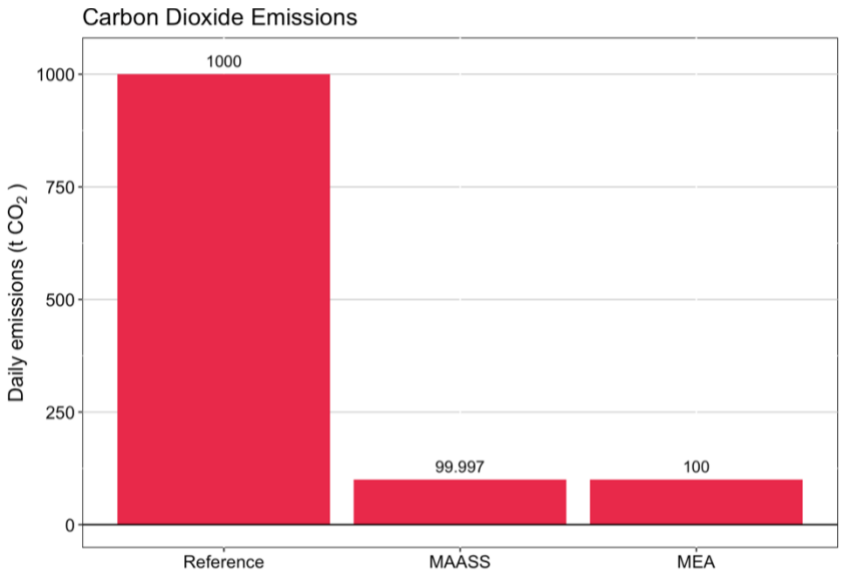

Figure 21. Carbon balance of the reference plant without carbon capture, and MAASS and MEA capture systems.

The life cycle impacts of a reference plant without capture and with capture using MEA have been previously studied [138, 140, 141, 147]. These studies represent a foundation for which the life cycle impacts of the MAASS solvent can be compared, hence the lack of comparison to a reference plant without capture in this LCA. While the degradation products and emissions profile of the MEA solvent have been previously studied and characterized, future studies are needed to investigate the degradation of the MAASS over 2,000 cycles and determine

if there are any harmful byproducts formed during this process. This lack of data for the MAASS is a limitation of this assessment and should be considered when comparing the two solvent systems.

The summary of life cycle impacts is a clear demonstration of the benefits of using MAASS instead of MEA for post-combustion carbon capture (Figure 22). Due to the observed stability and non-toxicity of the MAASS, and in the absence of more specific data, there were no life cycle impacts for acidification, ecotoxicity, and smog formation. The degradation of MEA resulted in daily air emissions of 31.5 kg ammonia, 0.150 kg acetaldehyde, 0.236 kg formaldehyde, and 56.7 kg MEA. Acidification and eutrophication impacts were solely the result of the daily ammonia emissions, while smog formation and ecotoxicity impacts were the result of contributions from acetaldehyde, formaldehyde, and MEA (Table 25). These impact results are comparable to other studies assessing the life cycle impacts of an MEA capture system [140].

Table 25. Life cycle impacts of the MAASS and MEA systems.

Impact Category	MAASS	MEA
Acidification (kg SO_2 eq./t CO_2 captured)	-	0.0658
Ecotoxicity (CTUeco/t CO_2 captured)	-	0.268
Eutrophication (kg N eq./t CO_2 captured)	$1.56x10^{-4}$	$4.51x10^{-3}$
Smog formation (kg O_3 eq./t CO_2 captured)	-	0.433

The small scale of cultivation resulted in relatively small mass flows of nutrients into the system, and thus, resulted in minor waterborne nitrogen and phosphorous emissions of less than 1 kg/day. On the other hand, the MEA system produced considerable amounts of airborne ammonia emissions every day. These mass flows resulted in significantly difference life cycle impacts, with the MEA system having much greater eutrophication than the MAASS system. This result is notable because of the common assumption that microalgal cultivation, and other cultivation systems, can result in significant local eutrophication. On the contrary, the ammonia

from MEA degradation led to much more impactful emissions and made a much larger contribution to eutrophication.

As previously noted, the MEA system required much more energy than the MAASS system (Table 23). The water consumption of the two systems was relatively similar, however, the MEA system consumed more water than the MAASS system at 720 m^3/day and 648 m^3/day. This difference is the result of the cooling water required for each solvent and the assumption that the MAASS capture process would only require 90% of the water consumed by the MEA process due to the lower regeneration temperature. While this result is significant considering the cultivation and preparation processes were included in the MAASS system assessment, further investigation is warranted to determine the exact water consumption.

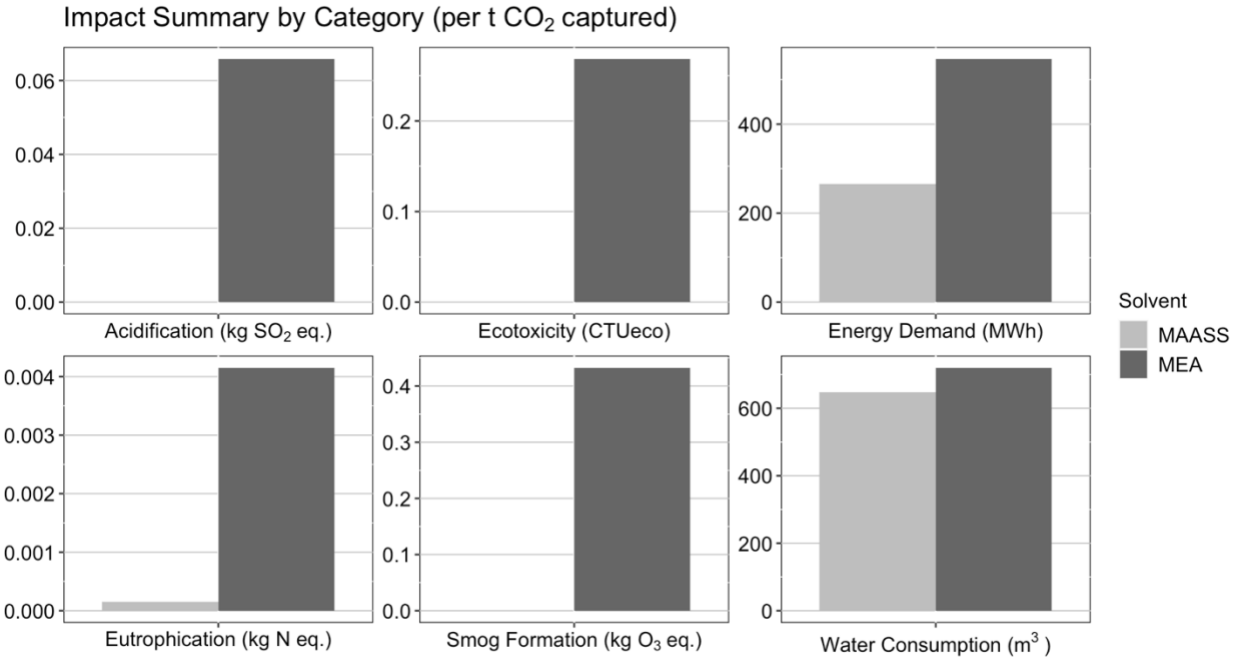

Figure 22. Impact assessment summary of MAASS and MEA solvents. Results are shown relative to the production of a functional unit (1 t captured CO_2).

Sensitivity analysis of the two systems impact results only confirm the conclusions made from the impact assessment. The MAASS system only resulted in eutrophication impacts, thus,

the sensitivity analysis was done only for this category. Figure 23 shows resulting change in eutrophication when the nitrogen and phosphorous flows were varied ± 30% while holding all other flows constant. Sensitivity analysis shows that the phosphorous flow, and the resulting impact, are much more sensitive to change than the nitrogen flow. This is caused by the magnitude of the mass flow and the characterization factors associated with the two chemicals.

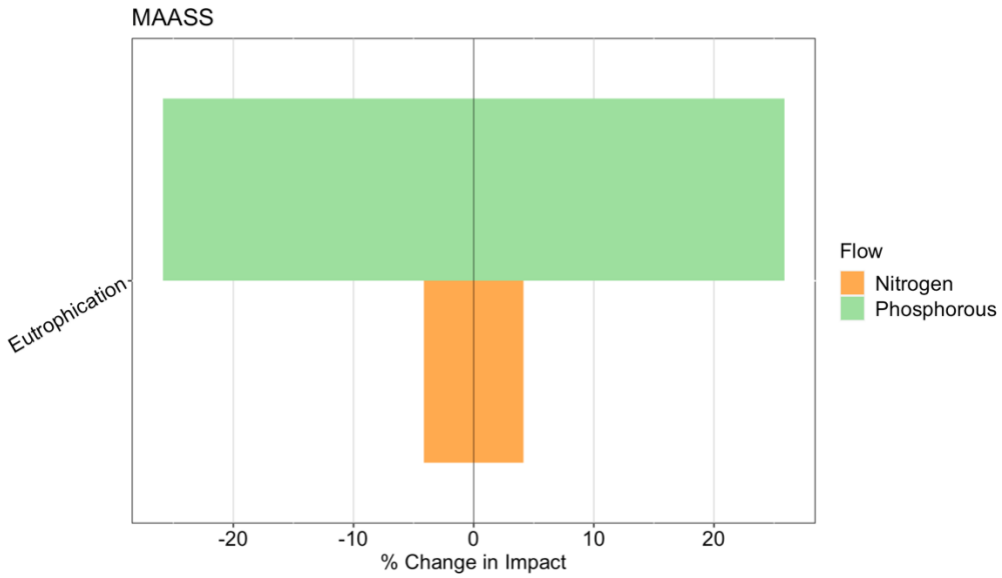

Figure 23. Life cycle impact sensitivity analysis of the MAASS solvent. Results show the percent change in each impact category when the original flows were varied ±30%.

For the MEA system, sensitivity analysis was carried out for all four life cycle impact categories (Figure 24). Ammonia was the only contributor to acidification and eutrophication impacts, and this is represented by one mass flow for each category. This also resulted in a change in impact that was proportional to the change in flow of ammonia. The result of the sensitivity analysis for ecotoxicity and smog formation impacts indicate that a similar relationship exists with these impact categories and MEA. This seemingly proportional change in impact is a result of the large flow of MEA, compared to acetaldehyde and formaldehyde. Although acetaldehyde and formaldehyde have similar, or larger, characterization factors for

these impact categories, they are present in much smaller amounts and contribute significantly less than MEA to the overall impact.

Despite the straightforward nature of these results, it's still important to note that the harmful degradation products of MEA should be strongly considered when searching for alternative solvents. In summary, the sensitivity analysis identified mass flows in each system that garner further examination and future research efforts should be dedicated to the reduction of these emissions.

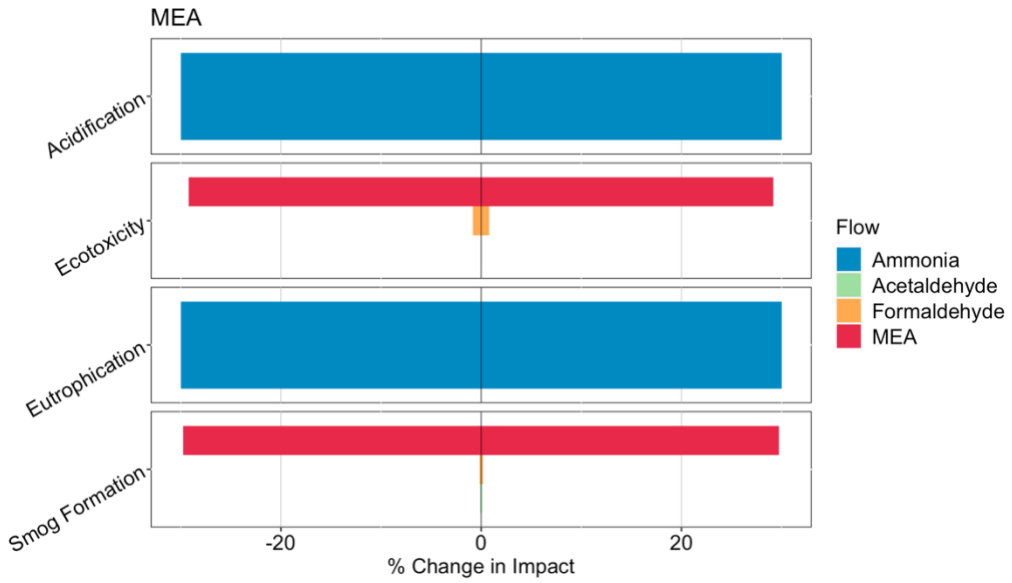

Figure 24. Life cycle impact sensitivity analysis of the MEA solvent. Results show the percent change in each impact category when the original flows were varied ±30%.

Techno-economic assessment

The capital costs for the capture system equipment were obtained from a previous report and applied for the MEA system, while the costs for the MAASS system were determined using the ratio of mass flow rates from each system and a cost-to-capacity method. In addition, the MAASS system cost was calculated with the equipment required for cultivation and harvesting of the microalgal biomass, as well as the production of the MAASS solvent. A complete list of equipment, indirect costs, and the total capital investment for both capture systems is provided in

Table 26. Due to the significant difference in solvent mass flows, the total capital investment for the MAASS system was considerably lower than for the MEA system, at $234,175,493 and $342,960,188, respectively. Based on a wet biomass production of 87.16 kg/day, the cultivation area was estimated to be 424 m^2 or approximately 0.10 acres. Thus, land purchase costs were not included in this analysis and it was assumed that the land requirements would be met by the existing infrastructure of the reference power plant. The low requirements for daily biomass and MAASS production resulted in minimal capital costs for cultivation and solvent preparation equipment, contributing approximately 1% to the overall capital investment.

Table 26. Capital costs of the MAASS and MEA carbon capture systems.

Item	MAASS	MEA
PBR	$6,549	-
Tank mixers (2)	$10,321	-
Mixing tank	$19,870	-
Hydrolysis reactor	$13,598	-
Centrifuge	$53,900	-
Acidification column	$118,112	-
Storage tank	$7,529,994	$7,529,994
Absorber	$57,786,583	$102,042,834
Stripper	$1,1051,067	$19,514,602
Plate heat exchanger	$14,992,595	$26,474,776
Compressor	$30,695,490	$30,695,490
Small blowers (2)	$1,365,160	-
Large blower	$13,149,200	$13,149,200
Production pumps (2)	$11,960	-
Solvent pumps (3)	$488,244	$488,244
Total equipment cost	**$137,292,643**	**$199,895,140**
Facility	$5,491,706	$7,995,806
Site development	$5,898,504	$9,861,555
Total direct cost	**$148,682,852**	**$217,752,500**
Construction fees, permits, start-up	$29,736,570	$43,550,500
Proratable expenses	$14,868,285	$21,775,250
Field expenses	$14,868,285	$21,775,250

Table 26 (cont'd)

Project contingency	$14,868,285	$21,775,250
Total indirect cost	**$74,341,426**	**$108,876,250**
Fixed capital investment	$223,024,279	**$326,628,750**
Working capital	$11,151,214	$16,331,438
Total capital investment	**$234,175,493**	**$342,960,188**

The annual fixed operational expenses of the MAASS and MEA systems were $1,364,260 and $1,147,180, respectively. The labor cost of the MAASS system was slightly higher because of the two chemical engineers tasked with solvent production. The annual variable operational expenses for the MAASS included the cost of CO_2 delivery, nitrogen, phosphorous, KOH, and electricity, totaling $1,844,818. Although the variable expenses for the amine system only included MEA and electricity, the price of MEA and the daily degradation rates of the solvent resulted in $2,697,999 in annual expenses. Collectively, the total capital investment and annual expenses resulted in a carbon capture cost of $113.53/t CO_2 and $163.31/t CO_2 for MAASS and MEA systems, respectively. This result is significant considering the scope of the MAASS system. A 30% lower cost of capture was achieved despite including microalgal cultivation and solvent production in the system boundary of the TEA. This means that the MAASS system is capable of producing the biobased solvent to be used for post-combustion carbon capture with a sustainable co-located operation, whereas MEA is produced off site using petrochemicals.

Table 27. Summary of TEA results, including annual fixed and variable expenses, and the cost of carbon capture determined using DCFROR analysis.

Metric	MAASS	MEA
Total capital investment	$234,175,493	$342,960,188
Fixed operational expenses	$1,364,260	$1,147,180
Variable operational expenses	$1,844,818	$2,697,999
Annual loan payment	$19,942,317	$26,206,389

Table 27 (cont'd)

Carbon capture (t/year)	296,101	296,100
Cost of carbon capture ($/t CO_2)	$113.53	$163.31

Sensitivity analysis of the TEA results for the MAASS system elucidated the lack of sensitivity of the material flows into the system. The results for the chemical and nutrient flows were not included in Figure 25 as they were negligible compared to the change in cost when the total capital investment and electricity demand were varied ± 30%. Varying the total capital investment and electricity demand changed the cost of capture by approximately $45.00 and $2.00, respectively. Comparatively, the changes in cost caused by varying the chemical flows were all less than $0.01. The absorption column and compressor account for nearly 40% of the total capital investment and therefore represent the equipment that should be re-evaluated. The cost of these key pieces of equipment could potentially be lowered with more accurate estimates or quotes from vendors. The electricity usage of the system was mostly due to the demand of the large flue gas blower for absorption and the solvent pumps in the capture system. While these operating conditions are difficult to reduce, more efficient equipment could be explored.

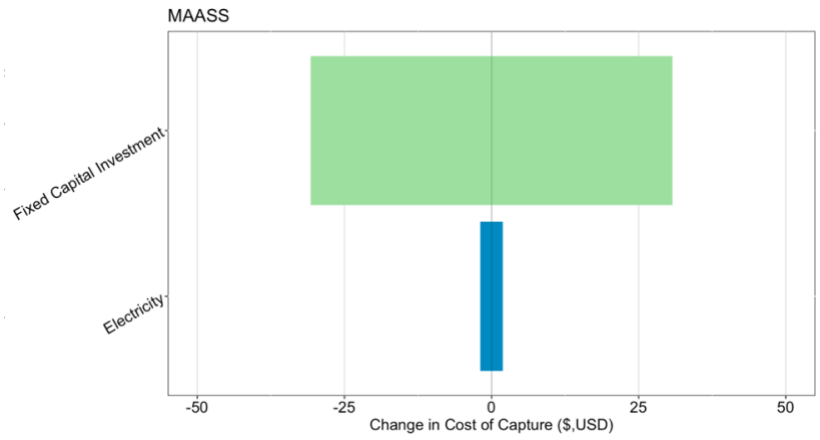

Figure 25. Techno-economic sensitivity analysis of the MAASS solvent. Results show the percent change in the cost of capture when the original flows were varied ±30%.

Unlike the MAASS system, the flow of MEA was not insensitive to changes and resulted in a $0.08 change in cost of capture. This indicates that while the MAASS system would be resilient to changing chemical prices, the MEA system would be impacted by this variability. This is particularly important in the case of MEA as it is a petrochemical and varies with the changing oil prices. The response of cost of capture to changes in the total capital investment and electricity demand mirrored that of the MAASS system. Varying the electricity usage changed the cost of capture by approximately the same dollar amounts as the MAASS system as well. These analogous responses are due to the similarity in total capital investment and electricity demand of the two systems and support the need for further analysis.

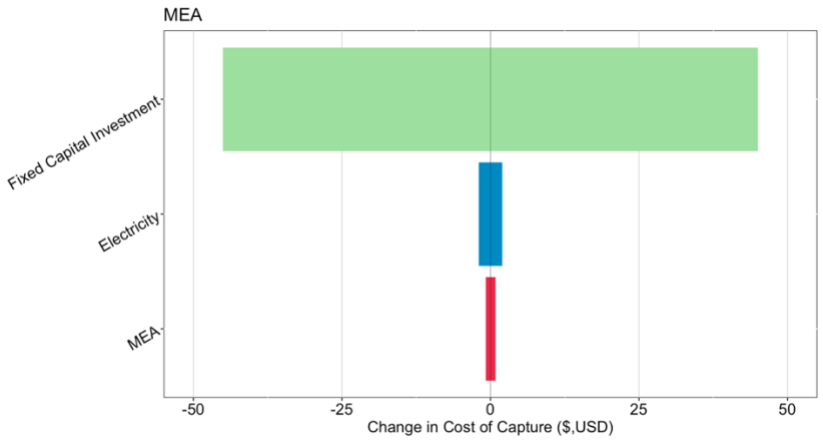

Figure 26. Techno-economic sensitivity analysis of the MEA solvent. Results show the percent change in the cost of capture when the original flows were varied ±30%.

The impact of the assumed carbon credits and capital grant can be seen in Figure 27. The dotted line represents the average cost of carbon capture from natural gas fired power plants, which was estimated to be approximately $74/t CO_2 captured [152]. The cost of carbon capture for both MEA and MAASS solvents was significantly reduced when applying a $31/t CO_2 carbon credit and assuming the allocation of a $25,000,000 capital grant. The cost of capture for both systems were reduced by approximately $14/t CO_2 and $32/t CO_2 when applying the capital grant and carbon credits, respectively. However, due to the lower baseline cost of capture for the

MAASS system, these policy-enabled reductions resulted in the cost of carbon capture reaching \$68.09/t CO_2. This is approximately \$6/t CO_2 lower than the reported average of \$74/t CO_2 and demonstrates the importance of policies when evaluating and implementing emerging technologies.

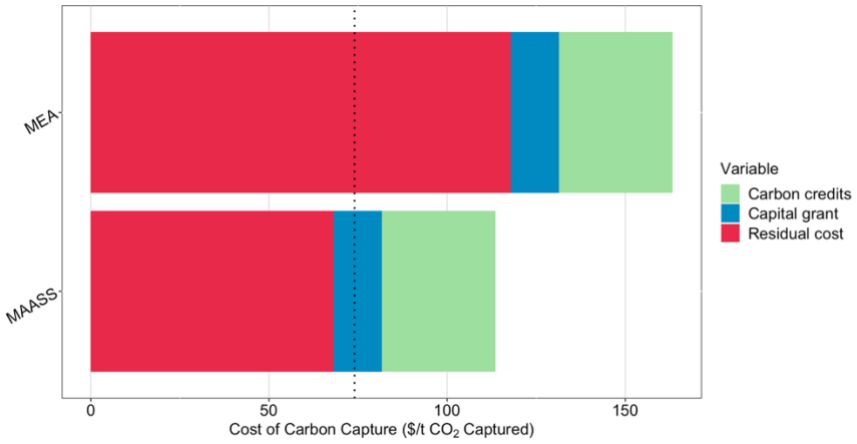

Figure 27. Cost of carbon capture when a policy scenario was considered, including carbon credits and a one-time capital grant.

Conclusions

This study elucidated that the MAASS production and capture processes are environmentally friendly, technically feasible, economically viable carbon capture technology that can significantly reduce CO_2 emissions from the power industry. Mass and energy analysis revealed that, due to a higher absorption capacity and lower mass flow rates, the MAASS system required significantly less heat energy for regeneration and solvent heat exchange when compared to MEA. The life cycle impact assessment revealed that the toxic byproducts of MEA degradation result in significantly higher life cycle impacts than the MAASS. The results of the TEA further demonstrated the advantages of the MAASS system, with the cost of the CO_2 capture being 30% lower than the MEA process. Policy plays a key role in the advancement and implementation of emerging technologies like the MAASS capture system. This was demonstrated by the results of

the policy scenario where the application of a realistic carbon credit and capital grant lowered the cost of carbon capture from \$113.53/t CO_2 to \$68.09/ t CO_2 using a MAASS capture system. This significant reduction results in a cost of capture that is less than the average at \$74/t CO_2. Based on these promising results, more studies on the MAASS, such as its potential degradation products, associated upstream and downstream impacts, and system optimization, need to be conducted to facilitate the technology transfer to the power industry.

CHAPTER 5: CONCLUSIONS AND FUTURE WORK

The results of the studies conducted herein support the feasibility of co-located microalgal cultivation and biomass utilization as a method for post-combustion carbon capture from the power industry. A 12-month continuous cultivation using natural gas fired flue gas was achieved and the optimal conditions of the culture were determined. A daily harvesting rate of 60% of the reactor volume with 24 hours of continuous light and using NH_4NO_3 as a nitrogen source and pH stabilization reagent resulted in optimal cultivation performance. The harvested biomass proved to be rich in protein, at 58.6% of the dry matter, despite the varying culture conditions. The different operating conditions were found to have no significant effect on culture performance and the microbial assemblage remained stable throughout the duration of the study, demonstrating the resilience of *C. sorokiniana*.

Biomass harvested from the 100 L PBR was used to optimize a mechanochemical protein extraction and recovery protocol. A protein extraction of $52.7 \pm 6.45\%$ was achieved and the acid precipitation method was able to recover 98.7% of proteins from a 20% w/w slurry. The energy analysis concluded that the energy demand of the cell disruption operation was 0.83 MJ/kg dry biomass. This is much lower than previous reports using high-pressure homogenization, making the mechanochemical method the preferred method for protein extraction. Collectively, this study suggests that mechanochemical protein extraction and recovery is an effective, low-energy processing method. Polyols were successfully synthesized from microalgal biomass harvested from the 100 L PBR and show a close similarity to the characteristics from reference polyols, indicating that microalgal polyols have the potential to be a viable alternative to petrochemical polyols. The results of the LCA indicate that microalgal polyols have some environmental tradeoffs, however the results of the TEA show that the MPSPs of the microalgal polyols are significantly lower than polyether polyol.

The LCA and TEA of the MAASS capture system demonstrated the advantages of using a biobased capture solvent as an alternative to amine solvents, like MEA. Mass and energy analyses concluded that the high absorption capacity of the MAASS led to significantly lower mass flow rates and thus, the MAASS system required significantly less heat energy for regeneration and solvent heat exchange when compared to MEA. The toxic byproducts of MEA degradation resulted in significantly higher life cycle impacts than the MAASS and the TEA concluded that MAASS solvent can achieve the same carbon capture efficiency with a 30% lower cost of the CO_2 compared to MEA.

A secondary outcome of this study was to identify the data gaps that still exist and the future work that needs to be completed based on the findings discussed herein. Although the protein extraction and recovery efficiencies indicate that the mechanochemical method was successful, the measured protein content of the protein isolate remained relatively low at 41.4% w/w. This suggests that the precipitation method is successful at recovering nearly all extracted proteins but is unsuccessful in the removal of non-protein cell matter. Future work needs to address the removal of all non-protein solids from the microalgal slurry to increase the purity of the protein isolate. In addition, further analysis should be completed to determine whether this method is viable on a process scale.

Sensitivity analyses of LCA and TEA results for the microalgal polyols elucidated that MEA and PC flows have the biggest impact on both the overall environmental impact and the MPSP. Future work should investigate the impact of modifying the polyol synthesis protocol to reduce PC consumption. The reduction of MEA could be achieved by using wet biomass as a feedstock with lower MEA mass ratios. Increasing the amount of biomass used while simultaneously reducing MEA consumption would increase the biobased content of the polyols and decrease the

environmental impacts of microalgal polyols. Finally, a cradle-to-grave LCA should be conducted to comprehensively evaluate the environmental impact of microalgal polyols compared to petrochemical polyols.

Despite the promising results of the LCA and TEA of a MAASS post-combustion carbon capture system, more studies on its potential degradation products, and the associated upstream and downstream impacts, are needed to affirm this result. The outlook on the results from future analyses of upstream processes is promising when comparing the two solvents, as MEA is a petrochemical and the MAASS does not rely on any petroleum-based products. Additional investigation and reassessment of the MAASS capture system is needed to continually prove the validity of the findings in this report.

The data and results reported in this document represent information that can be used by policymakers and industry to advance microalgal research and promote the adoption of sustainable microalgal technologies. Mass, energy, life cycle, and techno-economic analyses provide results that decision-makers can use to advance the implementation of emerging technologies. These frameworks are critical tools for communication of research findings and should be utilized as such. The results in this document represent the outcomes of collaboration between industry and research and demonstrate the actionable solutions that can come from such collaborations. Cooperation between industry, government, and research creates opportunities for real change to be made. The results of such opportunities have the potential to be policy changes, or new policy altogether, that will lead us to a more sustainable future.

APPENDICES

APPENDIX A:

Original Codes

```
   ## Statistical analysis
## Long Term algal cultivation

# Load libraries -----
  library (MASS)
  library(ggplot2)
  library(grid)
  library(gridExtra)
  library(ggpubr)
  library(plyr)
  library(inferr)
  library(extrafont)
  font_import()
  loadfonts(device="win")

# Plot bar chart with standard deviation -----
  #data: a data frame
  #varname: the name of a column containing the variable to be summarized
  #groupnames: vector of column names to be used as
  data_summary <- function(data, varname, groupnames){
    require(plyr)
    summary_func <- function(x, col){
      c(mean = mean(x[[col]], na.rm=TRUE),
        sd = sd(x[[col]], na.rm=TRUE))
    }
    data_sum<-ddply(data, groupnames, .fun=summary_func,
                    varname)
    data_sum <- rename(data_sum, c("mean" = varname))
    return(data_sum)
  }

# Choose data file metadata_main.txt -----
con <-file.choose(new = FALSE)
mastermetadata <- read.table(con, header = T, row.names = 1, fill = TRUE)
head(mastermetadata)
metadata<-mastermetadata[-c(1:9),] # removes data with missing NO3/NH3 measur
ements and places it into the metadata DF
head(metadata)

# Define factors for metadata and mastermetadata -----
metadata$Harvesting_amount <- factor(metadata$Harvesting_amount)
metadata$SO2_supplement <- factor(metadata$SO2_supplement)
metadata$Light_cycle <- factor(metadata$Light_cycle)
metadata$NaOH_addition <- factor(metadata$NaOH_addition)

mastermetadata$Harvesting_amount <- factor(mastermetadata$Harvesting_amount)
mastermetadata$SO2_supplement <- factor(mastermetadata$SO2_supplement)
mastermetadata$Light_cycle <- factor(mastermetadata$Light_cycle)
```

```r
mastermetadata$NaOH_addition<-factor(mastermetadata$NaOH_addition)

# Section 1: Effects of dark-light cycle on the cultivation -----
  # Select light cycle data; 30% harvesting with SO2 addition and no NaOH
  data1 <- metadata[which(metadata$Harvesting_amount=="30" & metadata$SO2_sup
plement=="Yes" & metadata$NaOH_addition=="No"),]
  data1$Light_cycle<-factor(data1$Light_cycle)

  ## Stats ##

  # Each data set is tested for normality
  # Normal data is tested for equal variance with an f test using var.test
  # Non-normal data is tested for equal variance with levenes test using infe
r_levene_test
  # Normal & equal variance-->t test, var.equal=TRUE
  # Normal & non-equal variance-->t test, var.equal=FALSE
  # Non-normal & equal variance-->KW test
  # Non-normal & non-equal varianve-->KW test

  # Biomass concentration
  # Normality
  shapiro.test(data1$Biomass_before_harvesting)
  # Variance
  infer_levene_test(data1, Light_cycle, Biomass_before_harvesting)
  # Significance
  kruskal.test(Biomass_before_harvesting ~ Light_cycle, data = data1)

  # Biomass productivity
  # Normality
  shapiro.test(data1$Biomass_productivity)
  # Variance
  var.test(Biomass_productivity ~ Light_cycle, data = data1)
  # Significance
  t.test(data1$Biomass_productivity ~ data1$Light_cycle,var.equal=FALSE)

  # pH
  # Normality
  shapiro.test(data1$pH_before_harvesting)
  # Variance
  var.test(pH_before_harvesting ~ Light_cycle, data = data1)
  # Significance
  t.test(data1$pH_before_harvesting ~ data1$Light_cycle,var.equal=TRUE)

  # TN reduction
  # Normality
  shapiro.test(data1$TN_reduction)
  # Variance
  infer_levene_test(data1, Light_cycle, TN_reduction)
  # Significance
  kruskal.test(TN_reduction ~ Light_cycle, data = data1)
```

```
  # TP reduction
  # Normality
  shapiro.test(data1$TP_reduction)
  # Variance
  infer_levene_test(data1, Light_cycle, TP_reduction)
  # Significance
  kruskal.test(TP_reduction ~ Light_cycle, data = data1)

  # NH3 reduction
  # Normality
  shapiro.test(data1$NH3_N_reduction)
  # Variance
  infer_levene_test(data1, Light_cycle, NH3_N_reduction)
  # Significance
  kruskal.test(NH3_N_reduction ~ Light_cycle, data = data1)

  # NO3 reduction
  # Normality
  shapiro.test(data1$NO3_N_reduction)
  # Variance
  var.test(NO3_N_reduction ~ Light_cycle, data = data1)
  # Significance
  t.test(data1$NO3_N_reduction ~ data1$Light_cycle,var.equal=TRUE)

  ## Plots ##

  #Biomass concentration
  box_1 <- ggplot(data1, aes(x=Light_cycle, y=Biomass_before_harvesting, fill
=Light_cycle)) +
    geom_boxplot() +
    xlab("Light-Dark Cycle")+
    ylab("Biomass Concentration (g/L)") + labs(title = "", subtitle=NULL) +
    theme_classic() +
    theme(title=element_text(size=20, family="Times New Roman"),
          axis.text.x = element_text(size=20, family="Times New Roman"),
          axis.text.y=element_text(size=20, family="Times New Roman"),
          axis.title.y = element_text(size = 20, family="Times New Roman"),
          axis.title.x=element_text(size=20, family="Times New Roman"), legen
d.position = "none") +
    scale_fill_manual(values=c("seagreen4", "darkgoldenrod1"))
  box_1

  # Biomass productivity
  box_2 <- ggplot(data1, aes(x=Light_cycle, y=Biomass_productivity, fill=Ligh
t_cycle)) +
    geom_boxplot() +
    xlab("Light-Dark Cycle")+
    ylab("Biomass Productivity (g/L/day)") + labs(title = "", subtitle=NULL)
+
```

```
    theme_classic() +
    theme(title=element_text(size=20, family="Times New Roman"),
          axis.text.x = element_text(size=20, family="Times New Roman"),
          axis.text.y=element_text(size=20, family="Times New Roman"),
          axis.title.y = element_text(size = 20, family="Times New Roman"),
          axis.title.x=element_text(size=20, family="Times New Roman"), legen
d.position = "none") +
    scale_fill_manual(values=c("seagreen4", "darkgoldenrod1"))
  box_2

  # pH
  box_3 <- ggplot(data1, aes(x=Light_cycle, y=pH_before_harvesting, fill=Ligh
t_cycle)) +
    geom_boxplot() +
    xlab("Light-Dark Cycle")+
    ylab("pH") + labs(title = "", subtitle=NULL) +
    theme_classic() +
    theme(title=element_text(size=20, family="Times New Roman"),
          axis.text.x = element_text(size=20, family="Times New Roman"),
          axis.text.y=element_text(size=20, family="Times New Roman"),
          axis.title.y = element_text(size = 20, family="Times New Roman"),
          axis.title.x=element_text(size=20, family="Times New Roman"), legen
d.position = "none") +
    scale_fill_manual(values=c("seagreen4", "darkgoldenrod1"))
  box_3

  # TN reduction
  box_4 <- ggplot(data1, aes(x=Light_cycle, y=TN_reduction, fill=Light_cycle)
) +
    geom_boxplot() +
    xlab("Light-Dark Cycle")+
    ylab("TN Consumed (mg/L/day)") + labs(title = "", subtitle=NULL) +
    theme_classic() +
    theme(title=element_text(size=20, family="Times New Roman"),
          axis.text.x = element_text(size=20, family="Times New Roman"),
          axis.text.y=element_text(size=20, family="Times New Roman"),
          axis.title.y = element_text(size = 20, family="Times New Roman"),
          axis.title.x=element_text(size=20, family="Times New Roman"), legen
d.position = "none") +
    scale_fill_manual(values=c("seagreen4", "darkgoldenrod1"))
  box_4

  # TP reduction
  box_5 <- ggplot(data1, aes(x=Light_cycle, y=TP_reduction, fill=Light_cycle)
) +
    geom_boxplot() +
    xlab("Light-Dark Cycle")+
    ylab("TP Consumed (mg/L/day)") + labs(title = "", subtitle=NULL) +
    theme_classic() +
    theme(title=element_text(size=20, family="Times New Roman"),
```

```
          axis.text.x = element_text(size=20, family="Times New Roman"),
          axis.text.y=element_text(size=20, family="Times New Roman"),
          axis.title.y = element_text(size = 20, family="Times New Roman"),
          axis.title.x=element_text(size=20, family="Times New Roman"), legen
d.position = "none") +
    scale_fill_manual(values=c("seagreen4", "darkgoldenrod1"))
  box_5

  # NH3 reduction
  box_6 <- ggplot(data1, aes(x=Light_cycle, y=NH3_N_reduction, fill=Light_cyc
le)) +
    geom_boxplot() +
    xlab("Light-Dark Cycle")+
    ylab("NH3 Consumed (mg/L/day)") + labs(title = "", subtitle=NULL) +
    theme_classic() +
    theme(title=element_text(size=20, family="Times New Roman"),
          axis.text.x = element_text(size=20, family="Times New Roman"),
          axis.text.y=element_text(size=20, family="Times New Roman"),
          axis.title.y = element_text(size = 20, family="Times New Roman"),
          axis.title.x=element_text(size=20, family="Times New Roman"), legen
d.position = "none") +
    scale_fill_manual(values=c("seagreen4", "darkgoldenrod1"))
  box_6

  # NO3 reduction
  box_7 <- ggplot(data1, aes(x=Light_cycle, y=NO3_N_reduction, fill=Light_cyc
le)) +
    geom_boxplot() +
    xlab("Light-Dark Cycle")+
    ylab("NO3 Consumed (mg/L/day)") + labs(title = "", subtitle=NULL) +
    theme_classic() +
    theme(title=element_text(size=20, family="Times New Roman"),
          axis.text.x = element_text(size=20, family="Times New Roman"),
          axis.text.y=element_text(size=20, family="Times New Roman"),
          axis.title.y = element_text(size = 20, family="Times New Roman"),
          axis.title.x=element_text(size=20, family="Times New Roman"), legen
d.position = "none") +
    scale_fill_manual(values=c("seagreen4", "darkgoldenrod1"))
  box_7

# Section 2: Effects of S on cultivation and biomass composition -----
  # Select SO2 data; 30% harvesting with no light cycle and no NaOH
  data2<-metadata[which(metadata$Harvesting_amount=="30" & metadata$NaOH_addi
tion=="No" & metadata$Light_cycle=="No"),]
  head(data2)

  ## Stats ##

  # Biomass concentration
  # Normality
```

```
  shapiro.test(data2$Biomass_before_harvesting)
  # Variance
  var.test(Biomass_before_harvesting ~ SO2_supplement, data = data2)
  # Significance
  t.test(data2$Biomass_before_harvesting ~ data2$SO2_supplement,var.equal=TRU
E)

  # Biomass productivity
  # Normality
  shapiro.test(data2$Biomass_productivity)
  # Variance
  infer_levene_test(data2, SO2_supplement, Biomass_productivity)
  # Significance
  kruskal.test(Biomass_productivity ~ SO2_supplement, data = data2)

  # pH
  # Normality
  shapiro.test(data2$pH_before_harvesting)
  # Variance
  var.test(pH_before_harvesting ~ SO2_supplement, data = data2)
  # Significance
  t.test(data2$pH_before_harvesting ~ data2$SO2_supplement,var.equal=TRUE)

  # TN reduction
  # Normality
  shapiro.test(data2$TN_reduction)
  # Variance
  infer_levene_test(data2, SO2_supplement, TN_reduction)
  # Significance
  kruskal.test(TN_reduction ~ SO2_supplement, data = data2)

  # TP reduction
  # Normality
  shapiro.test(data2$TP_reduction)
  # Variance
  infer_levene_test(data2, SO2_supplement, TP_reduction)
  # Significance
  kruskal.test(TP_reduction ~ SO2_supplement, data = data2)

  # NH3 reduction
  # Normality
  shapiro.test(data2$NH3_N_reduction)
  # Variance
  var.test(NH3_N_reduction ~ SO2_supplement, data = data2)
  # Significance
  t.test(data2$NH3_N_reduction ~ data2$SO2_supplement,var.equal=TRUE)

  # NO3 reduction
  # Normality
  shapiro.test(data2$NO3_N_reduction)
```

```
  # Variance
  var.test(NO3_N_reduction ~ SO2_supplement, data = data2)
  # Significance
  t.test(data2$NO3_N_reduction ~ data2$SO2_supplement,var.equal=TRUE)

  ## Plots ##

  #Biomass concentration
  box_8 <- ggplot(data2, aes(x=SO2_supplement, y=Biomass_before_harvesting, f
ill=SO2_supplement)) +
    geom_boxplot() +
    xlab("SO2 Supplement")+
    ylab("Biomass Concentration (g/L)") + labs(title = "", subtitle=NULL) +
    theme_classic() +
    theme(title=element_text(size=20, family="Times New Roman"),
          axis.text.x = element_text(size=20, family="Times New Roman"),
          axis.text.y=element_text(size=20, family="Times New Roman"),
          axis.title.y = element_text(size = 20, family="Times New Roman"),
          axis.title.x=element_text(size=20, family="Times New Roman"), legen
d.position = "none") +
    scale_fill_manual(values=c("seagreen4", "darkgoldenrod1"))
  box_8

  # Biomass productivity
  box_9 <- ggplot(data2, aes(x=SO2_supplement, y=Biomass_productivity, fill=S
O2_supplement)) +
    geom_boxplot() +
    xlab("SO2 Supplement")+
    ylab("Biomass Productivity (g/L/day)") + labs(title = "", subtitle=NULL)
+
    theme_classic() +
    theme(title=element_text(size=20, family="Times New Roman"),
          axis.text.x = element_text(size=20, family="Times New Roman"),
          axis.text.y=element_text(size=20, family="Times New Roman"),
          axis.title.y = element_text(size = 20, family="Times New Roman"),
          axis.title.x=element_text(size=20, family="Times New Roman"), legen
d.position = "none") +
    scale_fill_manual(values=c("seagreen4", "darkgoldenrod1"))
  box_9

  # pH
  box_10 <- ggplot(data2, aes(x=SO2_supplement, y=pH_before_harvesting, fill=
SO2_supplement)) +
    geom_boxplot() +
    xlab("SO2 Supplement")+
    ylab("pH") + labs(title = "", subtitle=NULL) +
    theme_classic() +
    theme(title=element_text(size=20, family="Times New Roman"),
          axis.text.x = element_text(size=20, family="Times New Roman"),
          axis.text.y=element_text(size=20, family="Times New Roman"),
```

```
          axis.title.y = element_text(size = 20, family="Times New Roman"),
          axis.title.x=element_text(size=20, family="Times New Roman"), legen
d.position = "none") +
    scale_fill_manual(values=c("seagreen4", "darkgoldenrod1"))
  box_10

  # TN reduction
  box_11 <- ggplot(data2, aes(x=SO2_supplement, y=TN_reduction, fill=SO2_supp
lement)) +
    geom_boxplot() +
    xlab("SO2 Supplement")+
    ylab("TN consumed (mg/L/day)") + labs(title = "", subtitle=NULL) +
    theme_classic() +
    theme(title=element_text(size=20, family="Times New Roman"),
          axis.text.x = element_text(size=20, family="Times New Roman"),
          axis.text.y=element_text(size=20, family="Times New Roman"),
          axis.title.y = element_text(size = 20, family="Times New Roman"),
          axis.title.x=element_text(size=20, family="Times New Roman"), legen
d.position = "none") +
    scale_fill_manual(values=c("seagreen4", "darkgoldenrod1"))
  box_11

  # TP reduction
  box_12 <- ggplot(data2, aes(x=SO2_supplement, y=TP_reduction, fill=SO2_supp
lement)) +
    geom_boxplot() +
    xlab("SO2 Supplement")+
    ylab("TP consumed (mg/L/day)") + labs(title = "", subtitle=NULL) +
    theme_classic() +
    theme(title=element_text(size=20, family="Times New Roman"),
          axis.text.x = element_text(size=20, family="Times New Roman"),
          axis.text.y=element_text(size=20, family="Times New Roman"),
          axis.title.y = element_text(size = 20, family="Times New Roman"),
          axis.title.x=element_text(size=20, family="Times New Roman"), legen
d.position = "none") +
    scale_fill_manual(values=c("seagreen4", "darkgoldenrod1"))
  box_12

  # NH3 reduction
  box_13 <- ggplot(data2, aes(x=SO2_supplement, y=NH3_N_reduction, fill=SO2_s
upplement)) +
    geom_boxplot() +
    xlab("SO2 Supplement")+
    ylab("NH3 consumed (mg/L/day)") + labs(title = "", subtitle=NULL) +
    theme_classic() +
    theme(title=element_text(size=20, family="Times New Roman"),
          axis.text.x = element_text(size=20, family="Times New Roman"),
          axis.text.y=element_text(size=20, family="Times New Roman"),
          axis.title.y = element_text(size = 20, family="Times New Roman"),
          axis.title.x=element_text(size=20, family="Times New Roman"), legen
```

```
d.position = "none") +
    scale_fill_manual(values=c("seagreen4", "darkgoldenrod1"))
  box_13

  # NO3 reduction
  box_14 <- ggplot(data2, aes(x=SO2_supplement, y=NO3_N_reduction, fill=SO2_s
upplement)) +
    geom_boxplot() +
    xlab("SO2 Supplement")+
    ylab("NO3 consumed (mg/L/day)") + labs(title = "", subtitle=NULL) +
    theme_classic() +
    theme(title=element_text(size=20, family="Times New Roman"),
          axis.text.x = element_text(size=20, family="Times New Roman"),
          axis.text.y=element_text(size=20, family="Times New Roman"),
          axis.title.y = element_text(size = 20, family="Times New Roman"),
          axis.title.x=element_text(size=20, family="Times New Roman"), legen
d.position = "none") +
    scale_fill_manual(values=c("seagreen4", "darkgoldenrod1"))
  box_14

# Section 3: pH stabilization using NH4NO3 and NaOH/NH4Cl -----
  # Data will be selected from modified metadata (mastermetadata) that includ
es dates missing NO3/NH3 data aka ph control days
  # Select pH data; 30% harvesting with no light cycle and no SO2
  data3<-mastermetadata[which(mastermetadata$Harvesting_amount=="30" & master
metadata$SO2_supplement=="No" & mastermetadata$Light_cycle=="No"),]
  head(data3)

  ## Stats ##

  # Biomass concentration
  # Normality
  shapiro.test(data3$Biomass_before_harvesting)
  # Variance
  infer_levene_test(data3, NaOH_addition, Biomass_before_harvesting)
  # Significance
  kruskal.test(Biomass_before_harvesting ~ NaOH_addition, data = data3)

  # Biomass productivity
  # Normality
  shapiro.test(data3$Biomass_productivity)
  # Variance
  infer_levene_test(data3, NaOH_addition, Biomass_productivity)
  # Significance
  kruskal.test(Biomass_productivity ~ NaOH_addition, data = data3)

  # pH
  # Normality
  shapiro.test(data3$pH_before_harvesting)
  # Variance
```

```
  var.test(pH_before_harvesting ~ NaOH_addition, data = data3)
  # Significance
  t.test(data3$pH_before_harvesting ~ data3$NaOH_addition,var.equal=TRUE)

  # TN reduction
  # Normality
  shapiro.test(data3$TN_reduction)
  # Variance
  infer_levene_test(data3, NaOH_addition, TN_reduction)
  # Significance
  kruskal.test(TN_reduction ~ NaOH_addition, data = data3)

  # TP reduction
  # Normality
  shapiro.test(data3$TP_reduction)
  # Variance
  var.test(TP_reduction ~ NaOH_addition, data = data3)
  # Significance
  t.test(data3$TP_reduction ~ data3$NaOH_addition,var.equal=TRUE)

  # There is no NH3 or NO3 data for the pH control data

  ## Plots ##

  #Biomass concentration
  box_15 <- ggplot(data3, aes(x=NaOH_addition, y=Biomass_before_harvesting, f
ill=NaOH_addition)) +
    geom_boxplot() +
    xlab("NaOH Supplement")+
    ylab("Biomass Concentration (g/L)") + labs(title = "", subtitle=NULL) +
    theme_classic() +
    theme(title=element_text(size=20, family="Times New Roman"),
          axis.text.x = element_text(size=20, family="Times New Roman"),
          axis.text.y=element_text(size=20, family="Times New Roman"),
          axis.title.y = element_text(size = 20, family="Times New Roman"),
          axis.title.x=element_text(size=20, family="Times New Roman"), legen
d.position = "none") +
    scale_fill_manual(values=c("seagreen4", "darkgoldenrod1"))
  box_15

  # Biomass productivity
  box_16 <- ggplot(data3, aes(x=NaOH_addition, y=Biomass_productivity, fill=N
aOH_addition)) +
    geom_boxplot() +
    xlab("NaOH Supplement")+
    ylab("Biomass Productivity (g/L/day)") + labs(title = "", subtitle=NULL)
+
    theme_classic() +
    theme(title=element_text(size=20, family="Times New Roman"),
          axis.text.x = element_text(size=20, family="Times New Roman"),
```

```
          axis.text.y=element_text(size=20, family="Times New Roman"),
          axis.title.y = element_text(size = 20, family="Times New Roman"),
          axis.title.x=element_text(size=20, family="Times New Roman"), legen
d.position = "none") +
    scale_fill_manual(values=c("seagreen4", "darkgoldenrod1"))
  box_16

  # pH
  box_17 <- ggplot(data3, aes(x=NaOH_addition, y=pH_before_harvesting, fill=N
aOH_addition)) +
    geom_boxplot() +
    xlab("NaOH Supplement")+
    ylab("pH") + labs(title = "", subtitle=NULL) +
    theme_classic() +
    theme(title=element_text(size=20, family="Times New Roman"),
          axis.text.x = element_text(size=20, family="Times New Roman"),
          axis.text.y=element_text(size=20, family="Times New Roman"),
          axis.title.y = element_text(size = 20, family="Times New Roman"),
          axis.title.x=element_text(size=20, family="Times New Roman"), legen
d.position = "none") +
    scale_fill_manual(values=c("seagreen4", "darkgoldenrod1"))
  box_17

  # TN reduction
  box_18 <- ggplot(data3, aes(x=NaOH_addition, y=TN_reduction, fill=NaOH_addi
tion)) +
    geom_boxplot() +
    xlab("NaOH Supplement")+
    ylab("TN consumed (mg/L/day)") + labs(title = "", subtitle=NULL) +
    theme_classic() +
    theme(title=element_text(size=20, family="Times New Roman"),
          axis.text.x = element_text(size=20, family="Times New Roman"),
          axis.text.y=element_text(size=20, family="Times New Roman"),
          axis.title.y = element_text(size = 20, family="Times New Roman"),
          axis.title.x=element_text(size=20, family="Times New Roman"), legen
d.position = "none") +
    scale_fill_manual(values=c("seagreen4", "darkgoldenrod1"))
  box_18

  # TP reduction
  box_19 <- ggplot(data3, aes(x=NaOH_addition, y=TP_reduction, fill=NaOH_addi
tion)) +
    geom_boxplot() +
    xlab("NaOH Supplement")+
    ylab("TP consumed (mg/L/day)") + labs(title = "", subtitle=NULL) +
    theme_classic() +
    theme(title=element_text(size=20, family="Times New Roman"),
          axis.text.x = element_text(size=20, family="Times New Roman"),
          axis.text.y=element_text(size=20, family="Times New Roman"),
          axis.title.y = element_text(size = 20, family="Times New Roman"),
```

```
          axis.title.x=element_text(size=20, family="Times New Roman"), legend.position = "none") +
    scale_fill_manual(values=c("seagreen4", "darkgoldenrod1"))
  box_19

  # There is no NH3 or NO3 data for the pH control data

# Section 4: Effects of cultivation conditions on biomass production and composition   -----
  # Select all data without light cycle
  data4<-metadata[which(metadata$Light_cycle=="No"),]
  head(data4)

  ## Stats ##

  # Each data set is tested for normality
  # Levenes test and KW test are used for all variance and significance testing when comparing harvesting amounts
  # var.test and t.test require grouping on two levels (yes/no) which can't be done with different harvesting amounts

  # Biomass concentration
  # Normality
  shapiro.test(data4$Biomass_before_harvesting)
  # Variance
  infer_levene_test(data4, Harvesting_amount, Biomass_before_harvesting)
  # Significance
  kruskal.test(Biomass_before_harvesting ~ Harvesting_amount, data = data4)

  # Biomass productivity
  # Normality
  shapiro.test(data4$Biomass_productivity)
  # Variance
  infer_levene_test(data4, Harvesting_amount, Biomass_productivity)
  # Significance
  kruskal.test(Biomass_productivity ~ Harvesting_amount, data = data4)

  # pH
  # Normality
  shapiro.test(data4$pH_before_harvesting)
  # Variance
  infer_levene_test(data4, Harvesting_amount, pH_before_harvesting)
  # Significance
  kruskal.test(pH_before_harvesting ~ Harvesting_amount, data = data4)

  # TN reduction
  # Normality
  shapiro.test(data4$TN_reduction)
  # Variance
  infer_levene_test(data4, Harvesting_amount, TN_reduction)
```

```r
  # Significance
  kruskal.test(TN_reduction ~ Harvesting_amount, data = data4)

  # TP reduction
  # Normality
  shapiro.test(data4$TP_reduction)
  # Variance
  infer_levene_test(data4, Harvesting_amount, TP_reduction)
  # Significance
  kruskal.test(TP_reduction ~ Harvesting_amount, data = data4)

  # NH3 reduction
  # Normality
  shapiro.test(data4$NH3_N_reduction)
  # Variance
  infer_levene_test(data4, Harvesting_amount, NH3_N_reduction)
  # Significance
  kruskal.test(NH3_N_reduction ~ Harvesting_amount, data = data4)

  # NO3 reduction
  # Normality
  shapiro.test(data4$NO3_N_reduction)
  # Variance
  infer_levene_test(data4, Harvesting_amount, NO3_N_reduction)
  # Significance
  kruskal.test(NO3_N_reduction ~ Harvesting_amount, data = data4)

  ## Plots ##

  #Biomass concentration
  box_20 <- ggplot(data4, aes(x=Harvesting_amount, y=Biomass_before_harvestin
g, fill=Harvesting_amount)) +
    geom_boxplot() +
    xlab("Harvesting Amount (%)")+
    ylab("Biomass Concentration (g/L)") + labs(title = "", subtitle=NULL) +
    theme_classic() +
    theme(title=element_text(size=20, family="Times New Roman"),
          axis.text.x = element_text(size=20, family="Times New Roman"),
          axis.text.y=element_text(size=20, family="Times New Roman"),
          axis.title.y = element_text(size = 20, family="Times New Roman"),
          axis.title.x=element_text(size=20, family="Times New Roman"), legen
d.position = "none") +
    scale_fill_manual(values=c("seagreen4", "darkgoldenrod1", "indianred", "d
odgerblue", "darkorange"))
  box_20

  # Biomass productivity
  box_21 <- ggplot(data4, aes(x=Harvesting_amount, y=Biomass_productivity, fi
ll=Harvesting_amount)) +
    geom_boxplot() +
```

```
    xlab("Harvesting Amount (%)")+
    ylab("Biomass Productivity (g/L/day)") + labs(title = "", subtitle=NULL)
+
    theme_classic() +
    theme(title=element_text(size=20, family="Times New Roman"),
          axis.text.x = element_text(size=20, family="Times New Roman"),
          axis.text.y=element_text(size=20, family="Times New Roman"),
          axis.title.y = element_text(size = 20, family="Times New Roman"),
          axis.title.x=element_text(size=20, family="Times New Roman"), legen
d.position = "none") +
    scale_fill_manual(values=c("seagreen4", "darkgoldenrod1", "indianred", "d
odgerblue", "darkorange"))
  box_21

  # pH
  box_22 <- ggplot(data4, aes(x=Harvesting_amount, y=pH_before_harvesting, fi
ll=Harvesting_amount)) +
    geom_boxplot() +
    xlab("Harvesting Amount (%)")+
    ylab("pH") + labs(title = "", subtitle=NULL) +
    theme_classic() +
    theme(title=element_text(size=20, family="Times New Roman"),
          axis.text.x = element_text(size=20, family="Times New Roman"),
          axis.text.y=element_text(size=20, family="Times New Roman"),
          axis.title.y = element_text(size = 20, family="Times New Roman"),
          axis.title.x=element_text(size=20, family="Times New Roman"), legen
d.position = "none") +
    scale_fill_manual(values=c("seagreen4", "darkgoldenrod1", "indianred", "d
odgerblue", "darkorange"))
  box_22

  # TN reduction
  box_23 <- ggplot(data4, aes(x=Harvesting_amount, y=TN_reduction, fill=Harve
sting_amount)) +
    geom_boxplot() +
    xlab("Harvesting Amount (%)")+
    ylab("TN consumed (mg/L/day)") + labs(title = "", subtitle=NULL) +
    theme_classic() +
    theme(title=element_text(size=20, family="Times New Roman"),
          axis.text.x = element_text(size=20, family="Times New Roman"),
          axis.text.y=element_text(size=20, family="Times New Roman"),
          axis.title.y = element_text(size = 20, family="Times New Roman"),
          axis.title.x=element_text(size=20, family="Times New Roman"), legen
d.position = "none") +
    scale_fill_manual(values=c("seagreen4", "darkgoldenrod1", "indianred", "d
odgerblue", "darkorange"))
  box_23

  # TP reduction
  box_24 <- ggplot(data4, aes(x=Harvesting_amount, y=TP_reduction, fill=Harve
```

```
sting_amount)) +
    geom_boxplot() +
    xlab("Harvesting Amount (%)")+
    ylab("TP consumed (mg/L/day)") + labs(title = "", subtitle=NULL) +
    theme_classic() +
    theme(title=element_text(size=20, family="Times New Roman"),
          axis.text.x = element_text(size=20, family="Times New Roman"),
          axis.text.y=element_text(size=20, family="Times New Roman"),
          axis.title.y = element_text(size = 20, family="Times New Roman"),
          axis.title.x=element_text(size=20, family="Times New Roman"), legen
d.position = "none") +
    scale_fill_manual(values=c("seagreen4", "darkgoldenrod1", "indianred", "d
odgerblue", "darkorange"))
  box_24

  # NH3 reduction
  box_25 <- ggplot(data4, aes(x=Harvesting_amount, y=NH3_N_reduction, fill=Ha
rvesting_amount)) +
    geom_boxplot() +
    xlab("Harvesting Amount (%)")+
    ylab("NH3 consumed (mg/L/day)") + labs(title = "", subtitle=NULL) +
    theme_classic() +
    theme(title=element_text(size=20, family="Times New Roman"),
          axis.text.x = element_text(size=20, family="Times New Roman"),
          axis.text.y=element_text(size=20, family="Times New Roman"),
          axis.title.y = element_text(size = 20, family="Times New Roman"),
          axis.title.x=element_text(size=20, family="Times New Roman"), legen
d.position = "none") +
    scale_fill_manual(values=c("seagreen4", "darkgoldenrod1", "indianred", "d
odgerblue", "darkorange"))
  box_25

  # NO3 reduction
  box_26 <- ggplot(data4, aes(x=Harvesting_amount, y=NO3_N_reduction, fill=Ha
rvesting_amount)) +
    geom_boxplot() +
    xlab("Harvesting Amount (%)")+
    ylab("NO3 consumed (mg/L/day)") + labs(title = "", subtitle=NULL) +
    theme_classic() +
    theme(title=element_text(size=20, family="Times New Roman"),
          axis.text.x = element_text(size=20, family="Times New Roman"),
          axis.text.y=element_text(size=20, family="Times New Roman"),
          axis.title.y = element_text(size = 20, family="Times New Roman"),
          axis.title.x=element_text(size=20, family="Times New Roman"), legen
d.position = "none") +
    scale_fill_manual(values=c("seagreen4", "darkgoldenrod1", "indianred", "d
odgerblue", "darkorange"))
  box_26
```

```
   ## Metagenomic analysis part A
## Alpha diversity, rarefaction, beta diversity
## Long Term Algal Cultivation

## Load libraries -----------------------------------------
  library(vegan)
  library(phyloseq)
  library (MASS)
  library(ggplot2)
  library(grid)
  library(gridExtra)
  library(ggpubr)
  #Gene frequency data from QIIME2

## Choose data files -----

 #Choose the FrequencyTable.txt
  con <- file.choose(new = FALSE)
  Frequency_Table <- read.table(con, header = T, row.names = 1)
  #Choose the FrequencyTable_Taxanomy.txt
  con1 <-file.choose(new = FALSE)
  Frequency_Table_taxonomy <- read.delim(con1, header = T, row.names = 1)

## Alpha Diversity -----
  #Create a matrix object with the data frame
  t.Frequency.table <- t(Frequency_Table)  # Transpose the data
  class(t.Frequency.table) # Check the class of the table

  #Alpha diversity analysis indexes
  #Shannon
  H <- diversity(t.Frequency.table, index = "shannon", MARGIN = 1, base = exp
(1))
  #Simpson
  D <- diversity(t.Frequency.table, "simpson", MARGIN = 1, base = exp(1))
  #Inverse Simpson
  iD <- diversity(t.Frequency.table, "inv")
  #Pielou's evenness
  J<-H/log(specnumber(t.Frequency.table))
  #List all indexes
  IN <- cbind(H,D,iD,J)
  IN
  write.csv(IN, "diversity.csv")

  #Plot H, D, iD, and J
  plot(H)
  plot(D)
  plot(iD)
  plot(J)

  #Estimate Chao1 and ACE
```

```
  estimateR(t.Frequency.table)

## ANOVA for Alpha Diversity -----

  #Using the H, D, iD, and J data to generate "alphadiversity.txt" to run one
way ANOVA
  #Choose alphadiversity.txt
  con3 <-file.choose(new = FALSE)
  alphadiversity <- read.table(con3, header = T, row.names = 1)

  #Define factors for alpha diversity
  alphadiversity$Harvesting_amount <- factor(alphadiversity$Harvesting_amount
)
  alphadiversity$SO2_supplement <- factor(alphadiversity$SO2_supplement)
  alphadiversity$NaOH_addition <- factor(alphadiversity$NaOH_addition)
  #Light cycle is not included because there are no microbial samples for "ye
s" light cycle

  #ANOVA of H index
  Hfit <- aov(H ~ Harvesting_amount*SO2_supplement*NaOH_addition, data = alph
adiversity)
  summary(Hfit)

  #ANOVA of D index
  Dfit <- aov(D ~ Harvesting_amount*SO2_supplement*NaOH_addition, data = alph
adiversity)
  summary(Dfit)

  #ANOVA of iD index
  iDfit <- aov(iD ~ Harvesting_amount*SO2_supplement*NaOH_addition, data = al
phadiversity)
  summary(iDfit)

  #ANOVA of J index
  Jfit <- aov(J ~ Harvesting_amount*SO2_supplement*NaOH_addition, data = alph
adiversity)
  summary(Jfit)

## Plots of H and J -----

  box_1 <- ggboxplot(alphadiversity, x = "Harvesting_amount", y = "H", color=
"Light_cycle")+ ylab("Shannon's Index (H)") +
    theme(legend.position="right",
          axis.text.x = element_text(size = 12, family="Times New Roman"),
          axis.title.x = element_blank(),
          axis.title.y = element_text(size = 14, family="Times New Roman"),
          axis.text.y = element_text(size = 12, family="Times New Roman"),
          legend.text = element_text(size = 12, family="Times New Roman"),
          legend.title = element_text(size = 14, family="Times New Roman"),
          plot.title= element_blank())
```

```
  box_1

  box_2 <- ggboxplot(alphadiversity, x = "Harvesting_amount", y = "J", color=
"Light_cycle")+ ylab("Pielou's Index (J)") +
    theme(legend.position="right",
          axis.text.x = element_text(size = 12, family="Times New Roman"),
          axis.title.x = element_blank(),
          axis.title.y = element_text(size = 14, family="Times New Roman"),
          axis.text.y = element_text(size = 12, family="Times New Roman"),
          legend.text = element_text(size = 12, family="Times New Roman"),
          legend.title = element_text(size = 14, family="Times New Roman"),
          plot.title= element_blank())
  box_2

## Rarefaction -----

  col <- c("black", "darkred", "forestgreen", "orange", "blue", "yellow", "ho
tpink")
  lty <- c("solid", "dashed", "longdash", "dotdash")
  pars <- expand.grid(col = col, lty = lty, stringsAsFactors = FALSE)
  head(pars)
  ra <- rarecurve(t.Frequency.table, step = 20, col =col,lty = lty, cex = 0.6
) # curve of rarefication
  rad <- rad.lognormal(t.Frequency.table) # Rank of Abundance
  rad1 <- plot(rad, xlab = "Rank", ylab = "Abundance") # Plotting the rank

## Beta diversity -----

  beta <- vegdist(t.Frequency.table, binary = TRUE)
  pcoa.obj <- capscale(t.Frequency.table ~ 1, distance = "bray")
  plot(pcoa.obj) #plot the PcoA plot
  text(scores(pcoa.obj)$sites[,1], scores(pcoa.obj)$sites[,2]) # change of th
e labes
  labels=row.names(t.Frequency.table)

## Vegan Tools -----

  #Rank Indexes study
  rankindex(scale(t.Frequency.table), t.Frequency.table, c("euc", "man", "bra
y", "jac", "kul"))

  #monMDS
  vare.mds <- metaMDS(t.Frequency.table, trace = FALSE)
  vare.mds
  plot(vare.mds, type ="t")
  stressplot(vare.mds)

  metaNMDS <- metaMDS(t.Frequency.table, distance = "bray",
                      k = 2, trymax = 20, engine = c("monoMDS"),
                      wascores = TRUE, expand = TRUE, trace = 1, plot = FALSE
```

```
) #Run the NMDS
  stressplot(metaNMDS)

  ordiplot(metaNMDS, type = "n")
  orditorp(metaNMDS, display = "species", choices = c(1,2), air = 1)

## Dendogram -----

  distance <-vegdist(t.Frequency.table, method="euclidean") ## Production of
Distance Matrix
  cluster <- hclust(distance, method="complete", members = NULL) ## Productio
n of Hierarchical Cluster Production
  tree_m <- plot(cluster, xlab = "Samples", sub = NULL, main ="Dendogram")

  range(distance)
  rect.hclust(cluster, k = 3, border = "red")
  grp <- cutree(cluster, k = 3)
```

```
   ## Metagenomic analysis part B, ANOVAs
## Relative abundance
## Long Term Algal Cultivation

## Load libraries -----
  library(vegan)
  library(phyloseq)
  library (MASS)
  library(ggplot2)
  library(grid)
  library(gridExtra)
  library(ggpubr)
  library(extrafont)
  font_import() #It may take a few minutes to import.
  loadfonts(device="win")

## Import data files -----

  #Choose RelativeFrequencyTable.txt
  con <- file.choose(new = FALSE)
  Frequency_Table <- read.table(con, header = T, row.names = 1)
  #Choose FrequencyTable_Taxanomy.txt
  con1 <-file.choose(new = FALSE)
  Frequency_Table_taxonomy <- read.delim(con1, header = T, row.names = 1)
  #Choose metadata_partb.txt
  con2 <-file.choose(new = FALSE)
  metadata <- read.table(con2, header = T, row.names = 1, fill = TRUE)

## Phyloseq -----
```

```
  Full_Frequency <- cbind.data.frame(Frequency_Table, Frequency_Table_taxonom
y)
  Frequency <- otu_table(Frequency_Table,taxa_are_rows = TRUE) #Frequency tab
le production for phyloseq
  TAX <- tax_table(as.matrix(Frequency_Table_taxonomy)) #Taxanomy production
for phyloseq
  physeq <- phyloseq(Frequency, TAX) #physeq document production
  physeq0 <- tax_glom(physeq, taxrank=rank_names(physeq)[7], NArm=TRUE, bad_e
mpty=c(NA, "", " ", "\t"))
  tax_table(physeq0)

## Overall abundances for Domain, Phylum, Class, Order, and Family ---------

  #Domain Abundance
  physeqa <-tax_glom(physeq, taxrank=rank_names(physeq)[1], NArm=TRUE, bad_em
pty=c(NA, "", " ", "\t"))
  tablea <- otu_table(physeqa)
  tablea
  write.csv(tablea, "domain.csv")

  #Phylum Abundance
  physeqa1 <-tax_glom(physeq, taxrank=rank_names(physeq)[2], NArm=TRUE, bad_e
mpty=c(NA, "", " ", "\t"))
  tablea1 <- otu_table(physeqa1)
  tablea1
  write.csv(tablea1, "Phylum.csv")

  #Class Abundance
  physeqa2 <-tax_glom(physeq, taxrank=rank_names(physeq)[3], NArm=TRUE, bad_e
mpty=c(NA, "", " ", "\t"))
  tablea2 <- otu_table(physeqa2)
  tablea2
  write.csv(tablea2, "Class.csv")

  #Order Abundance
  physeqa3 <-tax_glom(physeq, taxrank=rank_names(physeq)[4], NArm=TRUE, bad_e
mpty=c(NA, "", " ", "\t"))
  tablea3 <- otu_table(physeqa3)
  tablea3
  write.csv(tablea3, "Order.csv")

  #Family Abundance
  physeqa4 <-tax_glom(physeq, taxrank=rank_names(physeq)[5], NArm=TRUE, bad_e
mpty=c(NA, "", " ", "\t"))
  tablea4 <- otu_table(physeqa4)
  tablea4
  write.csv(tablea4, "Family.csv")

  #Genus Abundance
  physeqa5 <-tax_glom(physeq, taxrank=rank_names(physeq)[6], NArm=TRUE, bad_e
```

```
mpty=c(NA, "", " ", "\t"))
  tablea5 <- otu_table(physeqa5)
  tablea5
  write.csv(tablea5, "Genus.csv")

## Abundance Plotbar Bacteria -----

  #Bacteria Abundance (Phylum)
  physeq2 <-subset_taxa(physeq, Domain== "Bacteria")
  physeq2_1 <-tax_glom(physeq2, taxrank=rank_names(physeq2)[2], NArm=TRUE, ba
d_empty=c(NA, "", " ", "\t"))
  table2_1 <- otu_table(physeq2_1)
  write.csv(table2_1, "bacterialPhylum.csv")

  #Bacteroidetes Abundance (Family)
  physeq3 <-subset_taxa(physeq, Phylum == "Bacteroidetes")
  physeq3_1 <-tax_glom(physeq3, taxrank=rank_names(physeq3)[5], NArm=TRUE, ba
d_empty=c(NA, "", " ", "\t"))
  table3_1 <- otu_table(physeq3_1)
  table3_1
  write.csv(table3_1, "BacteroidetesFamily.csv")

  #Proteobacteria Abundance (Family)
  physeq5 <-subset_taxa(physeq, Phylum == "Proteobacteria")
  physeq5_1 <-tax_glom(physeq5, taxrank=rank_names(physeq5)[5], NArm=TRUE, ba
d_empty=c(NA, "", " ", "\t"))
  table5_1 <- otu_table(physeq5_1)
  table5_1
  write.csv(table5_1, "ProteobacteriaFamily.csv")

## ANOVA on abundances of key microbial communities -----

  #ANOVA Bacteria (Domain)
  Bacteria <- aov(Bacteria ~ Harvesting_amount*SO2_supplement*NaOH_addition,
data = metadata)
  summary(Bacteria)

  #ANOVA Eukarya (Domain)
  Eukarya <- aov(Eukarya ~ Harvesting_amount*SO2_supplement*NaOH_addition, da
ta = metadata)
  summary(Eukarya)

  #ANOVA Bacteroidetes (Phylum)
  Bacteroidetes <- aov(Bacteroidetes ~ Harvesting_amount*SO2_supplement*NaOH_
addition, data = metadata)
  summary(Bacteroidetes)

  #ANOVA Proteobacteria (Phylum)
  Proteobacteria <- aov(Proteobacteria ~ Harvesting_amount*SO2_supplement*NaO
H_addition, data = metadata)
```

```
  summary(Proteobacteria)

  #ANOVA Proteobacteria_unclassified (Class)
  Proteobacteria_unclassified <- aov(Proteobacteria_unclassified ~ Harvesting
_amount*SO2_supplement*NaOH_addition, data = metadata)
  summary(Proteobacteria_unclassified)

  #ANOVA Gammaproteobacteria (Class)
  Gammaproteobacteria <- aov(Gammaproteobacteria ~ Harvesting_amount*SO2_supp
lement*NaOH_addition, data = metadata)
  summary(Gammaproteobacteria)

  #ANOVA Alphaproteobacteria (Class)
  Alphaproteobacteria <- aov(Alphaproteobacteria ~ Harvesting_amount*SO2_supp
lement*NaOH_addition, data = metadata)
  summary(Alphaproteobacteria)

  #ANOVA Betaproteobacteria (Class)
  Betaproteobacteria <- aov(Betaproteobacteria ~ Harvesting_amount*SO2_supple
ment*NaOH_addition, data = metadata)
  summary(Betaproteobacteria)

  #ANOVA Actinobacteria (Class)
  Actinobacteria <- aov(Actinobacteria ~ Harvesting_amount*SO2_supplement*NaO
H_addition, data = metadata)
  summary(Actinobacteria)

  #ANOVA Bacteroidetes_unclassified (Family)
  Bacteroidetes_unclassified <- aov(Bacteroidetes_unclassified ~ Harvesting_a
mount*SO2_supplement*NaOH_addition, data = metadata)
  summary(Bacteroidetes_unclassified)

  #ANOVA Chitinophagaceae (Family)
  Chitinophagaceae <- aov(Chitinophagaceae ~ Harvesting_amount*SO2_supplement
*NaOH_addition, data = metadata)
  summary(Chitinophagaceae)

  #ANOVA Cytophagales_unclassified (Family)
  Cytophagales_unclassified <- aov(Cytophagales_unclassified ~ Harvesting_amo
unt*SO2_supplement*NaOH_addition, data = metadata)
  summary(Cytophagales_unclassified)

  #ANOVA Gammaproteobacteria_unclassified (Family)
  Gammaproteobacteria_unclassified <- aov(Gammaproteobacteria_unclassified ~
Harvesting_amount*SO2_supplement*NaOH_addition, data = metadata)
  summary(Gammaproteobacteria_unclassified)

  #ANOVA Proteobacteria_unclassified (Family)
  Proteobacteria_unclassified <- aov(Proteobacteria_unclassified ~ Harvesting
_amount*SO2_supplement*NaOH_addition, data = metadata)
```

```
  summary(Proteobacteria_unclassified)

  #ANOVA Rhizobiales_unclassified (Family)
  Rhizobiales_unclassified <- aov(Rhizobiales_unclassified ~ Harvesting_amoun
t*SO2_supplement*NaOH_addition, data = metadata)
  summary(Rhizobiales_unclassified)

## Network -----

  n <- make_network(physeq, max.dist =0.35)
  plot_network(n, physeq, color = NULL, shape = NULL)

## Beta-diversity analysis -------------------------------------------------

  t.Frequency.table <- t(Frequency_Table)  #transpose the data
  class(t.Frequency.table) #check the class of the table
  View(Frequency_Table)
  View(t.Frequency.table)

  #Permutational analysis of variance
  #adonis

  betad <-betadiver(t.Frequency.table, 'z')

  adonis(betad~Archaea, metadata, perm=200)
  adonis(betad~Bacteria, metadata, perm=200)

  adonis(betad~Euryarchaeota, metadata, perm=200)
  adonis(betad~Bacteria_unclassified_phylum, metadata, perm=200)

  adonis(betad~Bacteroidetes, metadata, perm=200)
  adonis(betad~Firmicutes, metadata, perm=200)
  adonis(betad~Proteobacteria, metadata, perm=200)

  adonis(betad~YC_E6_unclassified_family, metadata, perm=200)
  adonis(betad~Bacteroidetes_unclassified_family, metadata, perm=200)
  adonis(betad~Clostridiaceae, metadata, perm=200)
```

```
   ## Metagenomic analysis part B, plots
## Relative abundance
## Long Term Algal Cultivation

## Load libraries -----
  library(vegan)
  library(phyloseq)
  library (MASS)
  library(ggplot2)
  library(grid)
```

```
  library(gridExtra)
  library(ggpubr)
  library(extrafont)
  font_import() #It may take a few minutes to import.
  loadfonts(device="win")

## Import data files -----
  #Choose RelativeFrequencyTable.txt
  con <- file.choose(new = FALSE)
  Frequency_Table <- read.table(con, header = T, row.names = 1)
  #Choose FrequencyTable_Taxanomy.txt
  con1 <-file.choose(new = FALSE)
  Frequency_Table_taxonomy <- read.delim(con1, header = T, row.names = 1)

## Phyloseq -----
  Full_Frequency <- cbind.data.frame(Frequency_Table, Frequency_Table_taxonom
y)
  Frequency <- otu_table(Frequency_Table,taxa_are_rows = TRUE) #Frequency tab
le production for phyloseq
  TAX <- tax_table(as.matrix(Frequency_Table_taxonomy)) #Taxanomy production
for phyloseq
  physeq <- phyloseq(Frequency, TAX) #physeq document production
  physeq0 <- tax_glom(physeq, taxrank=rank_names(physeq)[7], NArm=TRUE, bad_e
mpty=c(NA, "", " ", "\t"))
  tax_table(physeq0)

  # Plot
  p = plot_bar(physeq0, fill = "Class", facet_grid=Domain~Phylum) +
    xlab("Run") + ylab("Relative Frequency (%)") +
    geom_bar(color = "black", size = .1, stat = "identity", position = "stack
")+
    theme(legend.position="right",
        axis.text.x = element_text(size = 11, family="Times New Roman", angle
= 45, hjust = 1),
        axis.text.y = element_text(size = 11, family="Times New Roman"),
        axis.title.x = element_text(size = 12, family="Times New Roman"),
        axis.title.y = element_text(size = 12, family="Times New Roman"),
        legend.text = element_text(size = 11, family="Times New Roman"),
        legend.title= element_text(size = 12, family="Times New Roman"))
  p

## Overall abundances for Domain, Phylum, Class, Order, and Family -----
  #Abundance Plotbar Domain
  physeqa <-tax_glom(physeq, taxrank=rank_names(physeq)[1], NArm=TRUE, bad_em
pty=c(NA, "", " ", "\t"))
  tablea <- otu_table(physeqa)

  a = plot_bar(physeqa, fill = "Domain") +
    geom_bar(aes(color=Domain, fill=Domain), stat = "identity", position = "s
tack") +
```

```
    xlab("Run") + ylab("Relative Frequency (%)") +
    theme(legend.position="right",
        axis.text.x = element_text(size = 11, family="Times New Roman", angle
= 45, hjust = 1),
        axis.text.y = element_text(size = 11, family="Times New Roman"),
        axis.title.x = element_text(size = 12, family="Times New Roman"),
        axis.title.y = element_text(size = 12, family="Times New Roman"),
        legend.text = element_text(size = 11, family="Times New Roman"),
        legend.title= element_text(size = 12, family="Times New Roman"))
  a

  #Abundance Plotbar Phylum
  physeqa1 <-tax_glom(physeq, taxrank=rank_names(physeq)[2], NArm=TRUE, bad_e
mpty=c(NA, "", " ", "\t"))
  tablea1 <- otu_table(physeqa1)

  a1 = plot_bar(physeqa1, fill = "Phylum") +
    geom_bar(aes(color=Phylum, fill=Phylum), stat = "identity", position = "s
tack") +
    xlab("Run") + ylab("Relative Frequency (%)")  +
    theme(legend.position="right",
          axis.text.x = element_text(size = 11, family="Times New Roman", ang
le = 45, hjust = 1),
          axis.text.y = element_text(size = 11, family="Times New Roman"),
          axis.title.x = element_text(size = 12, family="Times New Roman"),
          axis.title.y = element_text(size = 12, family="Times New Roman"),
          legend.text = element_text(size = 11, family="Times New Roman"),
          legend.title= element_text(size = 12, family="Times New Roman"))
  a1

  #Abundance Plotbar Class
  physeqa2 <-tax_glom(physeq, taxrank=rank_names(physeq)[3], NArm=TRUE, bad_e
mpty=c(NA, "", " ", "\t"))
  tablea2 <- otu_table(physeqa2)

  a2 = plot_bar(physeqa2, fill = "Class") +
    geom_bar(aes(color=Class, fill=Class), stat = "identity", position = "sta
ck") +
    xlab("Run") + ylab("Relative Frequency (%)") +
    theme(legend.position="right",
          axis.text.x = element_text(size = 11, family="Times New Roman", ang
le = 45, hjust = 1),
          axis.text.y = element_text(size = 11, family="Times New Roman"),
          axis.title.x = element_text(size = 12, family="Times New Roman"),
          axis.title.y = element_text(size = 12, family="Times New Roman"),
          legend.text = element_text(size = 11, family="Times New Roman"),
          legend.title= element_text(size = 12, family="Times New Roman"))
  a2
  ## Stop at the Class level
  grid.arrange(a,a1,a2, ncol=1)
```

```
## Abundance Plotbar Bacteria------------
  #Abundance Plotbar Bacteria (Phylum)
  physeq2 <-subset_taxa(physeq, Domain== "Bacteria")
  physeq2_1 <-tax_glom(physeq2, taxrank=rank_names(physeq2)[2], NArm=TRUE, ba
d_empty=c(NA, "", " ", "\t"))
  table2_1 <- otu_table(physeq2_1)

  c = plot_bar(physeq2_1, fill = "Phylum") +
    geom_bar(aes(color=Phylum, fill=Phylum), stat = "identity",position = "st
ack") +
    xlab("Run") + ylab("Relative Frequency (%)") +
    theme(legend.position="right",
          axis.text.x = element_text(size = 11, family="Times New Roman", ang
le = 45, hjust = 1),
          axis.text.y = element_text(size = 11, family="Times New Roman"),
          axis.title.x = element_text(size = 12, family="Times New Roman"),
          axis.title.y = element_text(size = 12, family="Times New Roman"),
          legend.text = element_text(size = 11, family="Times New Roman"),
          legend.title= element_text(size = 12, family="Times New Roman"))
  c

  #Abundance Plotbar Bacteroidetes (Family)
  physeq3 <-subset_taxa(physeq, Phylum == "Bacteroidetes")
  physeq3_1 <-tax_glom(physeq3, taxrank=rank_names(physeq3)[5], NArm=TRUE, ba
d_empty=c(NA, "", " ", "\t"))
  table3_1 <- otu_table(physeq3_1)
  table3_1

  d = plot_bar(physeq3_1, fill = "Family")+ geom_bar(aes(color=Family, fill=F
amily), stat = "identity",position = "stack") +
    xlab("Run") + ylab("Bacteroidetes Relative Frequency (%)") +
    theme(legend.position="right",
          axis.text.x = element_text(size = 11, family="Times New Roman", ang
le = 45, hjust = 1),
          axis.text.y = element_text(size = 11, family="Times New Roman"),
          axis.title.x = element_text(size = 12, family="Times New Roman"),
          axis.title.y = element_text(size = 12, family="Times New Roman"),
          legend.text = element_text(size = 11, family="Times New Roman"),
          legend.title= element_text(size = 12, family="Times New Roman"))
  d

  #Abundance Plotbar Proteobacteria (Family)
  physeq5 <-subset_taxa(physeq, Phylum == "Proteobacteria")
  physeq5_1 <-tax_glom(physeq5, taxrank=rank_names(physeq5)[5], NArm=TRUE, ba
d_empty=c(NA, "", " ", "\t"))
  table5_1 <- otu_table(physeq5_1)
  table5_1
  # write.csv(table5_1, "ProteobacteriaFamily.csv")
```

```
  f = plot_bar(physeq5_1, fill = "Family")+ geom_bar(aes(color=Family, fill=F
amily), stat = "identity",position = "stack") +
    xlab("Run") + ylab("Proteobacteria Relative Frequency (%)") +
    theme(legend.position="right",
          axis.text.x = element_text(size = 11, family="Times New Roman", ang
le = 45, hjust = 1),
          axis.text.y = element_text(size = 11, family="Times New Roman"),
          axis.title.x = element_text(size = 12, family="Times New Roman"),
          axis.title.y = element_text(size = 12, family="Times New Roman"),
          legend.text = element_text(size = 11, family="Times New Roman"),
          legend.title= element_text(size = 12, family="Times New Roman"))
  f

  #Put plots d and f next to each other
  grid.arrange(d, f, ncol=1)
```

CHAPTER 3

```
   ## Statistical analysis
## Mechanochemical cell disruption of algal biomass

## Load libraries and data -------------------------------------------
library(ggplot2)
library(grid)
library(gridExtra)
library(ggpubr)
library(dplyr)
library(knitr)
library(tidyverse)
library(broom)
library(extrafont)
library(RColorBrewer)
font_import()
loadfonts(device="win")

# Data file: ballmillTN
con1 <- file.choose(new = FALSE)
nitrogendata <- read.table(con1, header = T, row.names = 1)

nitrogendata$Ball.Material<- factor(nitrogendata$Ball.Material)
nitrogendata$Ball.Biomass.Ratio <- factor(nitrogendata$Ball.Biomass.Ratio)
nitrogendata$Milling.Speed <- factor(nitrogendata$Milling.Speed)
nitrogendata$Milling.Time <- factor(nitrogendata$Milling.Time)
nitrogendata$KOH.Biomass.Ratio <- factor(nitrogendata$KOH.Biomass.Ratio)

## ANOVA and Tukey's ------------------------------------
# All sample sizes are equal and large (95 ea), don't need to test for normal
ity or variance, assume normal distribution and equal variance
# Factorial ANOVA to see interactions of factors
factorial <- aov(Percent.TN.Recovery ~ Ball.Material*Ball.Biomass.Ratio*Milli
```

```
ng.Speed*Milling.Time*KOH.Biomass.Ratio, nitrogendata)
csvfactorial <- tidy(factorial)
write.csv(csvfactorial, "factorial.csv")

factorialtukey <- TukeyHSD(factorial, conf.level=0.95)
csvfactorialtukey <- tidy(factorialtukey)
write.csv(csvfactorialtukey, "factorial.tukey.csv")

# One-way ANOVA for ball material
oneway.ballmaterial <- aov(Percent.TN.Recovery ~ Ball.Material, nitrogendata)
csvoneway.ballmaterial <- tidy(oneway.ballmaterial)
# write.csv(csvoneway.ballmaterial, "oneway.ballmaterial.csv")

onewaytukey.ballmaterial <- TukeyHSD(oneway.ballmaterial, conf.level=0.95)
csvonewaytukey.ballmaterial <- tidy(onewaytukey.ballmaterial)
# write.csv(csvonewaytukey.ballmaterial, "onewaytukey.ballmaterial.csv")

# One-way ANOVA for ball to biomass ratio
oneway.ballratio <- aov(Percent.TN.Recovery ~ Ball.Biomass.Ratio, nitrogendat
a)
csvoneway.ballratio <- tidy(oneway.ballratio)
# write.csv(csvoneway.ballratio, "oneway.ballratio.csv")

onewaytukey.ballratio <- TukeyHSD(oneway.ballratio, conf.level=0.95)
csvonewaytukey.ballratio  <- tidy(onewaytukey.ballratio )
# write.csv(csvonewaytukey.ballratio , "onewaytukey.ballratio.csv")

# One-way ANOVA for milling speed
oneway.millingspeed <- aov(Percent.TN.Recovery ~ Milling.Speed, nitrogendata)
csvoneway.millingspeed <- tidy(oneway.millingspeed)
# write.csv(csvoneway.millingspeed, "oneway.millingspeed.csv")

onewaytukey.millingspeed <- TukeyHSD(oneway.millingspeed, conf.level=0.95)
csvonewaytukey.millingspeed  <- tidy(onewaytukey.millingspeed)
# write.csv(csvonewaytukey.millingspeed, "onewaytukey.millingspeed.csv")

# One-way ANOVA for milling time
oneway.millingtime <- aov(Percent.TN.Recovery ~ Milling.Time, nitrogendata)
csvoneway.millingtime <- tidy(oneway.millingtime)
# write.csv(csvoneway.millingtime, "oneway.millingtime.csv")

onewaytukey.millingtime <- TukeyHSD(oneway.millingtime, conf.level=0.95)
csvonewaytukey.millingtime <- tidy(onewaytukey.millingtime)
# write.csv(csvonewaytukey.millingtime, "onewaytukey.millingtime.csv")

# One-way ANOVA for KOH to biomass ratio
oneway.koh <- aov(Percent.TN.Recovery ~ KOH.Biomass.Ratio, nitrogendata)
csvoneway.koh<- tidy(oneway.koh)
# write.csv(csvoneway.koh, "oneway.koh.csv")
```

```
onewaytukey.koh <- TukeyHSD(oneway.koh, conf.level=0.95)
csvonewaytukey.koh <- tidy(onewaytukey.koh)
# write.csv(csvonewaytukey.koh, "onewaytukey.koh.csv")

## Bar charts: TN recovery for all factors individually ----------------------
----------------------
# TN recovery by ball material
ballmaterialrecovery <- nitrogendata %>% group_by(Ball.Material) %>% summaris
e(bmmean = mean(Percent.TN.Recovery),bmsd = sd(Percent.TN.Recovery))

bar00 <- ggplot(ballmaterialrecovery, aes(x=Ball.Material, y=bmmean, fill=Bal
l.Material)) +
  geom_bar(stat="identity", position=position_dodge(0.9)) +
  geom_errorbar(aes(ymin=bmmean-bmsd, ymax=bmmean+bmsd), width=0.2, position=
position_dodge(0.9)) +
  xlab("Ball Material")+ ylab("Total Nitrogen Recovery (%)") +
  ylim(0, 100)  + labs(title = "", subtitle=NULL) +
  scale_fill_manual(values=c("#d7191c","#2b83ba")) +
  theme(title=element_text(size=10, family="Helvetica"),
        axis.text.x = element_text(size=10, family="Helvetica"),
        axis.text.y=element_text(size=12, family="Helvetica"),
        axis.title.y = element_text(size =12, family="Helvetica"),
        axis.title.x=element_text(size=12, family="Helvetica"),
        legend.title = element_text(size=12, family="Helvetica"),
        legend.text = element_text(size=10, family="Helvetica"),
        legend.position = "none")
bar00

# TN recovery by KOH to biomass ratio
kohrecovery <- nitrogendata %>% group_by(KOH.Biomass.Ratio) %>% summarise(koh
mean = mean(Percent.TN.Recovery),kohsd = sd(Percent.TN.Recovery))

bar01 <- ggplot(kohrecovery, aes(x=KOH.Biomass.Ratio, y=kohmean, fill=KOH.Bio
mass.Ratio)) +
  geom_bar(stat="identity", position=position_dodge(0.9))+
  geom_errorbar(aes(ymin=kohmean-kohsd, ymax=kohmean+kohsd), width=0.2, posit
ion=position_dodge(0.9)) +
  xlab("KOH to Biomass Ratio")+ ylab("Total Nitrogen Recovery (%)") +
  ylim(0, 100)  + labs(title = "", subtitle=NULL) +
  scale_fill_manual(values=c("#d7191c","#2b83ba")) +
  theme(title=element_text(size=10, family="Helvetica"),
        axis.text.x = element_text(size=10, family="Helvetica"),
        axis.text.y=element_text(size=12, family="Helvetica"),
        axis.title.y = element_text(size =12, family="Helvetica"),
        axis.title.x=element_text(size=12, family="Helvetica"),
        legend.title = element_text(size=12, family="Helvetica"),
        legend.text = element_text(size=10, family="Helvetica"),
        legend.position = "none")
bar01
```

```
# TN recovery by milling time
millingtimerecovery <- nitrogendata %>% group_by(Milling.Time) %>% summarise(
mtmean = mean(Percent.TN.Recovery),mtsd = sd(Percent.TN.Recovery))

bar02 <- ggplot(millingtimerecovery, aes(x=Milling.Time, y=mtmean, fill=Milli
ng.Time)) +
  geom_bar(stat="identity", position=position_dodge(0.9))+
  geom_errorbar(aes(ymin=mtmean-mtsd, ymax=mtmean+mtsd), width=0.2, position=
position_dodge(0.9)) +
  xlab("Milling Time (min)")+ ylab("Total Nitrogen Recovery (%)") +
  ylim(0, 100)  + labs(title = "", subtitle=NULL) +
  scale_fill_brewer(palette="Spectral") +
  theme(title=element_text(size=10, family="Helvetica"),
        axis.text.x = element_text(size=10, family="Helvetica"),
        axis.text.y=element_text(size=12, family="Helvetica"),
        axis.title.y = element_text(size =12, family="Helvetica"),
        axis.title.x=element_text(size=12, family="Helvetica"),
        legend.title = element_text(size=12, family="Helvetica"),
        legend.text = element_text(size=10, family="Helvetica"),
        legend.position = "none")
bar02

## Bar charts: TN recovery grouped by ball material ----------------------
-----------------
# TN recovery by Ball material & Ball-biomass ratio
bmbbrecovery <- nitrogendata %>% group_by(Ball.Material, Ball.Biomass.Ratio)
%>% summarise(bmbbmean = mean(Percent.TN.Recovery),bmbbsd = sd(Percent.TN.Rec
overy))

bar1 <- ggplot(bmbbrecovery, aes(x=Ball.Biomass.Ratio, y=bmbbmean, fill=Ball.
Material)) +
  geom_bar(stat="identity", position=position_dodge(0.9))+
  geom_errorbar(aes(ymin=bmbbmean-bmbbsd, ymax=bmbbmean+bmbbsd), width=0.2, p
osition=position_dodge(0.9)) +
  xlab("Ball to Biomass Ratio")+ ylab("Total Nitrogen Recovery (%)") +
  ylim(0, 100)  + labs(title = "", subtitle=NULL) +
  theme(title=element_text(size=10,family="Times New Roman"),
        axis.text.x = element_text(size=10, family="Times New Roman"),
        axis.text.y=element_text(size=12, family="Times New Roman"),
        axis.title.y = element_text(size =12, family="Times New Roman"),
        axis.title.x=element_text(size=12, family="Times New Roman"),
        legend.title = element_text(size=12, family="Times New Roman"),
        legend.text = element_text(size=10, family="Times New Roman"))
bar1

# TN recovery by Ball material & Milling rotation speed
bmmsrecovery <- nitrogendata %>% group_by(Ball.Material, Milling.Speed) %>% s
ummarise(bmmsmean = mean(Percent.TN.Recovery),bmmssd = sd(Percent.TN.Recovery
))
```

```
bar2 <- ggplot(bmmsrecovery, aes(x=Milling.Speed, y=bmmsmean, fill=Ball.Mater
ial)) +
  geom_bar(stat="identity", position=position_dodge(0.9))+
  geom_errorbar(aes(ymin=bmmsmean-bmmssd, ymax=bmmsmean+bmmssd), width=0.2, p
osition=position_dodge(0.9)) +
  xlab("MIlling Speed (rpm)")+ ylab("Total Nitrogen Recovery (%)") +
  ylim(0, 100)  + labs(title = "", subtitle=NULL) +
  theme(title=element_text(size=10,family="Times New Roman"),
        axis.text.x = element_text(size=10, family="Times New Roman"),
        axis.text.y=element_text(size=12, family="Times New Roman"),
        axis.title.y = element_text(size =12, family="Times New Roman"),
        axis.title.x=element_text(size=12, family="Times New Roman"),
        legend.title = element_text(size=12, family="Times New Roman"),
        legend.text = element_text(size=10, family="Times New Roman"))
bar2

# TN recovery by Ball material & Milling time
bmmtrecovery <- nitrogendata %>% group_by(Ball.Material, Milling.Time) %>% su
mmarise(bmmtmean = mean(Percent.TN.Recovery),bmmtsd = sd(Percent.TN.Recovery)
)

bar3 <- ggplot(bmmtrecovery, aes(x=Milling.Time, y=bmmtmean, fill=Ball.Materi
al)) +
  geom_bar(stat="identity", position=position_dodge(0.9))+
  geom_errorbar(aes(ymin=bmmtmean-bmmtsd, ymax=bmmtmean+bmmtsd), width=0.2, p
osition=position_dodge(0.9)) +
  xlab("Milling Time (min)")+ ylab("Total Nitrogen Recovery (%)") +
  ylim(0, 100)  + labs(title = "", subtitle=NULL) +
  theme(title=element_text(size=10,family="Times New Roman"),
        axis.text.x = element_text(size=10, family="Times New Roman"),
        axis.text.y=element_text(size=12, family="Times New Roman"),
        axis.title.y = element_text(size =12, family="Times New Roman"),
        axis.title.x=element_text(size=12, family="Times New Roman"),
        legend.title = element_text(size=12, family="Times New Roman"),
        legend.text = element_text(size=10, family="Times New Roman"))
bar3

# TN recovery by Ball material  & KOH biomass ratio
bmkohrecovery <- nitrogendata %>% group_by(Ball.Material, KOH.Biomass.Ratio)
%>% summarise(bmkohmean = mean(Percent.TN.Recovery),bmkohsd = sd(Percent.TN.R
ecovery))

bar4 <- ggplot(bmkohrecovery, aes(x=KOH.Biomass.Ratio, y=bmkohmean, fill=Ball
.Material)) +
  geom_bar(stat="identity", position=position_dodge(0.9))+
  geom_errorbar(aes(ymin=bmkohmean-bmkohsd, ymax=bmkohmean+bmkohsd), width=0.
2, position=position_dodge(0.9)) +
  xlab("KOH to Biomass Ratio")+ ylab("Total Nitrogen Recovery (%)") +
  ylim(0, 100)  + labs(title = "", subtitle=NULL) +
  scale_fill_manual(values=c("#d7191c","#2b83ba")) +
```

```
  theme(title=element_text(size=10, family="Helvetica"),
        axis.text.x = element_text(size=10, family="Helvetica"),
        axis.text.y=element_text(size=12, family="Helvetica"),
        axis.title.y = element_text(size =12, family="Helvetica"),
        axis.title.x=element_text(size=12, family="Helvetica"),
        legend.title = element_text(size=12, family="Helvetica"),
        legend.text = element_text(size=10, family="Helvetica")) +
        guides(fill=guide_legend(title="Ball Material"))
bar4

## Bar charts: ZIRCONIA TN recovery grouped by KOH ------------------------
----------------
zirconia <- subset(nitrogendata, Ball.Material == "Zirconia", select = Ball.B
iomass.Ratio:Percent.TN.Recovery)

# TN recovery by KOH-biomass ratio & Ball-biomass ratio
zkohbbrecovery <- zirconia %>% group_by(KOH.Biomass.Ratio, Ball.Biomass.Ratio
) %>% summarise(zkohbbmean = mean(Percent.TN.Recovery),zkohbbsd = sd(Percent.
TN.Recovery))

bar5 <- ggplot(zkohbbrecovery, aes(x=Ball.Biomass.Ratio, y=zkohbbmean, fill=K
OH.Biomass.Ratio)) +
  geom_bar(stat="identity", position=position_dodge(0.9))+
  geom_errorbar(aes(ymin=zkohbbmean-zkohbbsd, ymax=zkohbbmean+zkohbbsd), widt
h=0.2, position=position_dodge(0.9)) +
  xlab("Ball to Biomass Ratio")+ ylab("Total Nitrogen Recovery (%)")+ ylim(0,
100) +
  theme(title=element_text(size=10,family="Times New Roman"),
        axis.text.x = element_text(size=10, family="Times New Roman"),
        axis.text.y=element_text(size=12, family="Times New Roman"),
        axis.title.y = element_text(size =12, family="Times New Roman"),
        axis.title.x=element_text(size=12, family="Times New Roman"),
        legend.title = element_text(size=12, family="Times New Roman"),
        legend.text = element_text(size=10, family="Times New Roman"))
bar5

# TN recovery by KOH-biomass ratio & Milling speed
zkohmsrecovery <- zirconia %>% group_by(KOH.Biomass.Ratio, Milling.Speed) %>%
summarise(zkohmsmean = mean(Percent.TN.Recovery),zkohmssd = sd(Percent.TN.Rec
overy))

bar6 <- ggplot(zkohmsrecovery, aes(x=Milling.Speed, y=zkohmsmean, fill=KOH.Bi
omass.Ratio)) +
  geom_bar(stat="identity", position=position_dodge(0.9))+
  geom_errorbar(aes(ymin=zkohmsmean-zkohmssd, ymax=zkohmsmean+zkohmssd), widt
h=0.2, position=position_dodge(0.9)) +
  xlab("Milling Speed (rpm)")+ ylab("Total Nitrogen Recovery (%)") + ylim(0,
100) +
  theme(title=element_text(size=10,family="Times New Roman"),
        axis.text.x = element_text(size=10, family="Times New Roman"),
```

```
        axis.text.y=element_text(size=12, family="Times New Roman"),
        axis.title.y = element_text(size =12, family="Times New Roman"),
        axis.title.x=element_text(size=12, family="Times New Roman"),
        legend.title = element_text(size=12, family="Times New Roman"),
        legend.text = element_text(size=10, family="Times New Roman"))
bar6

# TN recovery by KOH-biomass ratio & Milling time
zkohmtrecovery <- zirconia %>% group_by(KOH.Biomass.Ratio, Milling.Time) %>%
summarise(zkohmtmean = mean(Percent.TN.Recovery),zkohmtsd = sd(Percent.TN.Rec
overy))

bar7 <- ggplot(zkohmtrecovery, aes(x=Milling.Time, y=zkohmtmean, fill=KOH.Bio
mass.Ratio)) +
  geom_bar(stat="identity", position=position_dodge(0.9))+
  geom_errorbar(aes(ymin=zkohmtmean-zkohmtsd, ymax=zkohmtmean+zkohmtsd), widt
h=0.2, position=position_dodge(0.9)) +
  xlab("Milling Time (min)")+ ylab("Total Nitrogen Recovery (%)") + ylim(0, 1
00) +
  theme(title=element_text(size=10,family="Times New Roman"),
        axis.text.x = element_text(size=10, family="Times New Roman"),
        axis.text.y=element_text(size=12, family="Times New Roman"),
        axis.title.y = element_text(size =12, family="Times New Roman"),
        axis.title.x=element_text(size=12, family="Times New Roman"),
        legend.title = element_text(size=12, family="Times New Roman"),
        legend.text = element_text(size=10, family="Times New Roman"))
bar7

## Bar charts: AGATE TN recovery grouped by KOH ----------------------------
--------------
agate <- subset(nitrogendata, Ball.Material == "Agate", select = Ball.Biomass
.Ratio:Percent.TN.Recovery)

# TN recovery by KOH-biomass ratio & Ball-biomass ratio
akohbbrecovery <- agate %>% group_by(KOH.Biomass.Ratio, Ball.Biomass.Ratio) %
>% summarise(akohbbmean = mean(Percent.TN.Recovery),akohbbsd = sd(Percent.TN.
Recovery))

bar8 <- ggplot(akohbbrecovery, aes(x=Ball.Biomass.Ratio, y=akohbbmean, fill=K
OH.Biomass.Ratio)) +
  geom_bar(stat="identity", position=position_dodge(0.9))+
  geom_errorbar(aes(ymin=akohbbmean-akohbbsd, ymax=akohbbmean+akohbbsd), widt
h=0.2, position=position_dodge(0.9))+
  xlab("Ball to Biomass Ratio")+ ylab("Total Nitrogen Recovery (%)") + ylim(0
, 100) +
  theme(title=element_text(size=10,family="Times New Roman"),
        axis.text.x = element_text(size=10, family="Times New Roman"),
        axis.text.y=element_text(size=12, family="Times New Roman"),
        axis.title.y = element_text(size =12, family="Times New Roman"),
        axis.title.x=element_text(size=12, family="Times New Roman"),
```

```
        legend.title = element_text(size=12, family="Times New Roman"),
        legend.text = element_text(size=10, family="Times New Roman"))
bar8

# TN recovery by KOH-biomass ratio & Mill rotation speed
akohmsrecovery <- agate %>% group_by(KOH.Biomass.Ratio, Milling.Speed) %>% su
mmarise(akohmsmean = mean(Percent.TN.Recovery),akohmssd = sd(Percent.TN.Recov
ery))

bar9 <- ggplot(akohmsrecovery, aes(x=Milling.Speed, y=akohmsmean, fill=KOH.Bi
omass.Ratio)) +
  geom_bar(stat="identity", position=position_dodge(0.9))+
  geom_errorbar(aes(ymin=akohmsmean-akohmssd, ymax=akohmsmean+akohmssd), widt
h=0.2, position=position_dodge(0.9))+
  xlab("Milling Speed (rpm)")+ ylab("Total Nitrogen Recovery (%)") + ylim(0,
100) +
        theme(title=element_text(size=10,family="Times New Roman"),
              axis.text.x = element_text(size=10, family="Times New Roman"),
              axis.text.y=element_text(size=12, family="Times New Roman"),
              axis.title.y = element_text(size =12, family="Times New Roman")
,
              axis.title.x=element_text(size=12, family="Times New Roman"),
              legend.title = element_text(size=12, family="Times New Roman"),
              legend.text = element_text(size=10, family="Times New Roman"))
bar9

# TN recovery by KOH-biomass ratio & Milling time
akohmtrecovery <- agate %>% group_by(KOH.Biomass.Ratio, Milling.Time) %>% sum
marise(akohmtmean = mean(Percent.TN.Recovery),akohmtsd = sd(Percent.TN.Recove
ry))

bar10 <- ggplot(akohmtrecovery, aes(x=Milling.Time, y=akohmtmean, fill=KOH.Bi
omass.Ratio)) +
  geom_bar(stat="identity", position=position_dodge(0.9))+
  geom_errorbar(aes(ymin=akohmtmean-akohmtsd, ymax=akohmtmean+akohmtsd), widt
h=0.2, position=position_dodge(0.9))+
  xlab("Milling Time (min)")+ ylab("Total Nitrogen Recovery (%)") + ylim(0, 1
00) +
  theme(title=element_text(size=10,family="Times New Roman"),
        axis.text.x = element_text(size=10, family="Times New Roman"),
        axis.text.y=element_text(size=12, family="Times New Roman"),
        axis.title.y = element_text(size =12, family="Times New Roman"),
        axis.title.x=element_text(size=12, family="Times New Roman"),
        legend.title = element_text(size=12, family="Times New Roman"),
        legend.text = element_text(size=10, family="Times New Roman"))
bar10
```

```
   ## Statistical analysis
## Isoelectric point protein extraction

# Load libraries and data -------------------------------------------
library(ggplot2)
library(grid)
library(gridExtra)
library(ggpubr)
library(dplyr)
library(knitr)
library(tidyverse)
library(car)
library(extrafont)
library(RColorBrewer)
font_import()
loadfonts(device="win")

# Data file: IEP FINAL
con1 <- file.choose(new = FALSE)
iepdata <- read.table(con1, header = T, row.names = 1)

iepdata$dilution.factor <- factor(iepdata$dilution.factor)

## Normality and variance tests ---------------------------------------
shapiro.test(iepdata$net.protein.recovered) #not normal
leveneTest(iepdata$net.protein.recovered ~ iepdata$dilution.factor, data=iepd
ata) #equal variance
ggqqplot(iepdata$net.protein.recovered)

shapiro.test(iepdata$percent.protein.recovered) #normal/not normal pvalue=0.0
4992
leveneTest(iepdata$percent.protein.recovered ~ iepdata$dilution.factor, data=
iepdata) #equal variance
ggqqplot(iepdata$percent.protein.recovered)

shapiro.test(iepdata$relative.protein.content) #normal
leveneTest(iepdata$relative.protein.content ~ iepdata$dilution.factor, data=i
epdata) #equal variance
ggqqplot(iepdata$relative.protein.content)

## ANOVA (assume ANOVA is robust enough for the violation of normality assump
tion) ----------------------------------------
fit1<-aov(net.protein.recovered ~ dilution.factor, data=iepdata)
summary(fit1)
# csvfit1<-tidy(fit1)
# write.csv(csvfit1, "fit1.csv")

fit2<-aov(percent.protein.recovered ~ dilution.factor, data=iepdata)
summary(fit2)
# csvfit2<-tidy(fit2)
```

```
# write.csv(csvfit2, "fit2.csv")

fit3<-aov(relative.protein.content ~ dilution.factor, data=iepdata)
summary(fit3)
# csvfit3<-tidy(fit3)
# write.csv(csvfit3, "fit3.csv")

## Tukeys Test ------------------------------------------
Tukey1 <- TukeyHSD(fit1, conf.level=0.95)
Tukey1
# csvTukey1<-tidy(Tukey1)
# write.csv(csvTukey1, "Tukey1.csv")

Tukey2 <- TukeyHSD(fit2, conf.level=0.95)
Tukey2
# csvTukey2 <-tidy(Tukey2)
# write.csv(csvTukey2, "Tukey2.csv")

Tukey3 <- TukeyHSD(fit3, conf.level=0.95)
Tukey3
# csvTukey3 <-tidy(Tukey3)
# write.csv(csvTukey3, "Tukey3.csv")

## Bar Charts ----------------------------------------

# Net protein
netprotein <- iepdata %>% group_by(dilution.factor) %>% summarise(npmean = me
an(net.protein.recovered),npsd = sd(net.protein.recovered))

bar1 <- ggplot(netprotein, aes(x=dilution.factor, y=npmean, fill=dilution.fac
tor)) + geom_bar(stat="identity", position=position_dodge(0.9))+
  geom_errorbar(aes(ymin=npmean-npsd, ymax=npmean+npsd), width=0.2, position=
position_dodge(0.9))+
  xlab("Dilution Factor")+ ylab("Recovered Protein (g)") + labs(fill="Dilutio
n Factor")+
  ylim(0, 5)  + labs(title = "", subtitle=NULL) +
  scale_fill_brewer(palette="Spectral") +
  theme(title=element_text(size=10, family="Helvetica"),
        axis.text.x = element_text(size=10, family="Helvetica"),
        axis.text.y=element_text(size=12, family="Helvetica"),
        axis.title.y = element_text(size =12, family="Helvetica"),
        axis.title.x=element_text(size=12, family="Helvetica"),
        legend.title = element_text(size=12, family="Helvetica"),
        legend.text = element_text(size=10, family="Helvetica"))
bar1

# Percent protein
precentprotein <- iepdata %>% group_by(dilution.factor) %>% summarise(ppmean
= mean(percent.protein.recovered),ppsd = sd(percent.protein.recovered))
```

```
bar2 <- ggplot(precentprotein, aes(x=dilution.factor, y=ppmean, fill=dilution
.factor)) + geom_bar(stat="identity", position=position_dodge(0.9))+
  geom_errorbar(aes(ymin=ppmean-ppsd, ymax=ppmean+ppsd), width=0.2, position=
position_dodge(0.9))+
  xlab("Dilution Factor")+ ylab("Recovered Protein (%)") + labs(fill="Dilutio
n Factor")+
  ylim(0, 115)  + labs(title = "", subtitle=NULL) +
  scale_fill_brewer(palette= "Spectral") +
  theme(title=element_text(size=10, family="Helvetica"),
        axis.text.x = element_text(size=10, family="Helvetica"),
        axis.text.y=element_text(size=12, family="Helvetica"),
        axis.title.y = element_text(size =12, family="Helvetica"),
        axis.title.x=element_text(size=12, family="Helvetica"),
        legend.title = element_text(size=12, family="Helvetica"),
        legend.text = element_text(size=10, family="Helvetica"))
bar2

# Relative protein
relativeprotein <- iepdata %>% group_by(dilution.factor) %>% summarise(rpmean
= mean(relative.protein.content),rpsd = sd(relative.protein.content))

bar3 <- ggplot(relativeprotein, aes(x=dilution.factor, y=rpmean, fill=dilutio
n.factor)) + geom_bar(stat="identity", position=position_dodge(0.9))+
  geom_errorbar(aes(ymin=rpmean-rpsd, ymax=rpmean+rpsd), width=0.2, position=
position_dodge(0.9))+
  xlab("Dilution Factor")+ ylab("Relative Protein Content (%)") + labs(fill="
Dilution Factor")+
  ylim(0, 115)  + labs(title = "", subtitle=NULL) +
  scale_fill_brewer(palette= "Spectral") +
  theme(title=element_text(size=10, family="Helvetica"),
        axis.text.x = element_text(size=10, family="Helvetica"),
        axis.text.y=element_text(size=12, family="Helvetica"),
        axis.title.y = element_text(size =12, family="Helvetica"),
        axis.title.x=element_text(size=12, family="Helvetica"),
        legend.title = element_text(size=12, family="Helvetica"),
        legend.text = element_text(size=10, family="Helvetica"))
bar3
```

APPENDIX B:

Supplemental Tables and Figures

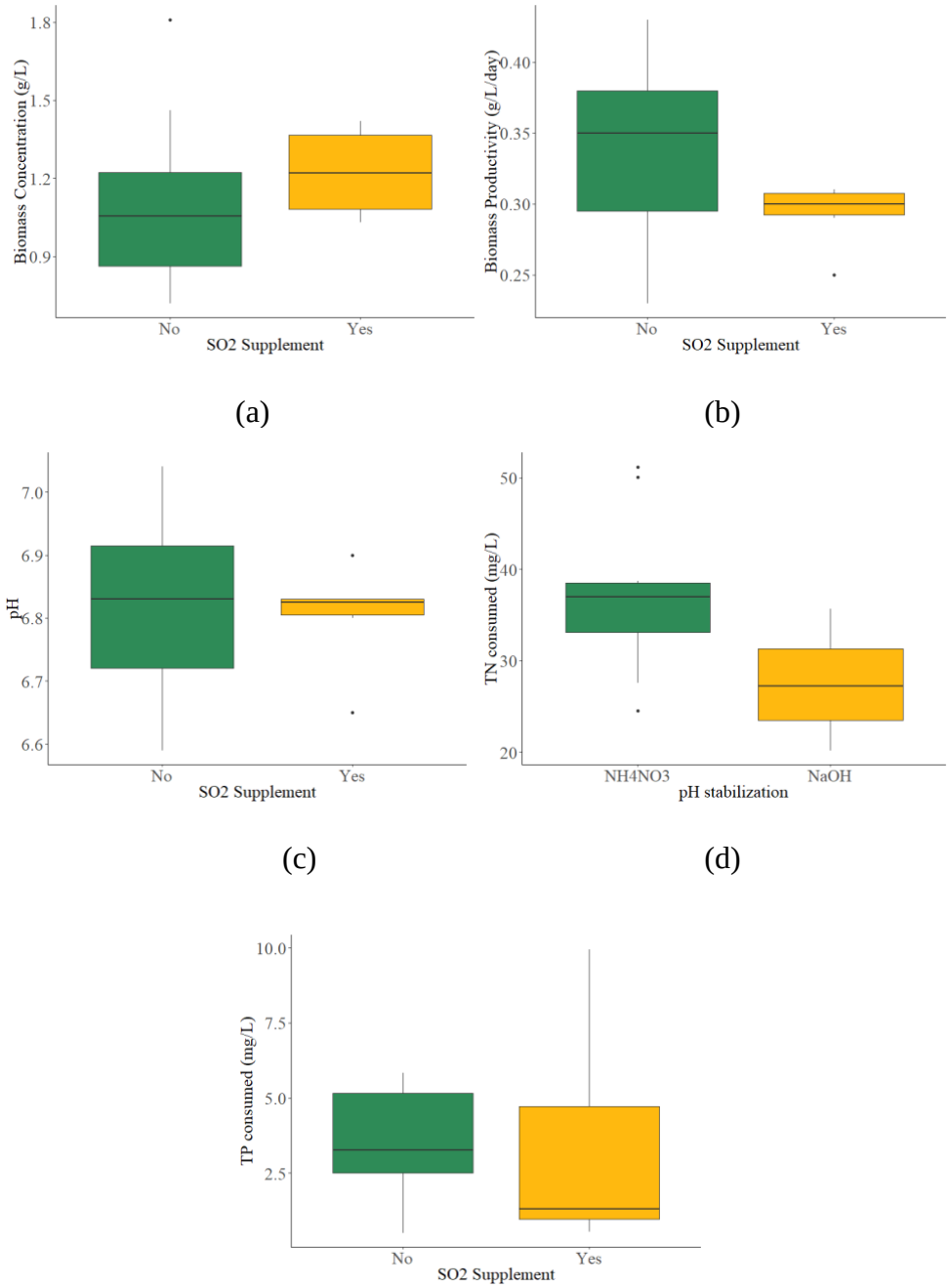

Figure 28. Effects of sulfur on algal cultivation discussed in Chapter 1, Section 3.2.1. (a) Biomass concentration; (b) Biomass Productivity; (c) pH; (d) TN consumed; (e) TP consumed.

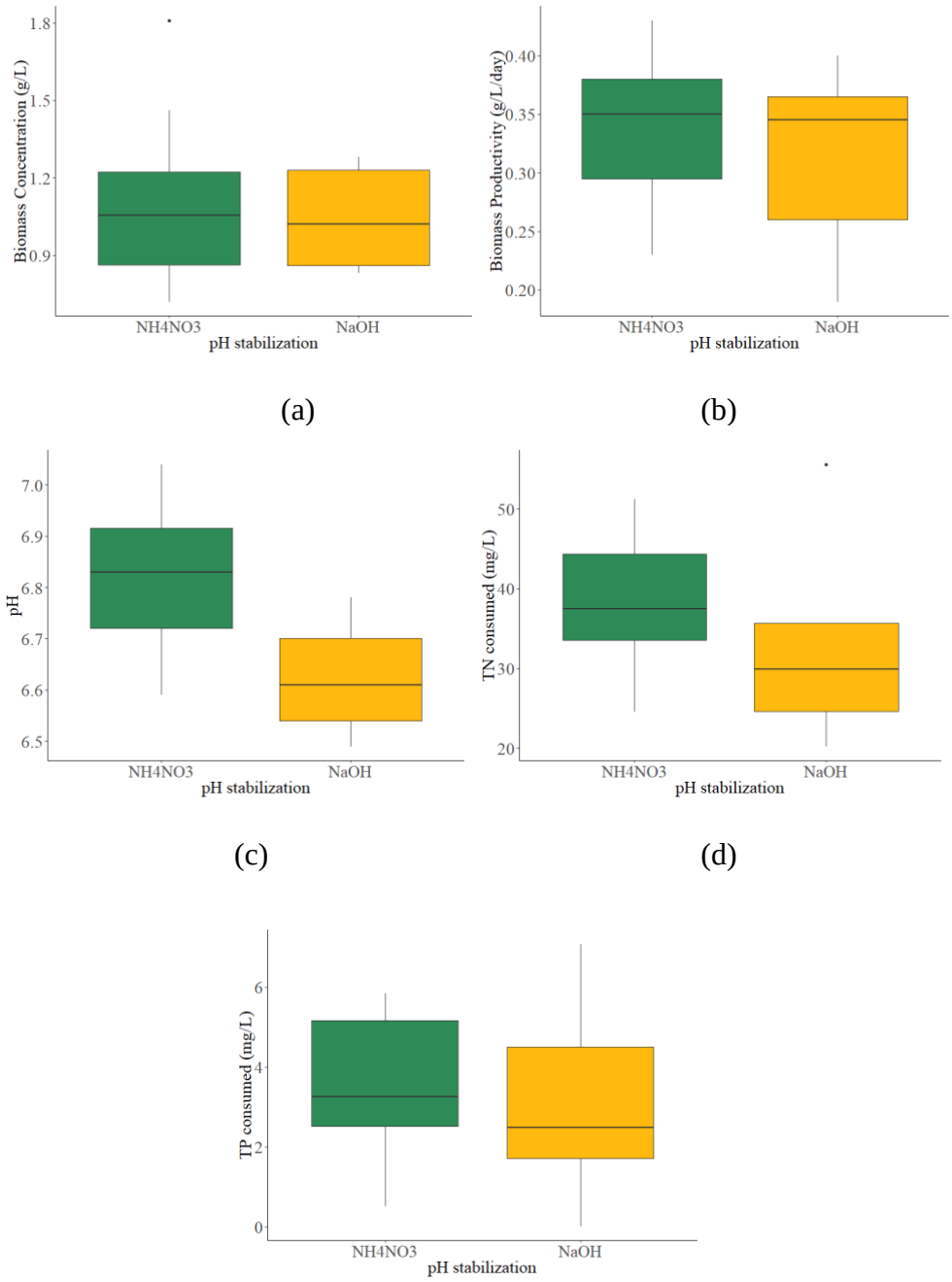

Figure 29. Effects of pH stabilization on algal cultivation discussed in Chapter1, Section 3.2.1. (a). Biomass concentration; (b). Biomass Productivity; (c). pH; (d). TN consumed; (e). TP consumed.

Table 28. Pairwise comparison of different harvesting amounts under no light cycle (light cycle OFF). Discussed in Chapter 1, Section 3.2.2.

Factors and levels		Harvesting Amount							
		30%	**50%**	**30%**	**60%**	**30%**	**70%**	**30%**	**100%**
Biomass concentration	Biomass concentration (g/L)	1.11±0.26	1.28±0.28	1.11±0.26	1.07±0.23	1.11±0.26	0.86±0.18	1.11±0.26	0.72±0.12
	Influence on biomass concentration	P=0.075		P=0.986		P=0.004		P=0	
Biomass productivity	Biomass productivity (g/L/day)	0.32±0.07	0.39±0.12	0.32±0.07	0.43±0.14	0.32±0.07	0.56±0.09	0.32±0.07	0.49±0.06
	Influence on biomass productivity	P=0.021		P=0.021		$P=1.52x10^{-9}$		$P=1.37x10^{-9}$	
pH	pH	6.74±0.15	6.44±0.23	6.74±0.15	6.70±0.10	6.74±0.15	6.56±0.18	6.74±0.15	5.20±0.55
	Influence on pH	$P=6.22x10^{-6}$		P=0.244		P=0.002		$P=5.24x10^{-11}$	
TN consumed	TN consumed (mg/L/day)	34.90±8.24	44.51±12.31	34.90±8.24	59.80±3.64	34.90±8.24	60.02±7.29	34.90±8.24	50.13±5.94
	Influence on TN consumed	P=0.018		$P=1.05x10^{-10}$		$P=1.04x10^{-9}$		$P=4.79x10^{-6}$	
TP consumed	TP consumed (mg/L/day)	3.34±2.48	5.03±2.19	3.34±2.48	5.88±1.58	3.34±2.48	7.99±1.51	3.34±2.48	6.50±1.85
	Influence on TP consumed	P=0.042		P=0.004		P=0		$P=2.21x10^{-5}$	

Factors and levels		Harvesting Amount					
		50%	**60%**	**50%**	**70%**	**50%**	**100%**
Biomass concentration	Biomass concentration (g/L)	1.28±0.28	1.07±0.23	1.28±0.28	0.86±0.18	1.28±0.28	0.72±0.12
	Influence on biomass concentration	P=0.057		$P=4.00x10^{-7}$		P=0	
Biomass productivity	Biomass productivity (g/L/day)	0.39±0.12	0.43±0.14	0.39±0.12	0.56±0.09	0.39±0.12	0.49±0.06

Table 28 (cont'd)

Biomass productivity	Influence on biomass productivity	P=0.372		P=1.52x10^{-4}		P=0.002	
pH	pH	6.44±0.23	6.70±0.10	6.44±0.23	6.56±0.18	6.44±0.23	5.20±0.55
	Influence on pH	P=8.43x10^{-5}		P=0.074		P=1.23x10^{-9}	
TN consumed	TN consumed (mg/L/day)	44.51±12.31	59.80±3.64	44.51±12.31	60.02±7.29	44.51±12.31	50.13±5.94
	Influence on TN consumed	P=2.73x10^{-6}		P=1.32x10^{-5}		P=0.053	
TP consumed	TP consumed (mg/L/day)	5.03±2.19	5.88±1.58	5.03±2.19	7.99±1.51	5.03±2.19	6.50±1.85
	Influence on TP consumed	P=0.708		P=2.02x10^{-4}		P=0.117	

Factors and levels		**Harvesting Amount**					
		60%	**70%**	**60%**	**100%**	**70%**	**100%**
Biomass concentration	Biomass concentration (g/L)	1.07±0.23	0.86±0.18	1.07±0.23	0.72±0.12	0.86±0.18	0.72±0.12
	Influence on biomass concentration	P=0.064		P=1.62x10^{-5}		P=0.131	
Biomass productivity	Biomass productivity (g/L/day)	0.43±0.14	0.56±0.09	0.43±0.14	0.49±0.06	0.56±0.09	0.49±0.06
	Influence on biomass productivity	P=0.135		P=0.214		P=0.015	
pH	pH	6.70±0.10	6.56±0.18	6.70±0.10	5.20±0.55	6.56±0.18	5.20±0.55
	Influence on pH	P=0.017		P=1.01x10^{-10}		P=2.66x10^{-10}	
TN consumed	TN consumed (mg/L/day)	59.80±3.64	60.02±7.29	59.80±3.64	50.13±5.94	60.02±7.29	50.13±5.94
	Influence on TN consumed	P=0.920		P=4.54x10^{-6}		P=2.27x10^{-4}	
TP consumed	TP consumed (mg/L/day)	5.88±1.58	7.99±1.51	5.88±1.58	6.50±1.85	7.99±1.51	6.50±1.85
	Influence on TP consumed	P=0.048		P=0.907		P=0.205	

Table 29. Effects of a 12-hour light cycle (light cycle ON) with different harvesting amounts. Discussed in Chapter 1, Section 3.2.2.

Factors and levels		**Harvesting Amount**					
		30%	**40%**	**30%**	**50%**	**40%**	**50%**
Biomass concentration	Biomass concentration (g/L)	0.67±0.14	0.50±0.09	0.67±0.14	0.42±0.07	0.50±0.09	0.42±0.07
	Influence on biomass concentration	$P=1.36x10^{-5}$		$P=8.70x10^{-6}$		P=0.156	
Biomass productivity	Biomass productivity (g/L/day)	0.20±0.05	0.18±0.05	0.20±0.05	0.17±0.02	0.18±0.05	0.17±0.02
	Influence on biomass productivity	P=0.201		P=0.222		P=0.852	
pH	pH	6.43±0.18	6.69±0.24	6.43±0.18	6.58±0.10	6.69±0.24	6.58±0.10
	Influence on pH	P=0.0002951		P=0.2384383		P=0.4175361	
TN consumed	TN consumed (mg/L/day)	23.98±10.70	21.20±6.82	23.98±10.70	21.30±1.96	21.20±6.82	21.30±1.96
	Influence on TN consumed	P=0.369		P=0.402		P=0.957	
TP consumed	TP consumed (mg/L/day)	2.74±2.01	2.13±1.47	2.74±2.01	2.77±0.24	2.13±1.47	2.77±0.24
	Influence on TP consumed	P=0.398		P=0.667		P=0.405	

Table 30. Effects of different harvesting amounts compared between a 12-hour light cycle and no light cycle (light cycle ON vs light cycle OFF). Discussed in Chapter 1, Section 3.2.2.

Factors and levels		Harvesting Amount			
		30% ON	**30% OFF**	**50% ON**	**50% OFF**
Biomass concentration	Biomass concentration (g/L)	0.67±0.14	1.11±0.26	0.42±0.07	1.28±0.28
	Influence on biomass concentration	$P=8.32x10^{-9}$		$P=2.94x10^{-12}$	
Biomass productivity	Biomass productivity (g/L/day)	0.20±0.05	0.32±0.07	0.17±0.02	0.39±0.12
	Influence on biomass productivity	$P=1.39x10^{-5}$		$P=1.19x10^{-9}$	
pH	pH	6.43±0.18	6.74±0.15	6.58±0.10	6.44±0.23
	Influence on pH	$P=7.48x10^{-8}$		P=0.045	
TN consumed	TN consumed (mg/L/day)	23.98±10.70	34.90±8.24	21.30±1.96	44.51±12.31
	Influence on TN consumed	P=0.003		$P=1.32x10^{-9}$	
TP consumed	TP consumed (mg/L/day)	2.74±2.01	3.34±2.48	2.77±0.24	5.03±2.19
	Influence on TP consumed	P=0.470		$P=3.10x10^{-5}$	

Table 31. Element composition of algal biomass from different culture conditions. Discussed in Chapter 1, Section 3.3.

Harvesting amount (L/day)	**Sulfur supplement**	**Light cycle**	**pH stabilization**	**C (% dry matter)**	**H (% dry matter)**	**N (% dry matter)**	**S (% dry matter)**	**P (% dry matter)**
30	No	No	NH_4NO_3	48.50	7.43	8.01	0.52	1.33
30	Yes	No	NH_4NO_3	49.50	7.34	9.30	0.54	1.60
30	No	No	NH_4NO_3	48.54	7.41	9.03	0.52	1.51
40	No	Yes	NH_4NO_3	46.79	6.98	9.40	0.71	1.65
40	No	Yes	NH_4NO_3	47.24	7.24	9.27	0.60	1.63
40	Yes	Yes	NH_4NO_3	47.46	7.28	9.26	0.60	1.56
40	Yes	Yes	NH_4NO_3	46.98	7.21	9.08	0.57	1.22
50	No	No	NaOH	48.78	7.11	9.07	0.53	1.43

Table 31 (cont'd)

50	Yes	No	NaOH	49.81	7.59	8.66	0.51	1.29
50	Yes	No	NaOH	52.82	7.33	9.88	0.59	1.41
50	No	Yes	NH_4NO_3	45.84	7.07	9.19	0.75	1.89
60	Yes	No	NH_4NO_3	48.54	7.42	8.87	0.44	1.25
60	Yes	No	NH_4NO_3	48.75	7.26	9.54	0.63	1.51
100	No	No	NaOH	48.31	7.39	8.81	0.45	1.83
100	No	No	NaOH	48.15	7.31	8.80	0.47	1.83

Table 32. Diversity of bacteria and eukarya communities calculated based on their 16S rRNA gene sequencing. Discussed in Chapter 1, Section 3.4.

Sample	Harvesting amount	SO_2 supplement	Light cycle	pH stabilization	H[a]	D[b]	iD[c]	J[d]
Scenario 2	50	no	no	NaOH	0.55	0.25	1.33	0.19
Scenario 3	100	no	no	NaOH	0.51	0.20	1.25	0.18
Scenario 4	50	yes	no	NaOH	0.60	0.23	1.30	0.22
Scenario 5	60	yes	no	NH_4NO_3	0.55	0.20	1.25	0.17
Scenario 8	30	yes	no	NH_4NO_3	0.47	0.18	1.22	0.16
Scenario 9	30	no	no	NH_4NO_3	0.31	0.11	1.12	0.10
Scenario 10	50	no	yes	NH_4NO_3	0.32	0.12	1.14	0.11
Scenario 11	40	no	yes	NH_4NO_3	0.66	0.31	1.44	0.21
Scenario 12	40	yes	yes	NH_4NO_3	0.70	0.33	1.49	0.23

a. H: Shannon's index which indicates the diversity of the microbial community.
b. D: Simpson's index which indicates the diversity of the microbial community.
c. iD: Inverse Simpson's index which indicates the diversity of the microbial community.
d. J: Pielou's index which indicates the evenness of the microbial community.

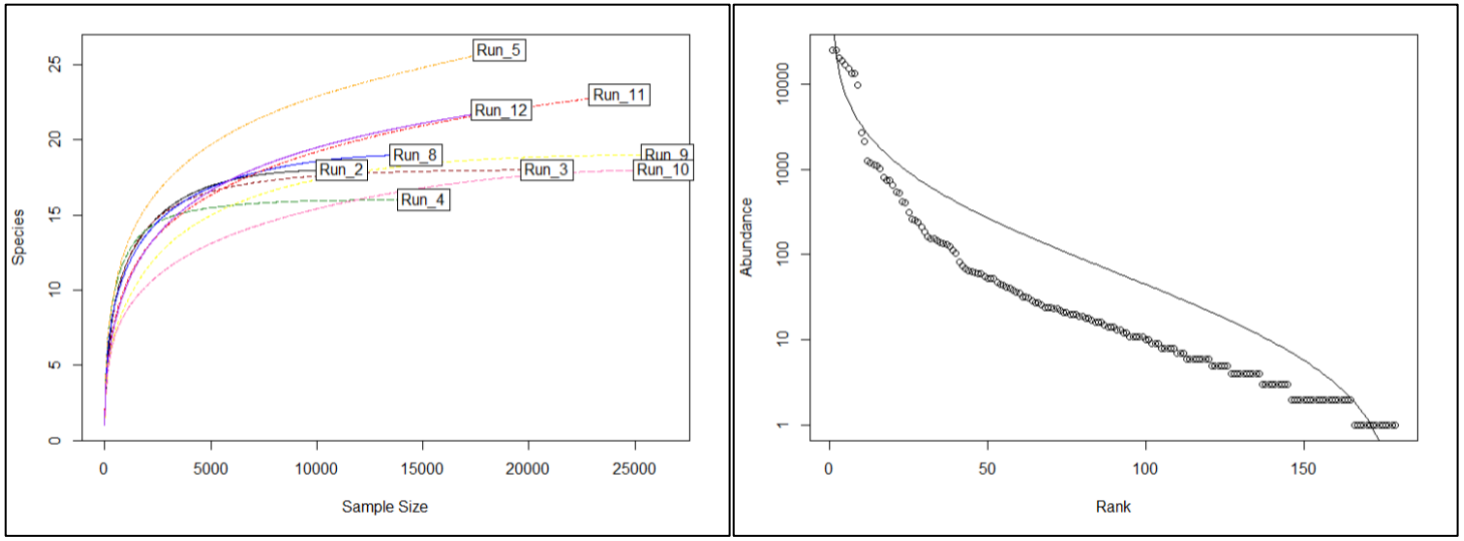

(a) (b)

Figure 30. Rarefaction and rank abundance discussed in Chapter 1, Section 3.4. (a). Rarefaction curves of all samples; (b). Rank abundance

Table 33. One-way analysis of variance of harvesting amount, SO_2 supplement, light cycle, and pH stabilization on key microbial communities. Discussed in Chapter 1, Section 3.4.

Microbial community	Statistic	Harvesting amount	SO_2 supplement	Light cycle	pH stabilization
Eukarya [a]	Degree of freedom	4	1	1	1
	Sum squared	125.44	10.74	28.45	1.79
	P	0.167	0.513	0.273	0.792
Proteobacteria [a]	Degree of freedom	4	1	1	1
	Sum squared	130.67	5.44	35.53	1.49
	P	0.145	0.647	0.219	0.812
Proteobacteria unclassified [b]	Degree of freedom	4	1	1	1
	Chi squared	4.2	0.06	1.0667	0.26667
	P	0.3796	0.8065	0.3017	0.6056
Alphaproteobacteria [b]	Degree of freedom	4	1	1	1
	Chi squared	4.3778	0.96	5.4	4.2667
	P	0.3573	0.3272	0.02014*	0.03887*
Betaproteobacteria [a]	Degree of freedom	4	1	1	1
	Sum squared	38.57	3.48	17.91	16.29
	P	0.00261*	0.415	0.0477*	0.0632
Gammaproteobacteria [b]	Degree of freedom	4	1	1	1
	Chi squared	2.80	0	3.2667	3.2667
	P	0.5918	1	0.0707	0.0707

a. Data are normally distributed. Regular one-way ANOVA is applied to analyze the data.
b. Data are not normally distributed. Kruskal-Wallis one-way ANOVA is applied to analyze the data.
c. " * " means significant difference.

Table 34. Mass and energy flows for process scale analysis of mechanochemical protein extraction and recovery.

Cell Disruption					
INPUT	*Unit*	*Value*	*OUTPUT*	*Unit*	*Value*
Dewatered biomass	kg/day	10,000	Losses (media and vessel, 5%)	kg/day	538
Potassium hydroxide	kg/day	760	Algal slurry	kg/day	10,222
Ball mill	kWh/day	441	*Algal slurry (protein, dry)*	*kg/day*	*631*
Centrifugation					
INPUT	*Unit*	*Value*	*OUTPUT*	*Unit*	*Value*
Algal slurry	kg/day	10222	Solids	kg/day	1227
Centrifuge	kWh/day	8.21	Protein supernatant	kg/day	8995
Precipitation					
INPUT	*Unit*	*Value*	*OUTPUT*	*Unit*	*Value*
Protein supernatant	kg/day	8,995	Precipitated proteins in supernatant	kg/day	14,954
1M H2SO4	kg/day	5,959			
Centrifugation					
INPUT	*Unit*	*Value*	*OUTPUT*	*Unit*	*Value*
Precipitated proteins in supernatant	kg/day	14,954	Supernatant	kg/day	14,336
Centrifuge	kWh/day	12.0	Protein isolate	kg/day	617

Table 35. Inventory for life cycle and techno-economic assessment of microalgal polyol production using a wet microalgal feedstock.

Cultivation					
INPUT	*Unit*	*Value*	*OUTPUT*	*Unit*	*Value*
Freshwater	m^3/day	3.00	Algae suspension	kg/day	500,000
Nitrogen	kg/day	28.1			
Phosphorous	kg/day	7.29			
Carbon dioxide	kg/day	375			
Cultivation electricity	kWh/day	76.5			
Harvesting and Dewatering					

Table 35 (cont'd)

INPUT	*Unit*	*Value*	*OUTPUT*	*Unit*	*Value*
Algae suspension	kg/day	500,000	Recycle nitrogen	kg/day	5.21
Centrifuge	kWh	280	Recycle phosphorous	kg/day	11.5
			Recycle water	m^3/day	496
			Waste nitrogen	kg/day	3.13
			Waste phosphorous	kg/day	4.79
			Waste water	m^3/day	3.00
			Dewatered biomass	kg/day	1250
Polyol synthesis					
INPUT	*Unit*	*Value*	*OUTPUT*	*Unit*	*Value*
Dewatered biomass	kg/day	1,250	Biomass losses	kg/day	62.5
MEA	kg/day	3,750	MEA losses	kg/day	188
PC	kg/day	5,045	MEA losses (air)	kg/day	7.50
Reactor	kWh	5,670	PC losses	kg/day	252
			PC losses (air)	kg/day	10.1
			Microalgal polyol	kg/day	9,525

Table 36. Inventory for life cycle and techno-economic assessment of microalgal polyol production using a dry microalgal feedstock.

Cultivation					
INPUT	*Unit*	*Value*	*OUTPUT*	*Unit*	*Value*
Freshwater	m^3/day	3.00	Algae suspension	kg/day	500,000
Nitrogen	kg/day	28.13			
Phosphorous	kg/day	7.29			
Carbon dioxide	kg/day	375			
Cultivation electricity	kWh/day	76.53			
Harvesting and Dewatering					
INPUT	*Unit*	*Value*	*OUTPUT*	*Unit*	*Value*
Algae suspension	kg/day	500,000	Recycle nitrogen	kg/day	5.21
Centrifuge	kWh	280	Recycle phosphorous	kg/day	11.46
Drying	kWh	503.3	Recycle water	m3/day	495.7
			Waste nitrogen	kg/day	3.13
			Waste phosphorous	kg/day	4.79
			Waste water	m^3/day	3.00
			Dewatered biomass	kg/day	1,250

Table 36 (cont'd)

			Dried biomass (80%)	kg/day	312.5
Polyol synthesis					
INPUT	*Unit*	*Value*	*OUTPUT*	*Unit*	*Value*
Dried biomass (80%)	kg/day	312.5	Biomass losses	kg/day	15.63
MEA	kg/day	937.5	MEA losses	kg/day	46.88
PC	kg/day	2,523	MEA losses (air)	kg/day	1.88
Reactor	kWh	2,129	PC losses	kg/day	126.1
			PC losses (air)	kg/day	5.05
			Microalgal polyol	kg/day	3,577

Table 37. Capital costs of process scale microalgal polyol production using a wet microalgal feedstock.

Item	Purchase cost	Installation factor	Installed cost
PBR	$53,221.93	1.2	$63,866.32
Centrifuge	$245,000.00	1.5	$367,500.00
Water tanks	$152,540.00	3	$457,620.00
Reactor set up	$35,012.48	1.7	$59,521.21
		Total equipment cost	**$948,507.53**
Facility	(4% of equipment costs)		$37,940.30
Site development	(9% of equipment costs)		$85,365.68
		Total direct cost	**$1,071,813.51**
Indirect Costs			
Construction fees, permits, start-up	20% of TDC		$214,362.70
Proratable expenses	10% of TDC		$107,181.35
Field expenses	10% of TDC		$107,181.35
Project contingency	10% of TDC		$107,181.35
		Total indirect cost	**$535,906.75**
		Fixed Capital Investment	$1,607,720.26
Working capital	5% of FCI		$80,386.01
		Total Capital Investment	**$1,688,106.28**

Table 38. Capital costs of process scale microalgal polyol production using a dry microalgal feedstock.

Item	Purchase cost	Installation factor	Installed cost
PBR	$53,221.93	1.2	$63,866.32
Centrifuge	$245,000.00	1.5	$367,500.00
Water tanks	$152,540.00	3	$457,620.00
Reactor set up	$35,012.48	1.7	$59,521.21

Table 38 (cont'd)

Dryer	$40,000.00	1.7	$68,000.00
		Total equipment cost	**$1,216,409.11**
Facility	(4% of equipment costs)		$48,656.36
Site development	(9% of equipment costs)		$109,476.82
		Total direct cost	**$1,071,813.51**
Indirect Costs			
Construction fees, permits, start-up	20% of TDC		$274,908.46
Proratable expenses	10% of TDC		$137,454.23
Field expenses	10% of TDC		$137,454.23
Project contingency	10% of TDC		$137,454.23
		Total indirect cost	**$687,271.14**
		Fixed Capital Investment	$2,061,813.43
Working capital	5% of FCI		$103,090.67
		Total Capital Investment	**$2,164,904.11**

Table 39. Fixed operational expenses for production of microalgal polyols using wet and dry feedstocks.

Employee	Salary	Number	Annual Cost
Chemical engineer	$108,540.00	1	$108,540.00
Chemical technician	$49,820.00	4	$199,280.00
		Total Labor Cost	$307,820.00
		Annualized fixed operational expenses	**$307,820.00**

Table 40. Variable operational expenses for production of microalgal polyols using wet feedstocks and an operating year of 329 days.

Item	Amount	Unit	Unit cost	Total cost
Carbon dioxide	375	kg/day	$0.05	$16.88
Nitrogen	28.13	kg/day	$1.06	$29.92
Phosphorous	7.29	kg/day	$1.90	$13.88
MEA	3,750	kg/day	$1.50	$5,630.76
PC	5,045	kg/day	$1.00	$5,045.00
Electricity	6,026	kWh/day	$0.12	$735.82
Daily polyol production	9,525	kg	$1.20	$11,472.26
Annual polyol production	3,133,778	kg		$3,774,372.36

Table 40 (cont'd)

Annualized variable operational expenses	$3,774,372.36

Table 41. Variable operational expenses for production of microalgal polyols using dry feedstocks and an operating year of 329 days.

Item	Amount	Unit	Unit cost	Total cost
Carbon dioxide	375	kg/day	$0.05	$16.88
Nitrogen	28.13	kg/day	$1.06	$29.92
Phosphorous	7.29	kg/day	$1.90	$13.88
MEA	938	kg/day	$1.50	$1,407.69
PC	2,523	kg/day	$1.00	$2,522.50
Electricity	2,989	kWh/day	$0.12	$364.96
Daily polyol production	3,577	kg	$1.22	$4,355.83
Annual polyol production	1,176,818	kg		$1,433,066.88
Annualized variable operational expenses				$1,433,066.88

CHAPTER 5

Table 42. Mass analysis of biological and chemical carbon capture for the MAASS solvent production and capture system.

Parameter	Value	Unit
CO_2 flow (to PBR)	1000000	kg/day
Biomass production	87.16	wet kg/day
	17.43	dry kg/day
Microalgae CO_2 consumption	0.30	kg CO_2/kg wet
Biomass to MAASS conversion	0.43	kg MAASS/kg wet
Biological CO_2 capture	26.15	kg/day
	0.00003	% of total capture
CO_2 flow (to capture system)	999974	kg/day
CO_2 content of flue gas	0.10	% (v/v)
Flue gas flow	5347454	m^3/day
	6684317	kg/day
Absorption capacity (MEA)	0.50	mol CO_2/mol amine
Absorption capacity (MAASS)	1.27	mol CO_2/mol amine
L/G ratio (MEA)	3.70	kg/m^3
L/G ratio (MAASS)	1.46	kg/m^3
MAASS flow	6330	m^3/day
	7786417	kg/day

Table 42 (cont'd)

Chemical CO_2 capture (90% eff.)	899976	kg/day
CO_2 Residual Emission	99997	kg/day

Table 43. Inventory for life cycle and techno-economic assessment of MAASS production and carbon capture.

Cultivation					
INPUT	*Unit*	*Value*	*OUTPUT*	*Unit*	*Value*
Freshwater	m^3/day	0.308	Algae suspension	kg/day	51272
Nitrogen	kg/day	1.961			
Phosphorous	kg/day	0.508			
CO_2	kg/day	26.15			
Cultivation electricity	kWh/day	8.140			
Harvesting and Dewatering					
INPUT	*Unit*	*Value*	*OUTPUT*	*Unit*	*Value*
Algae suspension	kg/day	51,272	Recycle nitrogen	kg/day	0.36
			Recycle phosphorous	kg/day	0.80
			Recycle water	m^3/day	50.88
			Waste nitrogen	kg/day	0.02
			Waste phosphorous	kg/day	0.05
			Waste water	m^3/day	0.31
			Dewatered biomass	kg/day	87.16
Hydrolysis					
INPUT	*Unit*	*Value*	*OUTPUT*	*Unit*	*Value*
Dewatered biomass	kg/day	87.16	MAASS (pre-centrifuge)	kg/day	121.3
Potassium hydroxide	kg/day	34.17			
Hydrolysis	kWh-E/day	2.79			
Feeding pump	kWh/day	0.01			
Reactor	kWh-E/day	0.66			
Centrifugation					
INPUT	*Unit*	*Value*	*OUTPUT*	*Unit*	*Value*
MAASS (pre-centrifuge)	kg/day	121.33	Solid removal	kg/day	40.67

Table 43 (cont'd)

Centrifuge	kWh/day	0.08	MAASS (post-centrifuge)	kg/day	80.67
Feeding pump	kWh/day	0.02			
Acidification					
INPUT	*Unit*	*Value*	*OUTPUT*	*Unit*	*Value*
MAASS (post-centrifuge)	kg/day	80.67	Precipitated carbon salts	kg/day	36.48
CO_2 (acidification)	kg/day	6.57	Transfer losses	kg/day	6.29
Feeding pump	kWh/day	0.01	MAASS (fresh)	kg/day	37.91
Flue gas blower	kWh/day	0.02			
Regeneration	kWh-E/day	0.21			
Production is separate from absorption and desorption; all are on 167 day cycle					
Absorption					
INPUT	*Unit*	*Value*	*OUTPUT*	*Unit*	*Value*
MAASS (lean)	kg/day	7,786,417	MAASS (rich)	kg/day	8,596,396
CO_2	kg/day	899,977	Uncaptured CO_2	kg/day	99,997
Flue gas blower	kWh/day	3342			
Pump	kWh/day	379.8			
Desorption					
INPUT	*Unit*	*Value*	*OUTPUT*	*Unit*	*Value*
MAASS (rich)	kg/day	8,596,396	CO_2	kg/day	899,977
Regeneration	kWh-E/day	33430	MAASS (lean)	kg/day	7,696,419
Pump	kWh/day	419.3			
HEX	kWh-E/day	186,988			
Compression					
INPUT	*Unit*	*Value*	*OUTPUT*	*Unit*	*Value*
CO_2	kg/day	899,977	CO_2	kg/day	899,977
Compressor	kWh/day	41,729			

Table 44. Mass analysis of chemical carbon capture for the MEA solvent capture system.

Parameter	Unit	Value
CO_2 flow	1,000,000	kg/day
CO_2 content of flue gas	0.10	% (v/v)
Flue gas flow	5,347,594	m^3/day
	6,684,492	kg/day
MEA absorption capacity	0.50	mol CO_2/mol amine

Table 44 (cont'd)

MEA concentration	30	% (w/w)
MEA solvent flow	19,719	m^3/day
	19,778,016	kg/day
MEA flow	5,875	m^3/day
	5,933,405	kg/day
Chemical CO_2 capture (90% eff.)	900,000	kg/day
CO_2 Residual Emission	100,000	kg/day

Table 45. Inventory for life cycle and techno-economic assessment of MEA carbon capture.

Solvent Addition					
INPUT	*Unit*	*Value*	*OUTPUT*	*Unit*	*Value*
Fresh MEA	kg/day	1,600	MEA (lean)	kg/day	19,778,016
Recycled MEA	kg/day	19,776,416			
Absorption					
INPUT	*Unit*	*Value*	*OUTPUT*	*Unit*	*Value*
MEA (lean)	kg/day	19,778,016	MEA (rich)	kg/day	20,588,016
CO_2	kg/day	900,000	Uncaptured CO_2	kg/day	100,000
Flue gas blower	kWh/day	3,342			
Pump	kWh/day	1,183			
Desorption					
INPUT	*Unit*	*Value*	*OUTPUT*	*Unit*	*Value*
MEA (rich)	kg/day	20,588,016	CO_2	kg/day	900,000
Regeneration	kWh-E/day	153,678	Recycled MEA	kg/day	19,686,505
Pump	kWh/day	1,232	MEA degradation	kg/day	1,511
HEX	kWh-E/day	345,062	Ammonia	kg/day	31.50
			Acetaldehyde	kg/day	0.150
			Formaldehyde	kg/day	0.236
			MEA	kg/day	56.70
Compression					
INPUT	*Unit*	*Value*	*OUTPUT*	*Unit*	*Value*
CO_2	kg/day	900,000	CO_2	kg/day	900,000
Compressor	kWh/day	41,730			

REFERENCES

REFERENCES

1. EPA. *Inventory of Greenhouse Gas Emissions and Sinks: 1990-2018*. 2018; Available from: https://www.epa.gov/ghgemissions/inventory-us-greenhouse-gas-emissions-and-sinks.

2. Wang, M., et al., *Post-combustion CO2 capture with chemical absorption: A state-of-the-art review.* Chemical Engineering Research & Design, 2011. **89**(9): p. 1609-1624.

3. Ullah, K., et al., *Assessing the potential of algal biomass opportunities for bioenergy industry: A review.* Fuel, 2015. **143**: p. 414-423.

4. Zhao, B. and Y. Su, *Process effect of microalgal-carbon dioxide fixation and biomass production: A review.* Renewable & Sustainable Energy Reviews, 2014. **31**: p. 121-132.

5. Terry, K.L. and L.P. Raymond, *SYSTEM-DESIGN FOR THE AUTOTROPHIC PRODUCTION OF MICROALGAE.* Enzyme and Microbial Technology, 1985. **7**(10): p. 474-487.

6. Carnegie Institution of Washington, *Algal Culture from Laboratory to Pilot Plant*. 1953.

7. Wu, W. and J.-S. Chang, *Integrated algal biorefineries from process systems engineering aspects: A review.* Bioresource Technology, 2019. **291**: p. 121939.

8. Khoo, C.G., et al., *Algae biorefinery: Review on a broad spectrum of downstream processes and products.* Bioresource Technology, 2019. **292**: p. 121964.

9. Beal, C.M., et al., *Flare gas recovery for algal protein production.* Algal Research-Biomass Biofuels and Bioproducts, 2016. **20**: p. 142-152.

10. Bhattacharya, M. and S. Goswami, *Microalgae – A green multi-product biorefinery for future industrial prospects.* Biocatalysis and Agricultural Biotechnology, 2020. **25**: p. 101580.

11. Davis, R. and B. Klein, *Algal Biomass Production via Open Pond Algae Farm Cultivation: 2020 State of Technology and Future Research*. 2021, National Renewable Energy Laboratory: Golden, CO.

12. Davis, R., et al., *Conceptual Basis and TechnoEconomic Modeling for Integrated Algal Biorefinery Conversion of Microalgae to Fuels and Products: 2019 NREL TEA Update: Highlighting Paths to Future Cost Goals via a New Pathway for Combined Algal Processing*. 2020, National Renewable Energy Laboratory: Golden, CO.

13. Wiatrowski, M. and R. Davis, *Algal Biomass Conversion to Fuels via Combined Algae Processing (CAP): 2020 State of Technology and Future Research*. 2021, National Renewable Energy Laboratory: Golden, CO.

14. Clippinger, J.N. and R.E. Davis, *Techno-Economic Analysis for the Production of Algal Biomass via Closed Photobioreactors: Future Cost Potential Evaluated Across a Range of Cultivation System Designs*. 2019: United States.

15. Eppink, M.H.M., et al., *From Current Algae Products to Future Biorefinery Practices: A Review*, in *Biorefineries*, K. Wagemann and N. Tippkotter, Editors. 2019, Springer International Publishing Ag: Cham. p. 99-123.

16. Gajraj, R.S., G.P. Singh, and A. Kumar, *Third-generation biofuel: algal biofuels as a sustainable energy source.* Biofuels: Greenhouse Gas Mitigation and Global Warming: Next Generation Biofuels and Role of Biotechnology, 2018: p. 307.

17. Bleakley, S. and M. Hayes, *Algal Proteins: Extraction, Application, and Challenges Concerning Production.* Foods (Basel, Switzerland), 2017. **6**(5): p. 33.

18. Miao, G., et al., *Efficient one-pot production of 1,2-propanediol and ethylene glycol from microalgae (Chlorococcum sp.) in water.* Green Chemistry, 2015. **17**(4): p. 2538-2544.

19. Arbenz, A., R. Perrin, and L. Avérous, *Elaboration and Properties of Innovative Biobased PUIR Foams from Microalgae.* Journal of Polymers and the Environment, 2018. **26**(1): p. 254-262.

20. Peyrton, J., et al., *Biobased Polyurethane Foams Based on New Polyol Architectures from Microalgae Oil.* ACS Sustainable Chemistry & Engineering, 2020. **8**(32): p. 12187-12196.

21. Phung Hai, T.A., et al., *Flexible polyurethanes, renewable fuels, and flavorings from a microalgae oil waste stream.* Green Chemistry, 2020. **22**(10): p. 3088-3094.

22. Kumar, S., et al., *Polyurethanes preparation using proteins obtained from microalgae.* Journal of Materials Science, 2014. **49**(22): p. 7824-7833.

23. Zeller, M.A., et al., *Bioplastics and their thermoplastic blends from Spirulina and Chlorella microalgae.* Journal of Applied Polymer Science, 2013. **130**(5): p. 3263-3275.

24. Rochelle, G.T., *Amine Scrubbing for CO2 Capture.* Science, 2009. **325**(5948): p. 1652-1654.

25. Mandal, B.P., et al., *Removal of carbon dioxide by absorption in mixed amines: modelling of absorption in aqueous MDEA/MEA and AMP/MEA solutions.* Chemical Engineering Science, 2001. **56**(21-22): p. 6217-6224.

26. Borowitzka, M.A., *Commercial production of microalgae: ponds, tanks, tubes and fermenters.* Journal of Biotechnology, 1999. **70**(1-3): p. 313-321.

27. Rawat, I., et al., *Biodiesel from microalgae: A critical evaluation from laboratory to large scale production.* Applied Energy, 2013. **103**: p. 444-467.

28. Kunjapur, A.M. and R.B. Eldridge, *Photobioreactor Design for Commercial Biofuel Production from Microalgae.* Industrial & Engineering Chemistry Research, 2010. **49**(8): p. 3516-3526.

29. Scherholz, M.L. and W.R. Curtis, *Achieving pH control in microalgal cultures through fed-batch addition of stoichiometrically-balanced growth media.* Bmc Biotechnology, 2013. **13**.

30. Cutshaw, A., et al., *A long-term pilot-scale algal cultivation on power plant flue gas – Cultivation stability and biomass accumulation.* Algal Research, 2020. **52**: p. 102115.

31. Zhang, B., et al., *Microalgal-bacterial consortia: From interspecies interactions to biotechnological applications.* Renewable & Sustainable Energy Reviews, 2020. **118**: p. 20.

32. Padmaperuma, G., et al., *Microbial consortia: a critical look at microalgae co-cultures for enhanced biomanufacturing.* Critical Reviews in Biotechnology, 2018. **38**(5): p. 690-703.

33. Richmond, A. and Q. Hu, *Handbook of Microalgal Culture : Applied Phycology and Biotechnology*. 2013, Hoboken, UNITED KINGDOM: John Wiley & Sons, Incorporated.

34. Coykendall, L.H., *Formation and Control of Sulfur Oxides in Boilers.* Journal of the Air Pollution Control Association, 1962. **12**(12): p. 567-591.

35. Zuccaro, G., et al., *Microalgae Cultivation for Biofuels Production,*. 2020: Academic Press.

36. Davis, R., et al., *Process Design and Economics for the Production of Algal Biomass: Algal Biomass Production in Open Pond Systems and Processing Through Dewatering for Downstream Conversion*. 2016: United States.

37. Ganesan, R., et al., *A review on prospective production of biofuel from microalgae.* Biotechnology Reports, 2020. **27**: p. e00509.

38. Rastogi, R.P., et al., *Algal Green Energy – R&D and technological perspectives for biodiesel production.* Renewable and Sustainable Energy Reviews, 2018. **82**: p. 2946-2969.

39. Peralta, E., C.G. Jerez, and F.L. Figueroa, *Centrate grown Chlorella fusca (Chlorophyta): Potential for biomass production and centrate bioremediation.* Algal Research, 2019. **39**: p. 101458.

40. Shalaby, S., *Quality of Novel Healthy Processed Cheese Analogue Enhanced with Marine Microalgae Chlorella vulgaris Biomass.* World Applied Sciences Journal, 2013. **23**: p. 914-925.

41. Ahuja, K. and S. Singh. *Algae Protein Market Size by Source*. 2020 [cited 2020; Available from: https://www.gminsights.com/industry-analysis/algae-protein-market.

42. Ursu, A.V., et al., *Extraction, fractionation and functional properties of proteins from the microalgae Chlorella vulgaris.* Bioresource Technology, 2014. **157**: p. 134-139.

43. Guenerken, E., et al., *Cell disruption for microalgae biorefineries.* Biotechnology Advances, 2015. **33**(2): p. 243-260.

44. Yap, B.H.J., et al., *Energy evaluation of algal cell disruption by high pressure homogenisation.* Bioresource Technology, 2015. **184**: p. 280-285.

45. Coons, J.E., et al., *Getting to low-cost algal biofuels: A monograph on conventional and cutting-edge harvesting and extraction technologies.* Algal Research, 2014. **6**: p. 250-270.

46. Balasundaram, B., S. Skill, and C. Llewellyn, *A low energy process for the recovery of bioproducts from cyanobacteria using a ball mill.* Biochemical Engineering Journal, 2012. **69**: p. 48-56.

47. Kabezya, K. and H. Motjotji, *The Effect of Ball Size Diameter on Milling Performance.* Journal of Material Sciences and Engineering, 2015. **4**(1).

48. t Lam, G.P., et al., *Multi-Product Microalgae Biorefineries: From Concept Towards Reality.* Trends in Biotechnology, 2018. **36**(2): p. 216-227.

49. Szycher, M., *Szycher's Handbook of Polyurethanes*. 2012, Baton Rouge, UNITED STATES: Taylor & Francis Group.

50. Ionescu, M., *Chemistry and Technology of Polyols for Polyurethanes; Volume 2*. Chemistry and Technology of Polyols for Polyurethanes. Vol. 2nd edition. 2016, Shrewsbury: Smithers Rapra.

51. Philp, J.C., R.J. Ritchie, and K. Guy, *Biobased plastics in a bioeconomy.* Trends in Biotechnology, 2013. **31**(2): p. 65-67.

52. Petrovic, Z.S., *Polyurethanes from vegetable oils.* Polymer Reviews, 2008. **48**(1): p. 109-155.

53. Guo, D.F., et al., *Amino Acids as Carbon Capture Solvents: Chemical Kinetics and Mechanism of the Glycine + CO2 Reaction.* Energy & Fuels, 2013. **27**(7): p. 3898-3904.

54. Rao, A.B. and E.S. Rubin, *A Technical, Economic, and Environmental Assessment of Amine-Based CO2 Capture Technology for Power Plant Greenhouse Gas Control.* Environmental Science & Technology, 2002. **36**(20): p. 4467-4475.

55. Singh, D., et al., *Techno-economic study of CO2 capture from an existing coal-fired power plant: MEA scrubbing vs. O-2/CO2 recycle combustion.* Energy Conversion and Management, 2003. **44**(19): p. 3073-3091.

56. Kumar, P.S., et al., *Equilibrium solubility of CO2 in aqueous potassium taurate solutions: Part 2. Experimental VLE data and model.* Industrial & Engineering Chemistry Research, 2003. **42**(12): p. 2841-2852.

57. Wei, C.-C., G. Puxty, and P. Feron, *Amino acid salts for CO2 capture at flue gas temperatures.* Chemical Engineering Science, 2014. **107**: p. 218-226.

58. Simons, K., et al., *Highly Selective Amino Acid Salt Solutions as Absorption Liquid for CO(2) Capture in Gas-Liquid Membrane Contactors.* ChemSusChem, 2010. **3**(8): p. 939-47.

59. Kumar, P.S., et al., *Kinetics of the reaction of CO2 with aqueous potassium salt of taurine and glycine.* Aiche Journal, 2003. **49**(1): p. 203-213.

60. Hu, G., et al., *Carbon dioxide capture by solvent absorption using amino acids: A review.* Chinese Journal of Chemical Engineering, 2018. **26**(11): p. 2229-2237.

61. Sanchez-Fernandez, E., et al., *New Process Concepts for CO2 Capture based on Precipitating Amino Acids.* Energy Procedia, 2013. **37**: p. 1160-1171.

62. Becker, E.W., *Micro-algae as a source of protein.* Biotechnology Advances, 2007. **25**(2): p. 207-210.

63. Ramezani, R., S. Mazinani, and R. Di Felice, *State-of-the-art of CO2 capture with amino acid salt solutions.* Reviews in Chemical Engineering, 2022. **38**(3): p. 273-299.

64. Fout, T., et al. *Cost and Performance Baseline for Fossil Energy Plants, Volume 1: Bituminous Coal and Natural Gas to Electricity, Revision 4*. in *Energy, Utility and Envrionment Conference*. 2019. United States.

65. Pavlik, D., et al., *Microalgae cultivation for carbon dioxide sequestration and protein production using a high-efficiency photobioreactor system.* Algal Research-Biomass Biofuels and Bioproducts, 2017. **25**: p. 413-420.

66. Paddock, M.B., J.D. Fernandez-Bayo, and J.S. VanderGheynst, *The effect of the microalgae-bacteria microbiome on wastewater treatment and biomass production.* Applied Microbiology and Biotechnology, 2020. **104**(2): p. 893-905.

67. de Carvalho, J.C., et al., *Culture media for mass production of microalgae*. Biomass, Biofuels and Biochemicals: Biofuels from Algae, 2nd Edition, ed. A. Pandey, et al. 2019, Amsterdam: Elsevier Science Bv. 33-50.

68. Praveen, P. and K.C. Loh, *Nutrient removal in an algal membrane photobioreactor: effects of wastewater composition and light/dark cycle.* Applied Microbiology and Biotechnology, 2019. **103**(8): p. 3571-3580.

69. Wang, X.Q., et al., *Two-stage photoautotrophic cultivation to improve carbohydrate production in Chlamydomonas reinhardtii.* Biomass & Bioenergy, 2015. **74**: p. 280-287.

70. Wan, M.X., et al., *The effect of iron on growth, lipid accumulation, and gene expression profile of the freshwater microalga Chlorella sorokiniana.* Applied Microbiology and Biotechnology, 2014. **98**(22): p. 9473-9481.

71. Hach. *EPA Compliant Methods*. 1996; Available from: https://www.hach.com/epa.

72. Undersander, D., D. Mertens, and N. Thiex, *Forage Analysis*, N.F.T. Association, Editor. 1993: Omaha, NE.

73. Bolyen, E., et al., *Reproducible, interactive, scalable and extensible microbiome data science using QIIME 2 (vol 37, pg 852, 2019).* Nature Biotechnology, 2019. **37**(9): p. 1091-1091.

74. Wang, L., et al., *Cultivation of Green Algae Chlorella sp. in Different Wastewaters from Municipal Wastewater Treatment Plant.* Applied Biochemistry and Biotechnology, 2010. **162**(4): p. 1174-1186.

75. Kim, S., et al., *Growth rate, organic carbon and nutrient removal rates of Chlorella sorokiniana in autotrophic, heterotrophic and mixotrophic conditions.* Bioresource Technology, 2013. **144**: p. 8-13.

76. Rückert, G.V. and A. Giani, *Effect of nitrate and ammonium on the growth and protein concentration of Microcystis viridis Lemmermann (Cyanobacteria).* Brazilian Journal of Botany, 2004. **27**: p. 325-331.

77. Burja, A.M., et al., *Identification of the green alga, Chlorella vulgaris (SDC1) using cyanobacteria derived 16S rDNA primers: targeting the chloroplast.* FEMS Microbiology Letters, 2001. **202**(2): p. 195-203.

78. Sukenik, A., T. Zohary, and J. Padisák, *Cyanoprokaryota and Other Prokaryotic Algae*, in *Encyclopedia of Inland Waters*, G.E. Likens, Editor. 2009, Academic Press: Oxford. p. 138-148.

79. Fulbright, S.P., et al., *Bacterial community changes in an industrial algae production system.* Algal research, 2018. **31**: p. 147-156.

80. Burrell, P.C., C.M. Phalen, and T.A. Hovanec, *Identification of Bacteria Responsible for Ammonia Oxidation in Freshwater Aquaria.* Applied and Environmental Microbiology, 2001. **67**(12): p. 5791.

81. McCaig, A.E., et al., *Nitrogen cycling and community structure of proteobacterial beta - subgroup ammonia-oxidizing bacteria within polluted marine fish farm sediments.* Applied and Environmental Microbiology, 1999. **65**(1): p. 213-220.

82. De Bie, M.J.M., et al., *Shifts in the dominant populations of ammonia-oxidizing beta - subclass Proteobacteria along the eutrophic Schelde Estuary.* Aquatic Microbial Ecology, 2001. **23**(3): p. 225-236.

83. Pepper, I.L. and C.P. Gerba, *Chapter 10 - Cultural Methods*, in *Environmental Microbiology (Third Edition)*, I.L. Pepper, C.P. Gerba, and T.J. Gentry, Editors. 2015, Academic Press: San Diego. p. 195-212.

84. Li, Y., et al., *Variance in bacterial communities, potential bacterial carbon sequestration and nitrogen fixation between light and dark conditions under elevated CO2 in mine tailings.* Science of the total environment, 2019. **652**: p. 234-242.

85. Warren, M.J., et al., *Alphaproteobacteria fix nitrogen in a Sphagnum-dominated peat bog using molybdenum-dependent nitrogenase.* bioRxiv, 2017: p. 114918.

86. Tsoy, O.V., et al., *Nitrogen Fixation and Molecular Oxygen: Comparative Genomic Reconstruction of Transcription Regulation in Alphaproteobacteria.* Frontiers in microbiology, 2016. **7**: p. 1343-1343.

87. Rezaei, F., et al., *SOx/NOx Removal from Flue Gas Streams by Solid Adsorbents: A Review of Current Challenges and Future Directions.* Energy & Fuels, 2015. **29**(9): p. 5467-5486.

88. Janssen, M., et al., *Specific growth rate of Chlamydomonas reinhardtii and Chlorella sorokiniana under medium duration light/dark cycles: 13-87 s*. 1999.

89. Khalid, A.A.H., et al., *Analysis of the elemental composition and uptake mechanism of Chlorella sorokiniana for nutrient removal in agricultural wastewater under optimized response surface methodology (RSM) conditions.* Journal of Cleaner Production, 2019. **210**: p. 673-686.

90. Rendón-Castrillón, L., et al., *Evaluation of the operational conditions in the production and morphology of Chlorella sp.* Brazilian Journal of Biology, 2020.

91. Williams, P.J.B. and L.M.L. Laurens, *Microalgae as biodiesel &; biomass feedstocks: Review &; analysis of the biochemistry, energetics &; economics.* Energy & Environmental Science, 2010. **3**(5): p. 554-590.

92. Goecke, F., et al., *Algae as an important environment for bacteria - phylogenetic relationships among new bacterial species isolated from algae.* Phycologia, 2013. **52**(1): p. 14.

93. Gupta, R.S. and A. Mok, *Phylogenomics and signature proteins for the alpha Proteobacteria and its main groups.* BMC Microbiology, 2007. **7**: p. 106.

94. Lian, J., et al., *The effect of the algal microbiome on industrial production of microalgae.* Microbial Biotechnology, 2018. **11**(5): p. 806-818.

95. Fuentes, J.L., et al., *Impact of Microalgae-Bacteria Interactions on the Production of Algal Biomass and Associated Compounds.* Marine drugs, 2016. **14**(5): p. 100.

96. Toyama, T., et al., *Growth promotion of three microalgae, Chlamydomonas reinhardtii, Chlorella vulgaris and Euglena gracilis, by in situ indigenous bacteria in wastewater effluent.* Biotechnology for biofuels, 2018. **11**(1): p. 176-p. 176.

97. *Climate Watch Historical GHG Emissions*. 2021; Available from: https://www.climatewatchdata.org/ghg-emissions?breakBy=sector&end_year=2018&gases=co2&start_year=1990.

98. Mortensen, L.M. and H.R. Gislerød, *The growth of Chlorella sorokiniana as influenced by CO2, light, and flue gases.* Journal of Applied Phycology, 2016. **28**(2): p. 813-820.

99. Jones, D.B., *Factors for converting percentages of nitrogen in foods and feeds into percentages of protein.* USDA Circ., 1931. **183**: p. 1-21.

100. Cavonius, L.R., E. Albers, and I. Undeland, *pH-shift processing of Nannochloropsis oculata microalgal biomass to obtain a protein-enriched food or feed ingredient.* Algal Research, 2015. **11**: p. 95-102.

101. Ursu, A.-V., et al., *Extraction, fractionation and functional properties of proteins from the microalgae Chlorella vulgaris.* Bioresource Technology, 2014. **157**: p. 134-139.

102. Doran, P.M., *Bioprocess Engineering Principles, 2nd Edition.* Bioprocess Engineering Principles, 2nd Edition, 2013: p. 1-919.

103. Tejano, L.A., et al., *Prediction of Bioactive Peptides from Chlorella sorokiniana Proteins Using Proteomic Techniques in Combination with Bioinformatics Analyses.* International Journal of Molecular Sciences, 2019. **20**(7): p. 1786.

104. Safi, C., et al., *Biorefinery of microalgal soluble proteins by sequential processing and membrane filtration.* Bioresource Technology, 2017. **225**: p. 151-158.

105. PlasticsEurope, *Plastics – the Facts 2021: An analysis of European plastics production, demand and waste data*. 2021.

106. Geyer, R., J.R. Jambeck, and K.L. Law, *Production, use, and fate of all plastics ever made.* Science Advances, 2017. **3**(7): p. e1700782.

107. Bote, S.D. and R. Narayan, *Synthesis of Biobased Polyols from Soybean Meal for Application in Rigid Polyurethane Foams.* Industrial & Engineering Chemistry Research, 2021. **60**(16): p. 5733-5743.

108. Daiek, C., W. Liao, and Y. Liu, *Effects of water recirculation on microalgae assemblage and corresponding sustainability of the photobioreactor cultivation system.* Biomass and Bioenergy, 2022. **157**: p. 106326.

109. Beal, C.M., et al., *Algal biofuel production for fuels and feed in a 100-ha facility: A comprehensive techno-economic analysis and life cycle assessment.* Algal Research, 2015. **10**: p. 266-279.

110. Huntley, M.E., et al., *Demonstrated large-scale production of marine microalgae for fuels and feed.* Algal Research, 2015. **10**: p. 249-265.

111. National Renewable Energy Laboratory, *U.S. Life Cycle Inventory Database*. 2012.

112. Franklin Associates and The Plastics Division of the American Chemistry Council, *Cradle-To-Gate Life Cycle Inventory of Nine Plastic Resins and Four Polyurethane Precursors.* 2010, Eastern Research Group Inc.,: Prairie Village, Kansas.

113. Edelen, A. and W. Ingwersen, *Guidance on Data Quality Assessment for Life Cycle Inventory Data*. 2016, Life Cycle Assessment Research Center, Systems Analysis Branch/ Sustainable Technology Division, National Risk Management Research Laboratory, U.S. Environmental Protection Agency.

114. U.S. Environmental Protection Agency. *Greenhouse Gas Equivalencies Calculator*. 2022 [cited 2022; Available from: https://www.epa.gov/energy/greenhouse-gas-equivalencies-calculator.

115. Plastic Mart. *Cone Bottom Tanks*. 2022; Available from: https://www.plastic-mart.com/product/11189/norwesco-10000-gallon-cone-bottom-tank-n-44103.

116. Chemical Engineering, *Plant Cost Index*. 2022.

117. Humbird, D., et al., *Process Design and Economics for Biochemical Conversion of Lignocellulosic Biomass to Ethanol: Dilute-Acid Pretreatment and Enzymatic Hydrolysis of Corn Stover*. 2011: United States.

118. Zhu, Y., S.B. Jones, and D.B. Anderson, *Algae Farm Cost Model: Considerations for Photobioreactors*. 2018: United States.

119. Garrett, D.E., *Chemical engineering economics*. 1989, New York: Van Nostrand Reinhold.

120. USDA Economic Research Service. *Fertilizer Use and Price*. 2019; Available from: https://www.ers.usda.gov/data-products/fertilizer-use-and-price.aspx.

121. Gibson, J., *Ethanolamines prices roll over.* ICIS Chemical Business, 2020. **298**(12): p. 19.

122. Alibaba. *Price Propylene Carbonate*. 2022; Available from: https://www.alibaba.com/showroom/price-propylene-carbonate.html.

123. U.S. Bureau of Labor Statistics. *Occupational Outlook Handbook*. 2021; Available from: https://www.bls.gov/ooh/.

124. Dessbesell, L., et al., *Bio-based polymers production in a kraft lignin biorefinery: techno-economic assessment.* Biofuels, Bioproducts and Biorefining, 2018. **12**(2): p. 239-250.

125. Huntsman Corporation. *Jeffol Polyether Polyols*. Available from: https://www.huntsman.com/products/detail/356/jeffol.

126. Ferro, L., et al., *Statistical Methods for Rapid Quantification of Proteins, Lipids, and Carbohydrates in Nordic Microalgal Species Using ATR-FTIR Spectroscopy.* Molecules (Basel, Switzerland), 2019. **24**(18): p. 3237.

127. Pretsch, E., P. Bühlmann, and M. Badertscher, *IR Spectroscopy*, in *Structure Determination of Organic Compounds: Tables of Spectral Data*. 2009, Springer Berlin Heidelberg: Berlin, Heidelberg. p. 1-67.

128. D'Alessandro, D.M., B. Smit, and J.R. Long, *Carbon Dioxide Capture: Prospects for New Materials.* Angewandte Chemie-International Edition, 2010. **49**(35): p. 6058-6082.

129. Aronu, U.E., H.F. Svendsen, and K.A. Hoff, *Investigation of amine amino acid salts for carbon dioxide absorption.* International Journal of Greenhouse Gas Control, 2010. **4**(5): p. 771-775.

130. Moioli, S., et al., *A comparison between amino acid based solvent and traditional amine solvent processes for CO2 removal.* Chemical Engineering Research and Design, 2019. **146**: p. 509-517.

131. Caporgno, M.P. and A. Mathys, *Trends in Microalgae Incorporation Into Innovative Food Products With Potential Health Benefits.* Frontiers in Nutrition, 2018. **5**(58).

132. Vizcaíno, A.J., et al., *Differential hydrolysis of proteins of four microalgae by the digestive enzymes of gilthead sea bream and Senegalese sole.* Algal Research, 2019. **37**: p. 145-153.

133. Kwak, N.-S., et al., *A study of the CO2 capture pilot plant by amine absorption.* Energy, 2012. **47**(1): p. 41-46.

134. Kim, Y.E., et al., *Comparison of Carbon Dioxide Absorption in Aqueous MEA, DEA, TEA, and AMP Solutions.* Bulletin of the Korean Chemical Society, 2013. **34**(3): p. 783-787.

135. Sanchez Fernandez, E., et al., *Conceptual Design of a Novel CO2 Capture Process Based on Precipitating Amino Acid Solvents.* Industrial & Engineering Chemistry Research, 2013. **52**(34): p. 12223-12235.

136. Amundsen, T.G., L.E. Øi, and D.A. Eimer, *Density and Viscosity of Monoethanolamine + Water + Carbon Dioxide from (25 to 80) °C.* Journal of Chemical & Engineering Data, 2009. **54**(11): p. 3096-3100.

137. Weiland, R.H., J.C. Dingman, and D.B. Cronin, *Heat Capacity of Aqueous Monoethanolamine, Diethanolamine, N-Methyldiethanolamine, and N-Methyldiethanolamine-Based Blends with Carbon Dioxide.* Journal of Chemical & Engineering Data, 1997. **42**(5): p. 1004-1006.

138. Fadeyi, S., H.A. Arafat, and M.R.M. Abu-Zahra, *Life cycle assessment of natural gas combined cycle integrated with CO2 post combustion capture using chemical solvent.* International Journal of Greenhouse Gas Control, 2013. **19**: p. 441-452.

139. van der Giesen, C., et al., *A Life Cycle Assessment Case Study of Coal-Fired Electricity Generation with Humidity Swing Direct Air Capture of CO2 versus MEA-Based Postcombustion Capture.* Environmental Science & Technology, 2017. **51**(2): p. 1024-1034.

140. Singh, B., A.H. Strømman, and E. Hertwich, *Life cycle assessment of natural gas combined cycle power plant with post-combustion carbon capture, transport and storage.* International Journal of Greenhouse Gas Control, 2011. **5**(3): p. 457-466.

141. Koiwanit, J., et al., *A life cycle assessment study of a Canadian post-combustion carbon dioxide capture process system.* The International Journal of Life Cycle Assessment, 2014. **19**(2): p. 357-369.

142. Veltman, K., B. Singh, and E.G. Hertwich, *Human and Environmental Impact Assessment of Postcombustion CO2 Capture Focusing on Emissions from Amine-Based Scrubbing Solvents to Air.* Environmental Science & Technology, 2010. **44**(4): p. 1496-1502.

143. Perevertaylenko, O.Y., et al., *Searches of cost effective ways for amine absorption unit design in CO2 post-combustion capture process.* Energy, 2015. **90**: p. 105-112.

144. Jilvero, H., et al., *Techno-economic Analysis of Carbon Capture at an Aluminum Production Plant – Comparison of Post-combustion Capture Using MEA and Ammonia.* Energy Procedia, 2014. **63**: p. 6590-6601.

145. Ray, M.S., *Distillation Design, by HZ. Kister, McGraw-Hill, New York, USA (1992). 710 pages. ISBN 0-07-034909-6.* Developments in Chemical Engineering and Mineral Processing, 1994. **2**(4): p. 255-256.

146. Jiang, Y., et al., *Techno-economic comparison of various process configurations for post-combustion carbon capture using a single-component water-lean solvent.* International Journal of Greenhouse Gas Control, 2021. **106**: p. 103279.

147. Schreiber, A., P. Zapp, and W. Kuckshinrichs, *Environmental assessment of German electricity generation from coal-fired power plants with amine-based carbon capture.* The International Journal of Life Cycle Assessment, 2009. **14**(6): p. 547-559.

148. Turner, M.J. and L.L. Pinkerton, *Quality Guidelines for Energy System Studies: Capital Cost Scaling Methodology*. 2013: United States.

149. Loh, H.P., J. Lyons, and C.W. White, *Process Equipment Cost Estimation, Final Report*. 2002: United States.

150. Chemical Weekly. *Price Track.* Available from: https://www.chemicalweekly.com/pricetrack.

151. California Air Resources Board. *Cap-and-Trade Program Recent Market Information*. 2022; Available from: https://ww3.arb.ca.gov/cc/capandtrade/market_info.htm.

152. Rubin, E.S., J.E. Davison, and H.J. Herzog, *The cost of CO2 capture and storage.* International Journal of Greenhouse Gas Control, 2015. **40**: p. 378-400.